The role of factor inhibiting HIF-1 in the cardiovascular responses to hypoxia



Simon Platt

School of Life Sciences

University of Nottingham

This dissertation is submitted for the degree of

Doctor of Philosophy

July 2021

Declaration

I declare that this thesis is entirely the product of my own work. I performed all experiments described myself within the School of Life Sciences during my registered period of study for this degree. No part of the work presented has been submitted previously for a degree at any University.

Simon Platt

July 2021

Acknowledgements

I gratefully acknowledge both the BBSRC and COMPARE for the funding support they provided, enabling me to complete this PhD.

I would like to thank my supervisors, Dr Mark Cole and Professor Jeanette Woolard, for the training and guidance they have provided allowing me to undertake this work. Furthermore, I would like to thank Professor Steve Hill, Dr Mark Soave, and Dr Laura Kilpatrick for all the help and support they provided in undertaking the work described in chapter 5. I also extend thanks to my fellow PhD students within both metabolic physiology and cell signalling, in the School of Life Sciences, for their help, support, and camaraderie during the course of my PhD.

I am very grateful to my family, who have always been encouraging and supportive throughout my education and in particular during the course of my PhD. Similarly, I am appreciative of the encouragement (and distraction!) provided by all of my friends outside of the lab.

Most importantly I thank Fiona for all the support you have given me, making the completion of this thesis possible.

Abstract

Many diseases of the cardiovascular system involve an element of hypoxia due to impairments in oxygen delivery. Central to the cellular responses to hypoxia is the hypoxia inducible factor (HIF) transcription factor signalling system. The HIF system is somewhat unique in that the labile α subunit is constantly expressed, but signalling constrained in an oxygen dependent manner by both prolyl hydroxylase domain (PHD) enzymes and an asparaginyl hydroxylase, factor inhibiting HIF1 (FIH1). PHD enzymes regulate the degradation of HIFα, whereas FIH1 inhibits co-factor binding needed to induce target gene expression, both in an oxygen dependent manner. This thesis aimed to understand the role of FIH1 in aspects of the cardiovascular responses to hypoxia.

In chapters three and four, a mouse model with a null mutation in the HIF1AN gene, which encodes for FIH1, was studied. Cardiac function and metabolism was assessed using Langendorff isolated heart perfusion, in combination with radioisotope tracers (^{3}H palmitate and glucose), and comparisons made to wild type (WT) littermate controls. FIH1$^{-/-}$ hearts were found to have equivalent rates of fatty acid oxidation to WT controls. Furthermore, there was no evidence of alterations in mitochondrial content or function in the hearts of FIH1$^{-/-}$ mice. Upon exposure to chronic hypoxia (11% O_2, 3 weeks duration) there was no evidence of differential response in FIH1$^{-/-}$ animals and no change in cardiac or skeletal muscle mitochondrial content in either genotype.

Hearts from WT and FIH1$^{-/-}$ mice were exposed to a Langendorff ischaemia-reperfusion model. FIH1 mice recovered a greater proportion of baseline function than WT controls. This enhanced recovery was associated with increased rate of glycolysis in both the pre ischaemic and reperfusion periods and an increased degree of lactate accumulation during ischaemia.

In chapter five, to study the effect of FIH1 inhibition upon angiogenic signalling, acute treatment with the selective FIH1 inhibitor DM-NOFD was applied to cell culture models. Hypoxia response element signalling assays revealed that DM-NOFD treatment approximately doubled the HIF signal induced by hypoxia (1% O_2) in HeLa cells. Novel bioluminescent techniques were combined with CRISPR Cas9 gene editing to append an 11 amino acid split luciferase tag on the C-terminal of the VEGF-A gene in human umbilical vein endothelial cells. This allowed for monitoring of VEGF-A production, and was used to assay the effect of DM-NOFD upon VEGF-A production in hypoxia (1% O_2), which was not enhanced by DM-NOFD treatment.

In summary, loss of FIH1 was shown to modulate carbohydrate, but not lipid metabolism in the heart. FIH1 loss is associated with a degree of protection from ischaemic injury in the isolated heart. Although the inhibition of FIH1 in HeLa cells demonstrated a doubling of hypoxia induced HIF signalling, this did not translate to an increase in VEGF-A production by vascular endothelial cells. The techniques developed for monitoring VEGF-A production (split luciferase tag by CRISPR editing), show promise for broader application.

Table of contents

List of figures **xi**

List of tables **xiv**

Nomenclature **xvi**

1 Review of literature **1**

1.1 General introduction 1

1.2 Cardiac pathophysiology 3

1.3 Cardiac Metabolism 4

1.4 Cardiac metabolism in hypoxia 16

1.4.1 Chronic hypoxia 16

1.4.2 Acute Hypoxia 17

1.5 Hypoxia in the cardiovascular system 18

1.5.1 Signalling responses to hypoxia 19

1.6 Factor inhibiting HIF-1α 21

1.6.1 FIH1 manipulation in vivo 22

1.7 Vascular endothelial growth factor (VEGF) 23

1.7.1 Alternative Splicing of VEGF-A 24

1.8 Chemical activation of HIF signalling 27

1.9 General project aims 32

2 General Methods 34

2.1 FIH1 KO generation 34

2.1.1 Confirmation of genotype 35

2.2 Chronic hypoxic housing 36

2.3 Blood Haemoglobin 37

2.4 Isolated heart perfusion 38

2.4.1 Heart excision 38

2.4.2 Langendorff isolated heart perfusion protocol 38

2.4.3 Measurement of metabolic flux in the isolated beating heart 40

2.4.4 Measurement of palmitate oxidation 40

2.4.5 Measurement of Glycolytic flux 42

2.4.6 Measurement of net lactate efflux 43

2.5 Western blotting 44

2.5.1 Protein Extraction 44

2.5.2 Protein Quantification 44

2.5.3 Electrophoresis and Protein Transfer 45

2.5.4 Antibody Detection of Proteins 45

2.6 Mitochondrial copy number quantification 46

2.7 Enzyme activity assays 49

2.7.1 Citrate Synthase 49

2.8 Tissue metabolites 50

2.8.1 Perchloric acid metabolite extract 51

2.8.2 Glucose-6-phosphate, Phosphocreatine, and ATP 51

2.8.3 Pyruvate, ADP, and AMP 53

2.8.4 Free creatine 56

2.8.5 Glycogen 57

2.8.6 Tissue lactate 59

2.9 Cell culture 59

2.9.1 Cell lines utilised 59
2.9.2 General cell culture conditions 60
2.9.3 Hypoxic Cell culture 61
2.10 Hypoxia response element (HRE) reporter assay 61
2.10.1 Transfection of HRE reporter 65
2.10.2 Measurement of HRE-Luciferase activity 65
2.11 CRISPR Cas9 HiBiT protein tagging 66
2.11.1 Design of CRISPR components 66
2.11.2 Assessment of suitability of selected CRISPR editing sites 66
2.11.3 Preparation of Ribonucleoprotein complexes 67
2.11.4 Delivery of CRISPR components to HUVECs 68
2.11.5 Assessment of CRISPR editing 68
2.12 Bioluminescent measurements of HiBiT tagged proteins 69
2.13 Evaluation of HiBiT tagged protein binding to receptor 70
2.13.1 Expression of LgBiT tagged VEGFR2 and NRP1 in HEK293T cells 70
2.13.2 Conditioned media treatment 70
2.13.3 Bioluminescence determination 71
2.14 Immunocytochemistry 71
2.15 Statistical Analysis 72

3 The effect of FIH1 loss on indices of cardiac mitochondrial content and function, and interaction with chronic hypoxic exposure 74

3.1 Abstract 75
3.2 Introduction 76
3.3 Methods 78
3.3.1 Animals 78
3.3.2 Cardiac fatty acid oxidation 78

3.3.3 Chronic hypoxic housing 78
3.3.4 Tissue analysis 79
3.4 Statistical analysis 80
3.5 Results 81
3.5.1 Fatty acid oxidation in FIH1$^{-/-}$ hearts 81
3.5.2 The mitochondrial consequences of the interaction of chronic hypoxia and FIH1 deletion in cardiac and skeletal muscle 86
3.6 Discussion 89

4 The effect of FIH1 loss on cardiac ischaemia reperfusion injury and glucose metabolism 94
4.1 Abstract 95
4.2 Introduction 97
4.3 Methods 102
4.4 Results 106
4.4.1 Tissue metabolites 113
4.5 Discussion 117

5 Development of a CRISPR mediated protein tagging strategy to study the ability of acute chemical FIH1 inhibition to potentiate hypoxia induced angiogenic signalling 122
5.1 Abstract 123
5.2 Introduction 125
5.3 Results 128
5.4 Discussion 146

6 General Discussion 154
6.1 Discussion of principle findings 155

6.2 Experimental models employed: limitations and potential for further development 160
6.2.1 Langendorff heart perfusion 160
6.2.2 FIH1$^{-/-}$ mouse 161
6.2.3 Cell models 163
6.3 Future Directions 164
6.4 Concluding remarks 165

References **166**

Appendix A Reagent details **189**

A.1 Sequence of CRISPR components for addition of HiBit sequence to VEGF-A exon 8a and 8b 189

Appendix B Professional internship for PhD students **191**

List of figures

1.1 Regulation of CPT1 activity via malonyl-CoA 7
1.2 Schematic description of glycolysis 11
1.3 Integration of metabolic pathways in the heart 15
1.4 HIF regulation by oxygen 21
1.5 Schematic representation of VEGF-A gene 24
1.6 VEGF-A receptor binding 27

2.1 Example gel from FIH1 genotyping 36
2.2 Hypoxic housing protocol 37
2.3 Example Langendorff pressure trace 39
2.4 Method of measuring fatty acid oxidation in the isolated perfused heart 41
2.5 Method of measuring glycolytic flux measurement in the isolated perfused heart 43
2.6 Mouse mitochondrial DNA 48
2.7 Example plot of raw absorbance during a citrate synthase activity assay 50
2.8 Hypoxia Response Element- luciferase plasmid 64

3.1 Fatty acid oxidation in WT and FIH1$^{-/-}$ hearts 82
3.2 Citrate synthase activity in WT and FIH1$^{-/-}$ hearts 83

3.3 Mitochondrial/nuclear DNA ratio of WT and FIH1$^{-/-}$ hearts . . . 84
3.4 Protein expression of mitochondrial complexes in WT and FIH1$^{-/-}$ heart . . . 85
3.5 Body weight responses of WT and FIH1$^{-/-}$ mice during chronic hypoxia . . . 86
3.6 Blood haemoglobin in normoxic and hypoxic WT and FIH1$^{-/-}$ mice 87
3.7 Mitochondrial/nuclear DNA ratio of WT and FIH1$^{-/-}$skeletal muscle 88
3.8 Mitochondrial/nuclear DNA ratio of WT and FIH1$^{-/-}$ hearts from normoxic and hypoxic mice . . . 88

4.1 Perfusion protocol for FIH1 ischaemia reperfusion experiments . 103
4.2 Cardiac function in WT and FIH1$^{-/-}$ hearts during ischaemia and reperfusion . . . 108
4.3 Heart rate, end diastolic, and developed pressure in WT and FIH1$^{-/-}$ hearts during ischaemia and reperfusion . . . 109
4.4 Glycolytic flux in FIH1$^{-/-}$ and WT hearts during ischaemia and reperfusion . . . 111
4.5 Net lactate efflux rates from FIH1$^{-/-}$ and WT hearts during ischaemia and reperfusion . . . 112
4.6 Glycogen content of WT and FIH1$^{-/-}$ hearts following ischaemia and ischaemia reperfusion . . . 113
4.7 Tissue lactate content of WT and FIH1$^{-/-}$ hearts following ischaemia and ischaemia reperfusion . . . 114
4.8 ATP content and energy charge of WT and FIH1$^{-/-}$ hearts following ischaemia and ischaemia reperfusion . . . 115
4.9 PCr, free, and total creatine content and energy charge of WT and FIH1$^{-/-}$ hearts following ischaemia and ischaemia reperfusion . . 116

5.1 Accumulation of HIF-1α in MG132 treated HeLa HIF-1α HiBiT cells. 129
5.2 HRE luciferase activity and HIF-1α stabilisation in HeLa HIF-1α HiBiT cells. 131
5.3 Strategy for CRISPR mediated HiBiT tagging of VEGF-A exons 8a and 8b 133
5.4 Initial experiment of VEGF secretion from HUVECs 134
5.5 Assessment of CRISPR mediated HiBiT tagging of VEGF-A exon 8a and 8b 136
5.6 Optimisation of CRISPR mediated HiBiT tagging of VEGF-A exon 8b 137
5.7 The effect of DM-NOFD (500 μM) and hypoxia (1% O2) upon VEGF-A production in HUVECs with HiBiT tagged Exon 8A . 139
5.8 Aggregate data from experiments using unique pools of CRISPR edited HUVECs on the effect of DM-NOFD and hypoxia upon VEGF-A production 141
5.9 CD31 expression in WT and CRISPR edited HUVECs 143
5.10 HiBiT tagged VEGF from CRISPR edited HUVECs binding to LgBiT tagged receptors 145

List of tables

1.1 VEGF-A splice variants 26

1.2 Compounds that enhance HIF signalling 29

2.1 Primers used for genotyping of FIH1 mice 35

2.2 Primer pairs for analysis of mitochondrial copy number 48

2.3 Primers used for HUVEC VEGF-A exon eight amplification and sequencing 67

3.1 Morphological characteristics of WT and FIH1$^{-/-}$ utilised for measurement of fatty acid oxidation 81

3.2 Cardiac function of WT and FIH$^{-/-}$ hearts utilised for measurement of Fatty acid oxidation 82

4.1 Summary of in and ex-vivo investigations of altered HIF signalling in ischaemia reperfusion injury 98

4.2 Characteristics-mice 106

4.3 Coronary flow of hearts undergoing ischaemia reperfusion . . . 107

A.1 CRISPR components for targeting HiBiT addition to VEGF-A . 190

List of Reactions

Reaction {1}: Pyruvate formation from lactate 44
Reaction {2}: Citrate Synthase 49
Reaction {3}: TNB formation in Citrate Synthase reaction 49
Reaction {4}: Glucose-6-phosphate oxidation 52
Reaction {5}: Hexokinase catalysed glucose phosphorylation 52
Reaction {6}: ADP phosphorylation, PCr assay 52
Reaction {7}: Hexokinase catalysed glucose phosphorylation 54
Reaction {8}: ADP phosphorylation 54
Reaction {9}: ADP phosphorylation 54
Reaction {10}: Creatine phosphorylation 56
Reaction {11}: ADP phosphorylation 56
Reaction {12}: Hexokinase catalysed glucose phosphorylation 56
Reaction {13}: Glucose-6-phosphate formation 58
Reaction {14}: Glucose-6-phosphate oxidation (glycogen assay) . . . 58

Nomenclature

Acronyms / Abbreviations

3'UTR	Three prime untranslated region
ACC	Acetyl-CoA carboxylase
AKD	Ankyrin repeat domain
AMPK	Adenosine monophosphate activated protein kinase
ATP	Adenosine triphosphate
BCAA	Branch chain amino acid
BCKADH	Branch chain α-ketoacid dehydrogenase complex
BDH1	D-beta-hydroxybutyrate dehydrogenase
BHB	Beta-hydroxybutyrate
bp	Base pair
BSA	Bovine serum albumin
CACT	Carnitine acylcarnitine translocase
CD31	Cluster of differentiation 31/ Platelet endothelial cell adhesion molecule (PECAM-1)

CD36 Cluster of differentiation 36

CPT1 Carnitine palmitoyltransferase I

CPT2 Carnitine palmitoyltransferase 2

CRISPR Clustered regularly interspaced short palindromic repeats

DM-NOFD Dimethyl N-oxalyl-D-phenylalanine

dm dry mass

DMOG Dimethyl N-oxalyl glycine

DMSO Dimethyl sulfoxide

DP Left ventricular developed pressure

ECL Enhanced chemiluminescence

ECM Extracellular matrix

EDP End diastolic pressure

EPO Erythropoietin

FABPpm Plasma membrane fatty acid binding protein

FAD Flavin adenine dinucleotide

$FADH_2$ Flavin adenine dinucleotide (reduced)

FAT Fatty acid translocase

FIH1 Factor inhibiting HIF-1

G1P Glucose 1-phosphate

G6P Glucose 6-phosphate

GAPDH Glyceraldehyde 3-phosphate dehydrogenase

GFP Green fluorescent protein

GLUT1 Glucose transporter 1

GLUT4 Glucose transporter 4

gww gram wet weight

HBP Hexosamine biosynthetic pathway

HBSS HEPES buffered saline solution

HDR Homology directed repair

HEK293T Human embryonic kidney 293T cells

HF Heart failure

HIF Hypoxia inducible factor

HK Hexokinase

HRE Hypoxia response element

HUVECs Human umbilical vein endothelial cells

KO Knock out

LAD Left anterior descending artery

LDH Lactate dehydrogenase

LVES Large vessel endothelial supplement

LV Left ventricle

MCD Malonyl CoA decarboxylase

MCT1 Monocarboxylate transporter 1

MEF Mouse embryonic fibroblasts

MI Myocardial infarction

mThiolase Acetyl CoA thiolase

NADH Nicotinamide adenine dinucleotide (reduced)

NAD Nicotinamide adenine dinucleotide (oxidised)

NADPH Nicotinamide adenine dinucleotide phosphate (reduced)

NEFA Non esterified fatty acid

NFAT Nuclear factor of activated T-cells

NRP1 Neuropilin 1

PAM Protospacer adjacent motif

PBS Phosphate buffered saline

PCA Perchloric acid

PCR Polymerase chain reaction

PCr Phosphocreatine

PDC Pyruvate dehydrogenase complex

PFK Phosphofructokinase

PGC1α Peroxisome proliferator-activated receptor gamma coactivator 1-alpha

PGM Phosphoglucomutase

PHD Prolyl hydroxylase domain

PK Pyruvate kinase

PP2A Protein phosphatase 2

PPAR Peroxisome proliferator-activated receptor

PPP Pentose phosphate pathway

PSP Peak systolic pressure

RIPA buffer Radioimmunoprecipitation assay buffer

RNP Ribonucleoprotein

ROS Reactive oxygen species

RPP Rate pressure product

SCOT 3-ketoacid CoA transferase

SLC27A Fatty acid transporter protein

SNP Single nucleotide polymorphism

SR Serine-arginine rich

ssODN Single-stranded donor oligonucleotide

TAC Transverse aortic constriction

TAG Esterified triacylglycerol

TAN Total adenine nucleotide

TCA cycle Tricarboxylic acid cycle

TERT2 Telomerase reverse transcriptase

UCP1 Uncoupling protein 1

UDPG Uridine diphosphate glucose

VEGFR2 Vascular endothelial growth factor receptor 2

VEGF Vascular endothelial growth factor

VHL von Hippel–Lindau tumour suppressor protein

VLDL Very low density lipoprotein

WT Wild type

Chapter 1

Review of literature

1.1 General introduction

Due to its role as the final electron acceptor in the mitochondrial electron transport chain, oxygen is critical to survival. Humans have complex systems of oxygen delivery, in which oxygen is captured from the environment and transported to tissues across the body. This process maintains tissue viability and allows metabolic demands to be met. In situations when oxygen delivery does not meet oxygen demand, a biological system is said to be in a state of hypoxia (Semenza, 2011). Hypoxia occurs in a range of pathophysiological conditions, including cardiovascular disease (Bishop and Ratcliffe, 2015).

Heart failure (HF) can be described as a global pandemic. Worldwide, there are in excess of 24 million people living with the disease (Ponikowski et al., 2014). The financial burden of HF is extreme, with an estimated cost of around $31 billion (£22.5 billion) in the USA in the year 2012 alone, this figure is predicted to increase by 127% by the year 2030 (Mozaffarian et al., 2016). More alarming to the patient is the very poor prognosis associated with HF. In the UK, for example, there were an estimated 800,000 HF patients in the year 2010, and the estimated death rate within 30 days of hospital admittance with acute

HF was 15% for men, and 10% for women (Townsend et al., 2012). Globally, ischaemic heart disease was the most common cause of death between 1990 and 2010 (Lozano et al., 2012; Moran et al., 2014). Furthermore, although the rate of myocardial infarction decreased globally through this period, the prevalence of HF has increased (Moran et al., 2014). As such there is a clear need to further understand the mechanisms of HF with a view to develop further therapies for the condition.

In normal health the adult human heart has huge metabolic demands, cycling around 6 kg adenosine triphosphate (ATP) per day. The failing heart, however, has been long considered to be energy starved as these energy demands are not met (Neubauer, 2007). The failing heart also sees adaptations in substrate preference. In normal health, the heart can be described as omnivorous organ, relying on circulating fatty acids, glucose, and ketone bodies, and endogenous glycogen and fatty acids for ATP production (Lopaschuk et al., 2010). In advanced heart failure, however, the metabolic profile changes to an increased reliance upon glucose metabolism and reduced fatty acid metabolism (Lopaschuk et al., 2010; Stanley et al., 2005).

In addition to metabolic disturbance in HF, several strands of evidence also implicate a role of hypoxia in the disease. Study of human HF patients has demonstrated that the myocardium experiences hypoperfusion and hypoxia (Karamitsos et al., 2013; Mahmod et al., 2014). Additionally, utilising more invasive techniques, rodent models of HF also demonstrate that the myocardium experiences hypoxia (Sano et al., 2007; Willam et al., 2006).

The molecular response to hypoxia is orchestrated by the hypoxia inducible factor (HIF) signalling pathway (Semenza, 2011). HIF signalling is controlled by O_2 sensitive hydroxylase enzymes. In hypoxia HIF signalling positively and negatively regulates the expression of thousands of genes, with different

expression profiles in different cell types, with the aim of restoring oxygen homeostasis (Semenza, 2011).

The above epidemiological data demonstrate that diseases of the heart are serious conditions, requiring more effective treatment to reduce mortality. The role that both hypoxia and metabolic abnormalities play in these conditions dictates that the underlying processes of hypoxia, particularly with relation to metabolic changes, deserve further study, with a view toward the development of improved therapies.

1.2 Cardiac pathophysiology

The manifestation of heart failure is complex, with underlying changes in physiology giving rise to a range of symptoms. Chief amongst symptoms are dyspnoea and fatigue, which act to limit exercise tolerance, and also fluid retention, leading to splanchnic and pulmonary congestion and peripheral oedema (Yancy et al., 2013). The core underlying feature of heart failure is impaired ejection of blood or ventricular filling (Yancy et al., 2013).

HF is often preceded by myocardial infarction (Mann and Bristow, 2005). MI occurs when there is a reduction in cardiac perfusion severe enough to cause cell damage and death. Typically, this is due to the formation of a thrombus in a coronary artery (Boateng and Sanborn, 2013). Typical symptoms of acute MI include severe chest pain, which often radiates into the arms (Boateng and Sanborn, 2013). Currently, approximately one quarter of patients will develop HF or die within one year of MI (Cung et al., 2015), highlighting the need for improved therapeutic strategies.

1.3 Cardiac Metabolism

The adult human heart is a constantly active organ, performing a huge amount of work. The heart beats around 100,000 times per day, pumping approximately 10 tons of blood around the body (Neubauer, 2007). This vast amount of mechanical work has a large associated metabolic cost, with the heart cycling around 6 kg of ATP per day (Neubauer, 2007; Opie, 2004). To support this large energy demand the healthy adult heart is metabolically omnivorous, integrating the utilisation of many substrates to maintain energy supply. In normal health, the heart generates the majority of its ATP requirement through oxidative phosphorylation (>95%) (Stanley et al., 2005). The utilisation of several substrates to support this, including fatty acids, glucose, lactate, pyruvate, and ketone bodies, is under several nodes of control (Kolwicz et al., 2013; Lopaschuk et al., 2010). These high rates of oxidative metabolism are facilitated by the fact cardiomyocytes are approximately one third mitochondria by volume (Schaper et al., 1985).

Fat

Fatty acids are transported in the circulation as either esterified triacylglycerol (TAG) or as non esterified fatty acids (NEFA). TAGs in circulation may be from a variety of sources, such as dietary derived (e.g. chylomicron-TAG) or endogenous from the liver (very low density lipoprotein (VLDL)). NEFAs enter the circulation by release from adipose tissue and circulate bound to albumin (Frayn and Evans, 2019).

The rate of fatty acid transport into the heart is proportional to the circulating concentration (Wisneski et al., 1987). The transport of fatty acids across the sarcolemma, into the cardiomyocyte occurs via both passive diffusion and active transport. The fatty acid translocase (FAT), of which the most common cardiac form is cluster of differentiation 36 (CD36) (van der Vusse et al., 2000), as well as

plasma membrane fatty acid binding protein (FABPpm), and fatty acid transporter protein (SLC27A) 1 (Hirsch et al., 1998) and 6 (Gimeno et al., 2003) contribute to the active transport of fatty acids into the cardiomyocyte. Once within the cytoplasm, the major fates for fatty acids are catabolism for energy production, or incorporation into more complex lipids (Lopaschuk et al., 2010). In the healthy human heart, the majority (approximately 86%) of free fatty acids extracted from the circulation undergo rapid oxidation (Wisneski et al., 1987).

In the cytoplasm fatty acids are esterified by acyl-CoA synthase and either incorporated into the intracellular lipid pool, or oxidised. The oxidative process begins with transport into the mitochondria, facilitated by the action of carnitine palmitoyltransferase I (CPT1), the rate limiting enzyme for long chain fatty acid mitochondrial entry and oxidation (McGarry and Brown, 1997). CPT1 catalyses the conversion of fatty acyl-CoA to fatty acyl carnitine. The resultant acyl-carnitine is shuttled into the mitochondrial matrix in a 1:1 exchange with free carnitine via the carnitine acylcarnitine translocase (CACT) (Pande, 1975). Inside the mitochondrial matrix, the acyl-carnitine is transesterified back to long chain acyl-CoA and free carnitine via carnitine palmitoyltransferase 2 (CPT2).

Within the mitochondrial matrix the fatty acyl-CoA undergoes beta oxidation, producing $FADH_2$, NADH, and acetyl-CoA. The acetyl-CoA enters the tricarboxylic acid (TCA) cycle generating further $FADH_2$ and NADH molecules, these, together with those generated through beta oxidation, enter the electron transport chain and generate ATP (Lopaschuk et al., 2010).

The function of CPT1 as a locus of control of mitochondrial fatty acid oxidation is due to its inhibition by malonyl-CoA. Acetyl-CoA carboxylase (ACC) acts to form malonyl-CoA via the carboxylation of acetyl-CoA. Phosphorylation of ACC by AMPK is inhibitory and de phosphorylation via protein phosphatase 2 (PP2A) is disinhibitory (Kudo et al., 1995). The decarboxylation of malonyl-CoA by malonyl CoA decarboxylase (MCD), acts to reduce its abundance (figure 1.1).

Studies in rodent hearts clearly illustrate the importance of this mechanism in the heart.

Cardiac specific deletion of ACC leads to an approximate 50% reduction in malonyl-CoA concentration in the heart and an approximate 60% increase in fatty acid oxidation in isolated perfused hearts (Kolwicz et al., 2012). Conversely, pharmacological inhibition of MCD acutely in the isolated perfused rat heart, caused a seven fold increase in malonyl-CoA, simultaneous to an approximately 0.6 fold reduction in fatty acid oxidation and approximately 4 fold increase in glucose oxidation, with no significant effect of the rate of glycolytic flux (Dyck et al., 2004). Further evidence of the importance of this mechanism to the control of cardiac fatty acid oxidation comes from a mouse genetic model of reduced sensitivity of CPT1 to malonyl-CoA. Fatty acid oxidation was 1.9 fold greater in mutants relative to wild type (WT) controls (Van Weeghel et al., 2018).

There is also tight transcriptional control of fatty acid metabolism. Prominent in the transcriptional control of fatty acid oxidation are the peroxisome proliferator-activated receptor (PPAR) family of nuclear receptor transcription factor proteins. PPARα overexpression in the heart leads to an increase in the expression of genes involved in fatty acid metabolism and an increase in fatty acid uptake. This metabolic phenotype led to cardiac dysfunction and ventricular hypertrophy, suggesting a degree of lipotoxicity (Finck et al., 2002). Conversely, hearts from PPARα null mice oxidise palmitate at approximately one third of the rate of WT controls when perfused in working mode, with compensatory increases in glycolysis and glucose oxidation (Campbell et al., 2002).

Cardiac specific PPARδ deletion, similarly to PPARα, causes a down regulation of fatty acid metabolism associated genes and decreased palmitate oxidation in isolated cardiac tissue (Cheng et al., 2004). These mice also display cardiac dysfunction associated with progressive lipid accumulation in the myocardium. Furthermore, genetic deletion of the peroxisome proliferator-activated receptor

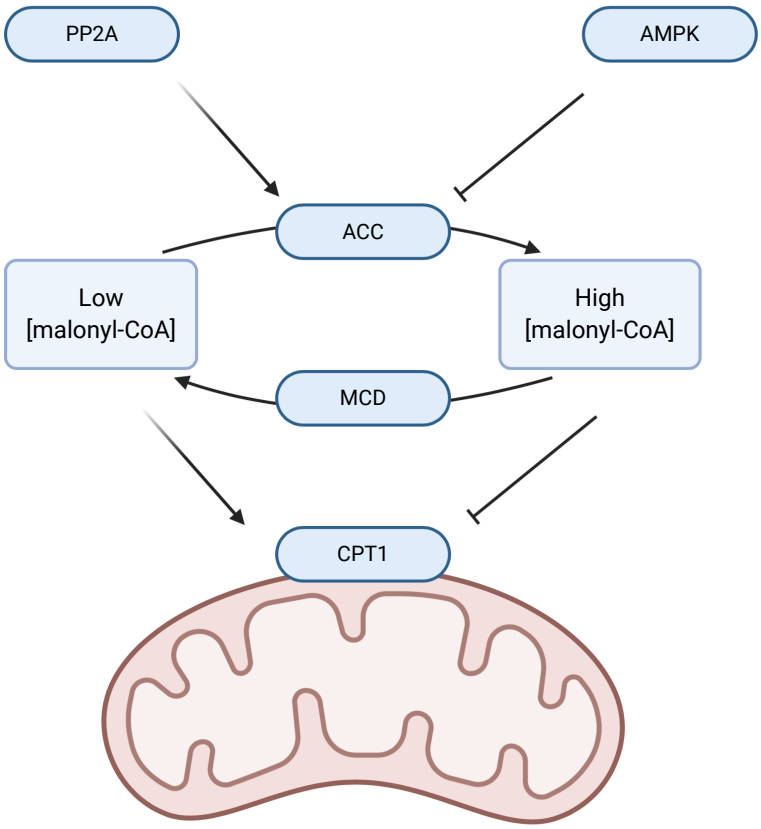


Fig. 1.1 Regulation of CPT1 activity via malonyl-CoA. High malonyl-CoA concentrations inhibit CPT1. Malonyl-CoA levels are decreased by malonyl-CoA decarboxylase (MCD), and increased by acetyl CoA carboxylase (ACC). The activity of ACC is in turn promoted by PP2A mediated dephosphorylation and inhibit by AMPK mediated phosphorylation.

gamma coactivator 1-alpha (PGC-1α), a master regulator of mitochondrial biogenesis, also causes a reduction of oxidative phosphorylation gene expression and a reduction in fatty acid oxidation in isolated working hearts (Lehman et al., 2008). PGC-1α null hearts also display a moderate degree of lipid accumulation, a compensatory increase in glucose oxidation but an overall impairment in cardiac efficiency.

Taken together, these studies of genetic disruption of PPAR signalling demonstrate the importance of transcriptional regulation of fatty acid metabolism in the heart and also provide evidence of the pathology associated with excessive accumulation of cardiac lipids.

Carbohydrate

Circulating glucose is transported into cardiomyocytes via glucose transporters. In the heart glucose transporter 1 (GLUT1) and glucose transporter (GLUT4) predominate. GLUT4 is the principal transporter in the adult heart, accounting for the majority of glucose uptake (Shao and Tian, 2016). GLUT1 is primarily responsible for basal glucose uptake (Kraegen et al., 1993), whereas GLUT4 is the insulin stimulated glucose transporter (James et al., 1988). Under basal conditions GLUT4 is located in intracellular vesicles and translocates to the plasma membrane with insulin stimulation (Slot et al., 1991). Cardiac ischaemic stress also results in the translocation of GLUT4 to the plasma membrane (Heather et al., 2013).

Once within the cell, glucose is readily phosphorylated to glucose-6-phosphate (G6P) by hexokinase (HK). G6P then undergoes a metabolic fate directly or is diverted towards storage as glycogen. The synthesis of glycogen proceeds via the conversion of G6P to glucose-1-phosphate (G1P) by phosphoglucomutase (PGM), and subsequent reaction of G1P with uridine triphosphate to give uridine

diphosphate glucose (UDPG). UDP glucose is transferred to existing glycogen by the action of glycogen synthase, or to glycogenin. Stored glycogen can then act as a substrate as required (Depre et al., 1999).

The majority of glucose is directed towards a metabolic fate via glycolysis: the conversion of G6P to pyruvate via nine enzyme linked steps within the cytosol (figure1.2) (Scrutton and Utter, 1968). There are four key enzymes in the rate of glycolytic flux: hexokinase (HK), phosphofructokinase (PFK), glyceraldehyde 3-phosphate dehydrogenase (GAPDH) and pyruvate kinase (PK) (Metallo and Vander Heiden, 2013). Glycolysis results in the net production of 2 ATP molecules and two NADH molecules and two molecules of pyruvate per glucose molecule. The fate of glycolytically derived pyruvate is dependent upon the energy demand and prevalence of other substrates (Depré et al., 1998).

Pyruvate can be converted to lactate via the action of lactate dehydrogenase, utilising glycolytically derived NADH, and exported out of the cell and into the circulation via monocarboxylate transporter 1 (MCT1), which is highly expressed in the cardiac tissue (Bonen, 2001). Alternatively, pyruvate enters the mitochondria to undergo an oxidative fate. Pyruvate is transported into the mitochondria via the mitochondrial pyruvate carrier and converted to acetyl CoA via the action of the pyruvate dehydrogenase complex (PDC), the rate limiting step in glucose oxidation (Holness and Sugden, 2003). The acetyl CoA produced from pyruvate enters the TCA cycle for oxidation, representing the point of convergence with fatty acid metabolism (figure 1.3; (Stanley et al., 2005)).

Alternative metabolic fates of glucose

Although the majority of glucose undergoes glycolysis, alternative fates are possible by way of the pentose phosphate pathway (PPP) and the hexosamine biosynthetic pathway (HBP) (figure 1.2). Glucose-6-phosphate can enter the pen-

tose phosphate pathway, producing nicotinamide adenine dinucleotide phosphate (NADPH) during the oxidative phase and 5-carbon sugars in the non oxidative phase. Entry of glucose-6-phosphate into the PPP is catalysed by glucose-6-phosphate-dehydrogenase, the rate limiting enzyme of the pathway (Zimmer, 1996).

Fructose-6-phosphate can diverge from glycolysis and enter the hexosamine biosynthetic pathway (HBP), figure 1.2). Entry of fructose-6-phosphate into the HBP is catalysed by L-Glutamine: D-fructose-6-phosphate amidotransferase (GFAT), the rate limiting enzyme of the pathway (Milewski, 2002). Analysis of the HBP in isolated working heart mouse hearts has demonstrated that the flux through the pathway is approximately 2.5 nmol/g protein/min (representing only 0.003–0.006% of glycolytic flux) and seems not to be increased by increasing glucose availability, despite large increases in glycolytic flux (Olson et al., 2020). The ultimate product of the HBP is uridine diphosphate-GlcNAc which serves as a substrate for O-linked–GlcNAc transferase (OGT), an enzyme that catalyses the O-GlcNAcylation of proteins (Wells et al., 2001). This post translational modification is important in the regulation of the behaviours of a wide range of cellular proteins and is increasingly implicated in a range of pathologies (Chatham et al., 2021). In the heart, there is evidence that acutely increased O-GlcNAcylation of proteins can be beneficial in the face of ischaemia reperfusion (Zuurbier et al., 2020). However, more chronically, excessive O-GlcNAcylation is associated with maladaptive cardiac remodelling and complications associated with the diabetic heart (Chatham et al., 2021; Lopaschuk et al., 2021; Wright et al., 2017).

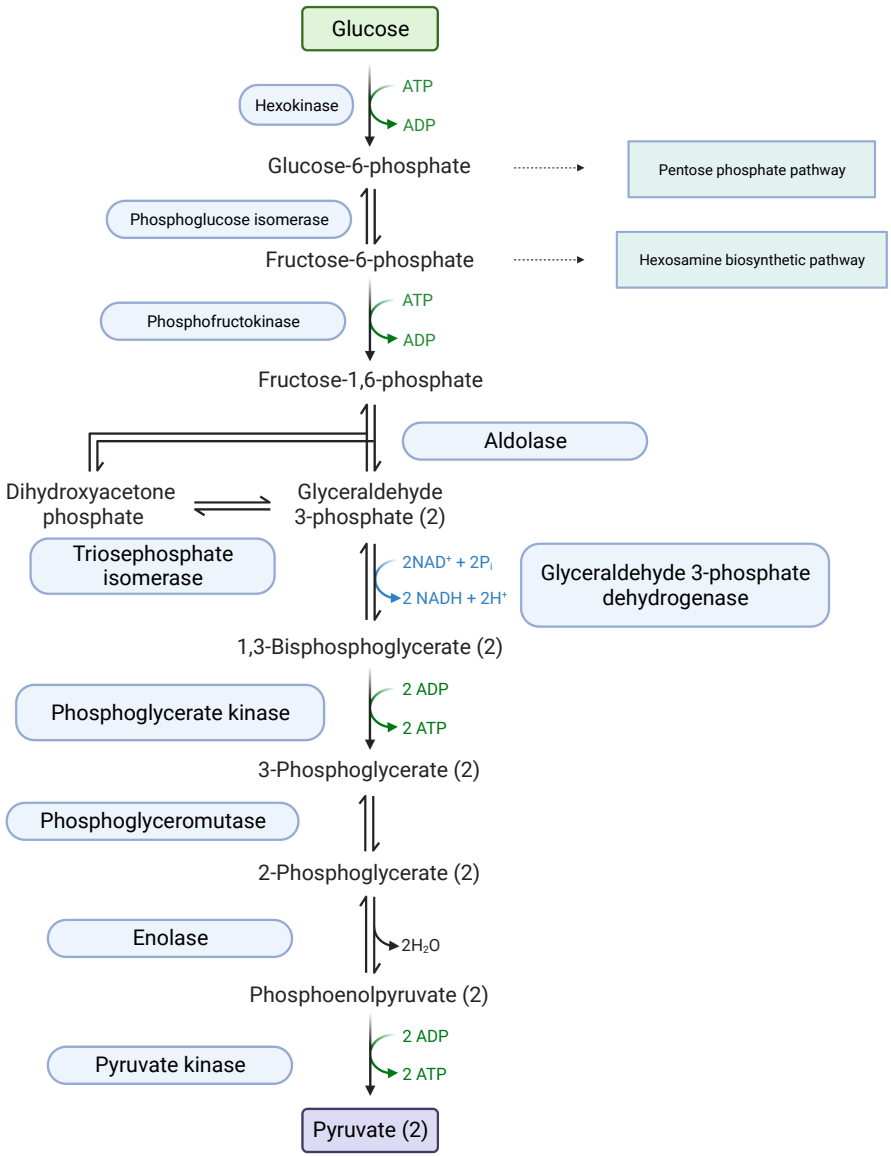


Fig. 1.2 Glycolysis: the conversion of glucose to pyruvate, with net gain of 2 ATP molecules per glucose molecule. Key rate limiting steps in the pathway are those catalysed by hexokinase, phosphofructokinase, and glyceraldehyde 3-phosphate dehydrogenase. Pyruvate can either be exported as lactate, via conversion by lactate dehydrogenase and transport via monocarboxylate transporter 1, or enter the mitochondria for an oxidative fate. Alternative metabolic fates for glucose by way of the pentose phosphate pathway and hexosamine biosynthetic pathway divert a very small fraction of glucose away from glycolysis.

Branch chain amino acids

The branch chain amino acids (BCAA), leucine, isoleucine, and valine, are transported into cells through specialised amino acid transporters (Hyde et al., 2003). Within the cell, BCAAs are transaminated then transported into the mitochondria and the branch chain α-ketoacid dehydrogenase complex (BCKADH), the rate limiting enzyme in BCAA metabolism, catalyses their oxidative decarboxylation. Ultimately the BCAAs enter the TCA cycle as acetyl CoA and in the case of valine and leucine, also as succinate.

BCAA metabolism contributes very little to the total ATP production of the mouse heart (approximately 1%) when perfused with physiologically relevant concentrations of BCAAs (Fillmore et al., 2018). There is an accumulation of BCAAs in left ventricular samples from patients with dilated cardiomyopathy, relative to controls, suggesting that BCAA catabolism is impaired (Uddin et al., 2019). Similarly, accumulation of BCAAs occurs in transverse aortic constriction (TAC) banded mouse hearts, but interestingly, promoting BCAA metabolism in the hypertrophied TAC banded heart improves contractile function (Uddin et al., 2019).

In summary BCAAs represent a minor substrate for the normal, healthy heart. In disease, however, there is dysregulation of BCAA metabolism.

Ketone Bodies

The two principal ketone bodies are beta-hydroxybutyrate (BHB) and acetoacetate, 4-carbon metabolites produced principally in hepatic mitochondria. They are derived from plasma NEFA, released from lipolysis of TAG in adipose tissue. In humans, circulating levels of total ketones in plasma ranges from approximately 100 μM in the fed state, to around 1 mM following a 24 hour fast (Cahill, 2006). BHB is a reduced form of acetoacetate and typically present in the plasma at

around five times the concentration of acetoacetate (Cahill, 2006; Robinson and Williamson, 1980).

Ketone bodies enter the cell via the monocarboxylate transporters. Non hepatic cells express the enzyme D-beta-hydroxybutyrate dehydrogenase (BDH1), which, once BHB is transported into the mitochondria via SLC16A, catalyses its oxidation to acetoacetate. Via the actions of the enzymes 3-ketoacid CoA transferase (SCOT) and acetyl CoA thiolase (mThiolase), each acetoacetate molecule is metabolised to two acetyl CoA molecules which enter the TCA cycle (Puchalska and Crawford, 2017; Robinson and Williamson, 1980). The complete oxidation of one BHB molecule gives a net yield of 21.25 ATP.

In the healthy adult heart ketone body oxidation represents a modest contribution to ATP production (Abdul Kadir et al., 2020). In the adult mouse heart, when perfused with a physiologically relevant concentration of BHB (200 μM) as part of a mixed substrate buffer, the oxidation of BHB contributes approximately 7% of total Acetyl CoA production (Ho et al., 2019). This contribution increases 3 fold with a three fold increase in BHB supply, intriguingly this occurred without any reduction in the flux of any other metabolic pathway (Ho et al., 2019).

In summary the oxidation of ketone bodies represents a minor contribution to energy production in the healthy adult heart, although the heart does have the capacity to increase the oxidation of this substrate in response to increases in supply.

Oxygen

Due to the high rates of oxidative metabolism described above, the heart has a large requirement for oxygen. At rest the adult human heart consumes 8-15 ml of O_2/minute/100 g tissue, which can increase several fold during exercise (Giordano, 2005). Deprivation of oxygen in the adult heart causes substantial

changes in metabolism (Essop, 2007), which will be discussed in more detail below.

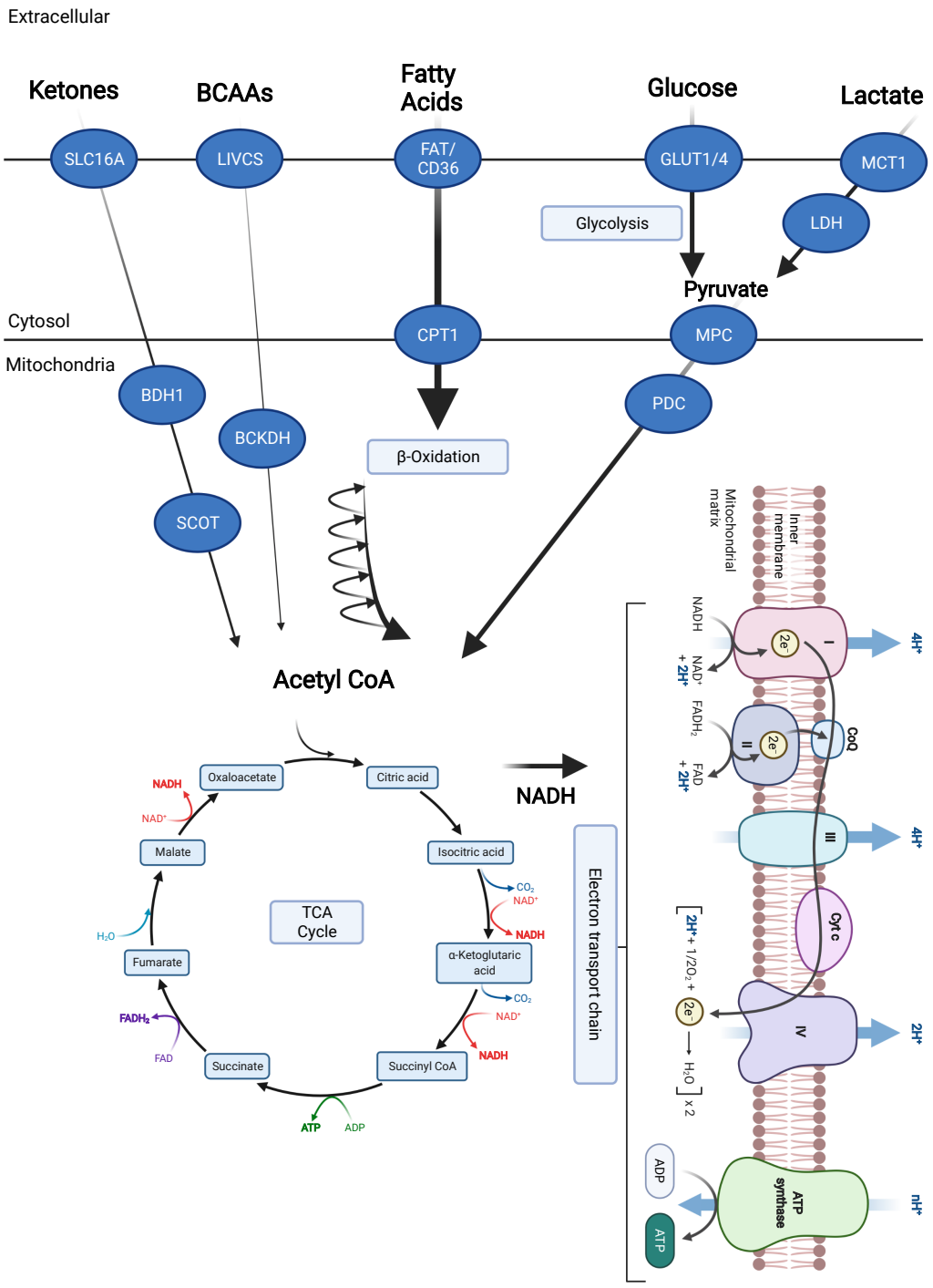


Fig. 1.3 Integration of metabolic pathways in the heart. Oxidation of major substrates in cardiac metabolism is shown, with key transporters (cells surface and mitochondrial), and key regulatory enzymes highlighted.

(continued overleaf)

Fig. 1.3 *(continued)* Oxidative metabolism of ketone bodies, branch chain amino acids (BCAAs), fatty acids, glucose, and lactate, all converges at the point of Acetyl-CoA in the mitochondria. The Acetyl-CoA produced from these different substrates enters the TCA cycle, generating $FADH_2$ and NADH, in turn entering the electron transport chain, which consumes oxygen to generate ATP.

1.4 Cardiac metabolism in hypoxia

Due to the high levels of oxidative metabolism in the heart described above, reductions in oxygen availability has a range of metabolic consequences in the heart. Broadly, the effects of hypoxia can be considered on two timescales- acutely and chronically. That is the immediate effects of reduction in oxygen availability to the heart over a period of minutes to hours, and chronic insufficiency in oxygen availability over a period of days, months, and years.

Complete oxidation of one molecule of palmitate generates 105 ATP molecules, whilst consuming 46 oxygen atoms, whereas the complete oxidation of glucose produces 31 molecules of ATP, consuming 12 oxygen atoms (Lopaschuk et al., 2010). Therefore, although palmitate can provide a greater amount of ATP, it is more costly in terms of oxygen consumption. The increased oxygen efficiency of glucose underlies why fatty acid metabolism is actively down regulated in the hypoxic heart, and a shift towards increased glucose metabolism is seen (Essop, 2007).

1.4.1 Chronic hypoxia

In response to chronic hypoxia, cardiac metabolism is modified in order to maintain function. Healthy lowland dwelling humans that undertook a trek to Everest base camp (5300 m) over 17 days, displayed a substantial decrease in left ventricular mass and function, coincidental with an 18% reduction in cardiac PCr/ATP ratio (Holloway et al., 2011b), indicative of an energy deficit in the heart. Ev-

idence from murine models provides evidence of how cardiac metabolism is reprogrammed with chronic hypoxic exposure.

Multiple rodent studies have utilised a paradigm of 3 weeks chronic hypoxic exposure, with inspired O_2 reduced to 11%. This has shown to induce reprogramming of both fatty acid and glucose metabolism. In the hearts of both rats (Mansor et al., 2016) and mice (Cole et al., 2016) there was an approximate 0.75 fold reduction in the rate of fatty acid oxidation. In mice, there was an overall reduction in the energy status of the heart, with a reduction in PCr/ATP ratio (Cole et al., 2016). Genetic evidence suggests that a reduction in PPARα expression in the hypoxic heart is pivotal to the metabolic reprogramming induced by chronic hypoxia and that this process is antagonised by the oversupply of fatty acids (Cole et al., 2016). Chronic hypoxia also upregulates glycolysis in both the rat (Mansor et al., 2016) and in the mouse heart (Cole et al., 2016; Handzlik et al., 2018).

In addition to the gross changes in substrate metabolism, chronic hypoxic exposure of this nature leads to reductions in activity of mitochondrial complex I, II, and IV activity in isolated subsarcolemmal mitochondria (Heather et al., 2012), and also citrate synthase activity (Mansor et al., 2016).

1.4.2 Acute Hypoxia

Holloway et al. (2011a) investigated the cardiac metabolic consequences of relatively short term hypoxia exposure (20 hours) in healthy adult male humans, utilising a protocol of normobaric hypoxia, maintaining subjects end tidal pO_2 between 50 and 60 mmHg, a value that may be expected at an altitude of around 3000-4000 m above sea level (Ortiz-Prado et al., 2019). Participants showed a 15% decrease in left ventricular PCr/ATP ratio following hypoxic exposure, demonstrating a rapid impairment in myocardial energetics due to reduced oxygen availability.

Acute hypoxia in isolated perfused hearts causes a rapid increase in the rate of glycolytic flux (approximate doubling) concurrent with a five fold reduction in palmitate oxidation (Handzlik et al., 2018). These data demonstrate the rapid switch to an increase in carbohydrate metabolism, particularly glycolysis, with sudden oxygen deprivation to the heart. These data are also of relevance to ischaemia, where the heart also experience a reduction in oxygen delivery. The acutely ischaemic heart also experiences a reduced rate of fatty acid oxidation (Heather et al., 2013), and increased lactate efflux (King et al., 1995).

1.5 Hypoxia in the cardiovascular system

Tissue hypoxia describes the state in which O_2 demand exceeds supply. This can occur due to reduced atmospheric O_2 concentration, such as at higher altitude, or, due to reduced oxygen delivery, such as in disease (Ratcliffe, 2013). The heart is particularly susceptible to hypoxia, due to the large oxygen and energy demands previously described. Myocardial oxygenation and perfusion are impaired in patients with hypertrophic cardiomyopathy, as assessed during vasodilator stress by magnetic resonance (Karamitsos et al., 2013). Furthermore, patients with severe aortic stenosis also experience impaired oxygenation during stress, which is related to the degree of metabolic derangement (Mahmod et al., 2014). Similarly, the heart experiences hypoxia in the event of myocardial infarction.

Animal models also demonstrate the relevance of hypoxia to the diseased heart. In a mouse model of cardiac pressure overload the heart has been demonstrated to experience hypoxia, by pimonidazole staining (Sano et al., 2007). In humans, HF is often preceded by a myocardial infarction (Mann and Bristow, 2005). This underlies the importance of the findings of Willam et al. (2006) who demonstrated that the tissue surrounding the necrotic infarcted region of the rat heart experiences hypoxia.

1.5.1 Signalling responses to hypoxia

All nucleated cells are capable of sensing and responding to hypoxia (Semenza, 2011). When cellular oxygen levels are low, oxygen sensing mechanisms detect and respond to the reduced oxygen availability (Semenza, 2011). Central to the molecular response to hypoxia is hypoxia inducible factor-1 (HIF-1) (Semenza, 2011). HIF-1 is a basic helix-loop-helix transcription factor. It is a heterodimer, consisting of an alpha (HIF-α) and beta (HIF-1β) sub-unit (Wang et al., 1995). There are three described alpha subunits: HIF-1α, HIF-2α, and HIF-3α (Ratcliffe, 2013). Total ablation of HIF-1α is embryonically lethal to mice mid gestation, underlining the importance of HIF signalling for normal development (Iyer et al., 1998).

HIF-α is constantly expressed, but rapidly degraded in cells in normoxia. Prolyl hydroxylase domain proteins (PHD) rapidly hydroxylate HIF-α at Proline 564 (Ivan et al., 2001; Jaakkola et al., 2001) and Proline 402 (Masson et al., 2001). This hydroxylation event promotes the binding of von Hippel–Lindau tumour suppressor protein (VHL). VHL binds to hydroxylated HIF-α and recruits the ubiquitin E3 ligase (Semenza, 2011). HIF-α is subsequently polyubiquitinated and targeted for proteasomal degradation by the 26S proteasome (Semenza, 2011). HIF-β does not display the same pattern of labile expression and is constitutively expressed (Semenza, 2012)

PHDs are members of the Fe(II) and 2-oxoglutarate-dependent oxygenase superfamily (Kaelin and Ratcliffe, 2008). Three PHD isoforms exist (PHD1-3), with differing locations. PHD1 is nuclear, PHD2 is located in the cytoplasm and PHD3 found both in the cytoplasm and the nucleus (Kaelin and Ratcliffe, 2008). These isoforms are widely expressed in various mouse tissues (Lieb et al., 2002). To an extent, there are patterns of tissue specific expression, with PHD3 mRNA

being particularly highly expressed in the heart, and PHD1 in the testes (Lieb et al., 2002).

As molecular oxygen is a crucial substrate for PHDs activity, they confer sensitivity to hypoxia upon the signalling pathway (Schofield and Ratcliffe, 2004). At lower oxygen concentrations, the activity of PHDs is inhibited, and thus HIF-α quickly accumulates and thus is able to heterodimerize and influence gene expression (Semenza, 2011). Of the three isoforms, PHD2 appears the primary control of HIF-1α stabilisation (Berra et al., 2003). This is underlined by the extreme polycythaemia displayed in mice with PHD2 inactivation (Minamishima et al., 2008). Furthermore, homozygous knock out of PHD2 is embryonically lethal, whereas PHD1 and PHD3 deletion are both viable and display less overt phenotypes than that of animals with PHD2 inactivation (Takeda et al., 2008). Although earlier reports suggested PHD isoforms have hydroxylase activity on targets other than HIF, when a thorough mass spectrometry screening approach was applied using recombinant PHDs, none of these non HIF proteins or peptides were hydroxylated (Cockman et al., 2019). These data suggest that the PHDs are in fact highly specific to HIF. The action of PHDs is schematically described in figure 1.4.

As previously described, homozygous deletion of HIF-1α is not viable in mice, although a heterozygous deletion is. Mice that are heterozygous HIF-1α knockouts (HIF-1$\alpha^{+/-}$) display an impaired adaptive response to three weeks of hypoxia (10% O_2) (Yu et al., 1999). More specifically to the heart, cardiac myocyte-specific HIF-1α deletion impairs left ventricular contractile function and also the energy status of the heart. Even in normoxia HIF-1α null hearts had an approximate 30% reduction in ATP and 15% reduction in phosphocreatine levels relative to wild type controls, emphasising the importance of HIF-1α in the regulation of cardiac metabolism (Huang et al., 2004). These data underline

the importance of HIF-1α to maintenance of homeostasis and maintenance of cardiac function.

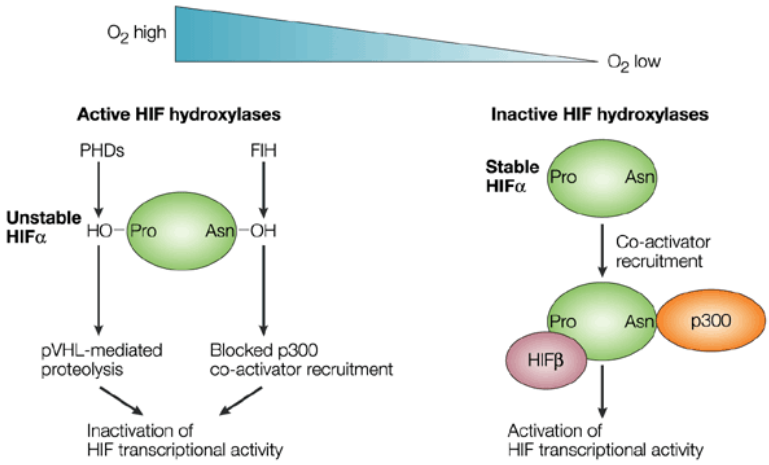


Fig. 1.4 Schematic representation of HIF regulation by oxygen from Schofield and Ratcliffe (2004). In normoxia (left hand side) oxygen availability is sufficient for PHDs and FIH1 to hydroxylate proline and asparagine residues respectively and thus limit the transcriptional activity of HIF. In hypoxia (right hand side), reduced oxygen availability limits hydroxylation, and therefore HIF-α dimerizes and is able to affect the transcription of target genes.

1.6 Factor inhibiting HIF-1α

The transcriptional activity of HIF-1 is under the control of FIH1 (figure 1.4, (Lando et al., 2002a,b; Mahon et al., 2001)). In conditions of normoxia FIH1 catalyses the hydroxylation of HIF-1α at asparagine residue 803 and HIF-2α at asparagine residue 851. This acts to inhibit the binding of cofactors required to promote gene expression (Lando et al., 2002a,b). As with hydroxylation of HIF-α by PHDs, the activity of FIH1 is O_2 dependent (Kaelin and Ratcliffe, 2008). As such, FIH1 acts as a cellular oxygen sensor and is involved in controlling the signalling response to hypoxia. The inhibitory action of FIH1 is seen to a greater extend on HIF-1α than HIF-2α (Bracken et al., 2006).

FIH1 is a ~40 kDa protein which is typically present as a dimer. Crystal structures of FIH1 have revealed its active site, which utilises molecular oxygen,

2-oxoglutarate, and iron to hydroxylate the c terminal activation domain of HIFα, producing succinate and CO_2 in the process (Dann et al., 2002; Elkins et al., 2003). FIH1 is primarily localised to the cytoplasm, but undergoes a degree of nuclear import in hypoxic conditions, orchestrated by a HIF-1α-importin β1 mechanism (Wang et al., 2018).

In vitro studies using isolated proteins and peptides have demonstrated that FIH1 is active at lower oxygen concentrations than PHDs. The observed Km for oxygen for FIH1 is in the region of 100 μM (Koivunen et al., 2004; Tarhonskaya et al., 2015), in comparison to PHD2 which has a Km for O_2 of approximately 229 μM (greater than atmospheric O_2 concentrations of ~200 μM, (Ehrismann et al., 2007)). These findings have been confirmed in whole cell assays, with FIH1 mediated hydroxylation occurring to lower oxygen concentrations than PHD mediated hydroxylation, therefore confirming that FIH1 controls HIF activity to lower oxygen concentrations than PHDs (Tian et al., 2011).

Hydroxylation of proteins other than HIFα occurs through the action of FIH1. The most abundant group of non HIF-α proteins affected are proteins containing ankyrin repeat domains (AKD) (Cockman et al., 2009; Masson et al., 2012). FIH1 also acts as a cellular peroxide sensor, and has been shown to be inhibited by hydrogen peroxide in vitro (Masson et al., 2012).

1.6.1 FIH1 manipulation in vivo

Study of FIH1 manipulation in vivo is limited. Reports from studies of genetic ablation of FIH1 in mice demonstrate that FIH1 affects the regulation of respiration, energy balance, and metabolism (Zhang et al., 2010). $FIH1^{-/-}$ animals display a phenotype of altered metabolism, with a reduced body weight, and a degree of protection from high fat diet induced obesity relative to wild type controls. This appears, in part at least, due to an elevation of UCP1 expression in

the brown adipose tissue of knock out (KO) mice and increased heat production (Zhang et al., 2010). At the cellular level, when cultured, embryonic fibroblasts from these animals display increased HIF transcriptional activity, as assessed by Luciferase assay (Zhang et al., 2010), confirming the basic proof of principle that FIH1 ablation increases HIF signalling.

In a zebra fish model of FIH1 deletion, upon exposure to hypoxia the loss of FIH1 was associated with a greater induction of HIF target genes, as may be anticipated. Furthermore, the loss of FIH1 was associated with an enhanced survival of the fish when exposed to hypoxia (2% O_2) (Cai et al., 2018). These data suggest that loss of FIH1 is protective in the face of hypoxia.

FIH1 is highly expressed in skeletal muscle, which led Sim and colleagues to generate a skeletal muscle specific FIH1 knock out mouse to study its effects specifically in this tissue (Sim et al., 2018). When these mice were exercised under hypoxia, there was a lower rate of oxygen consumption relative to WT controls, demonstrating a greater suppression of oxidative metabolism under conditions of limited oxygen availability.

Besides a modest tachycardia described in FIH1 KO mice (Zhang et al., 2010), there have been no previous publications on the effect of FIH1 manipulation on the heart. Due to enhanced physiological function in the face of hypoxia with FIH1 loss described above, the effect of FIH1 loss or inhibition in the heart in the context of hypoxia provides an interesting avenue of study.

1.7 Vascular endothelial growth factor (VEGF)

Vascular endothelial growth factors are a group of secreted proteins that promote angiogenesis (Holmes and Zachary, 2005). VEGF-A is the subtype principally responsible for angiogenesis. VEGF-A signalling is important in the cellular response to hypoxia, in order to promote oxygen delivery to hypoxic tissues, and

was one of the earliest discovered target genes of HIF-1α signalling (Forsythe et al., 1996).

VEGF-A is secreted by a variety of cell types, including endothelial cells (Uchida et al., 1994), cardiomyocytes (Giordano et al., 2001), fibroblasts (Nissen et al., 1998), and in a range of cancers (Carmeliet, 2005). The angiogenic signalling of VEGF-A is mediated by its binding to vascular endothelial growth factor receptors (VEGFR), of which there are three subtypes, 1-3. The receptor of principal importance for angiogenic signalling is VEGFR2 (Simons et al., 2016). Expression of VEGFR2 is detectable in a broad range of human organs (Wang et al., 2019), with both endothelial cells (Witmer et al., 2002), and smooth muscle cells (Ishida et al., 2001) being key sites of expression.

1.7.1 Alternative Splicing of VEGF-A

The VEGF-A gene is alternatively spliced to produce 16 distinct VEGF-A splice variants. The gene contains 8 exons, with exons 6, 7, and 8 being subdivided into 'a' and 'b', by splice site selection, as depicted in figure 1.5. VEGFR1 binding sites are encoded by exon 3, and VEGFR2 binding sites by exon 4, which are present in all isoforms (Peach et al., 2018). Exons 7 and 8a also encodes for a residue which binds to neuropilin 1 (NRP1), which selectively enhances VEGF-A signalling effects (Guo and Vander Kooi, 2015).

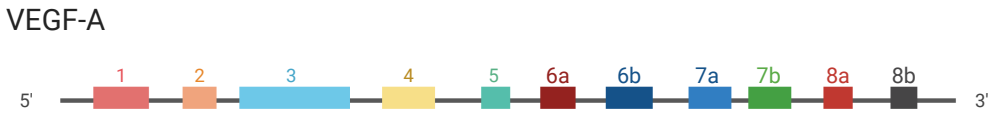


Fig. 1.5 Schematic representation of VEGF-A gene with all exons shown. Alternative splicing results in a multitude of VEGF-A isoforms, with distinct characteristics and signalling behaviours, described in table 1.1.

Differential splicing and the exons included in the VEGF-A protein modulate its activity and function. Exon 8 is a site of a great deal of variation in VEGF-

A splicing, with selection of the proximal splice site, resulting in a protein with exon 8a and the distal splice site with exon 8b. The originally described isoform of VEGF-A is a 165 amino acid protein, containing exons 1-5, 7a,b & 8a (Leung et al., 1989). This is the most abundant isoform and a full agonist of VEGFR2 signalling (Kilpatrick et al., 2017), and therefore considered the 'prototypical'VEGF-A. A corresponding isoform, with the 8b exon included rather than the 8a, was first described following investigation of human kidney biopsies (Bates et al., 2002). In vivo 165b has been shown not to be angiogenic and to inhibit angiogenesis promoted by the prototypical VEGF-A isoform (Woolard et al., 2004). The differential effects of VEGF-A isoforms containing the 8a versus the 8b exon upon binding VEGFR2 are described schematically in figure 1.6.

A number of the described VEGF-A isoforms are listed in table 1.1, together with their characteristic features. An interesting development in this area is the description of a splice variant denoted as VEGF-Ax, which is generated by a programmed translational readthrough (Eswarappa et al., 2014). This protein is due to the presence of an alternative stop codon in the three prime untranslated region (3'UTR), meaning the protein contains both exon 8a and 8b. The physiological role of this isoform is not comprehensively defined, with evidence of both pro-angiogenic (Eswarappa et al., 2014) and anti-angiogenic (Xin et al., 2016) signalling.

Table 1.1 Key alternative splice variants of the VEGF-A gene

Splice Variant	Characteristics
$VEGF_{111}a$	111 amino acid protein containing exons 1-5 & 8a, produced in response to genotoxic stress. Pro angiogenic and proteolysis resistant, does not bind extracellular matrix (ECM) (Mineur et al., 2007).
$VEGF_{121}a$	121 amino acid protein containing exons 1-5, & 8a. Does not bind ECM, does not interact with NRP1.
$VEGF_{145}a$	145 amino acid protein containing exons 1-5, 6a, & 8a.
$VEGF_{165}a$	165 amino acid protein, containing exons 1-5, 7a, & 8a. Prototypical isoform, most abundant, and is a full agonist of VEGFR2 signalling.
$VEGF_{165}b$	165 amino acid protein, containing exons 1-5, 7a, & 8b. Partial agonist of VEGFR2 signalling (Kilpatrick et al., 2017), shows anti-angiogenic effects in vivo (Woolard et al., 2004).
$VEGF_{189}a$	189 amino acid protein containing exons 1-5, 6a, 7a, & 8a. Interacts strongly with ECM (Chen et al., 2010).
$VEGF_{206}a$	206 amino acid protein containing exons 1-5, 6a &b, 7 a & b, & 8a. Interacts strongly with ECM (Chen et al., 2010).
$VEGF_{xxx}a$	Generic notation for VEGF-A of xxx amino acids in length, containing the 8a exon
$VEGF_{xxx}b$	Generic notation for VEGF-A of xxx amino acids in length, containing the 8b exon
VEGF -Ax	Translational read through, contains exons1-5, 7a, 8a, & 8b, and the 'intron' in-between them. Has been demonstrated to show both pro and anti angiogenic properties (Eswarappa et al., 2014; Xin et al., 2016).

Regulation of alternative splicing

Splicing of mRNA is regulated by the nuclear spliceosome. Within the nucleus, introns are excised from transcribed pre-mRNA by the constituent small nuclear ribonucleoproteins (U1, U2, U4, U5, AND U6), and accessory proteins U2AF and SF1 (Bowler and Oltean, 2019). The splicing of VEGF-A is also controlled by a number of RNA binding proteins, principally the serine/arginine rich (SR) proteins SRSF1, SRSF2, SRSF5, SRSF6 (Guyot and Pagès, 2015). SR proteins are located in the cytoplasm and transportation into the nucleus is facilitated

by phosphorylation. Within the nucleus SR proteins bind to regulatory sites in VEGF-A pre-mRNA leading to exon removal. Important to the alternative splicing of VEGF-A is the constitutively active kinase SRPK1 (Amin et al., 2011; Bowler and Oltean, 2019; Oltean et al., 2012). SRPK1 is instrumental in the alternative splicing of VEGF-A exon 8. Inhibition of SRPK1 has been shown to inhibit angiogenesis by promoting $VEGF_{xxx}b$ expression over $VEGF_{xxx}a$ (Amin et al., 2011; Oltean et al., 2012). Although there is no hypoxia response element present in the SPRK1 gene, there is some evidence of upregulation of mRNA expression due to hypoxia (Bowler et al., 2018).

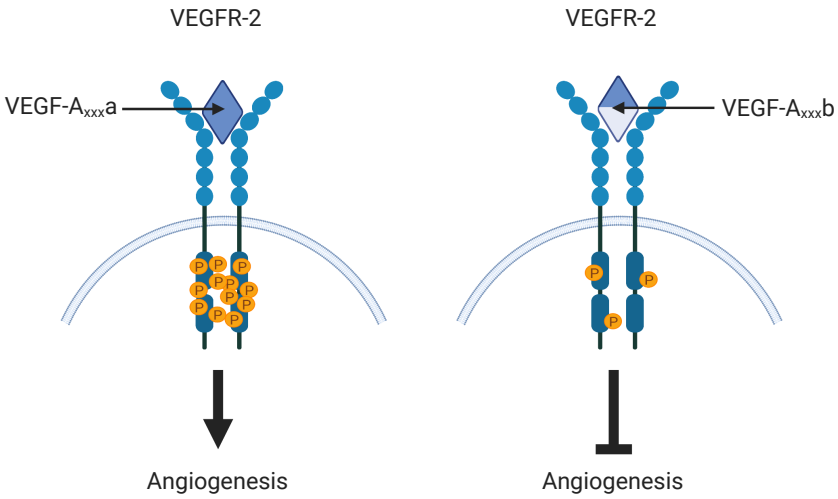


Fig. 1.6 Schematic representation of alternatively spliced VEGF-A binding to the VEGFR-2 receptor. The prototypical $VEGF\text{-}A_{xxx}a$ binds VEGFR2, causes autophosphorylation and promotes angiogenesis. $VEGF\text{-}A_{xxx}b$ is a partial agonist of the VEGFR-2 receptor, causes a lesser degree of autophosphorylation, and reduced angiogenic response.

1.8 Chemical activation of HIF signalling

HIF signalling can be promoted by a number of chemical compounds. There are several categories of HIF activating compounds, examples of which are given in table 1.2. Although the method of action for each of these groups is different,

the common theme is that these compounds prevent the hydroxylation of HIF, or negate the effects of its hydroxylation, therefore enhancing HIF signalling.

HIF activators with a method of action of hydroxylase inhibition can be either pan hydroxylase inhibitors, or more specific to either PHDs or FIH1. Pan hydroxylase inhibitors display more off target effects. Interestingly, however, there is some evidence that broad pan hydroxylase inhibitors (such as dimethyl N-oxalyl glycine (DMOG)) better mimic the transcriptional response to hypoxia than do PHD specific inhibitors (Chan et al., 2016). This may be due to off target effects on other dioxygenases (i.e. not PHDs or FIH1), that are also inhibited in hypoxic conditions.

As described in table 1.2, the majority of compounds that developed to augment HIF signalling are PHD specific inhibitors, acting to reduce proline hydroxylation of HIF. In cell based assays specific inhibition of PHDs, utilising a range of different inhibitors, has been shown to have relatively modest effects on HIF signalling, assessed with hypoxia response element (HRE) reporter assays. However, the addition of FIH1 specific inhibition (DM-NOFD) to targeted PHD inhibition can increase HIF transcriptional activity (Sulser et al., 2020). The maintained FIH1 activity at oxygen tensions where PHDs become inhibited (Tian et al., 2011), leads to the interesting hypothesis that in conditions of modest hypoxia, chemical inhibition of FIH1 may provide an increase of HIF signalling and therefore an enhancement in cellular function.

Table 1.2 Compounds that enhance HIF signalling

Compound Class	Compound	Method of Action	Current Usage
Hypoxia mimetic compounds	Cobalt Chloride	Binds HIF-1α and prevents VHL binding, thereby blocking proteasomal degradation (Yuan et al., 2003)	Used as a tool compound in pre clinical and cell culture models
Iron chelators	Desferrioxamine	Complexes with iron and inhibits PHD activity	Shown to be safe in phase two clinical trials in patients with intracerebral haemorrhage, although limited clinical utility in this setting (Selim et al., 2019)
	Hydralazine	Complexes with iron and inhibits PHD activity	Used as an antihypertensive since 1953, more recently shown to be a HIF activator (Knowles et al., 2004)
	AKB-4924 (GB004)	Complexes with iron and stabilises HIF (Okumura et al., 2012)	Phase 1 trials in healthy volunteers (NCT02914262) and patients with active ulcerative colitis (NCT03860896)
Alpha-ketoglutarate mimetics	Dimethyloxalylglycine (DMOG)	A prodrug form of N-oxalylglycine, an inhibitor of α-KG dependent dioxygenases (including PHDs)	Widely used as a tool compound in pre clinical and cell culture models

Continued on next page

Table 1.2 – continued from previous page

Compound Class	Compound	Method of Action	Current Usage
	Dimethyl N-oxalyl-D-phenylalanine (DM-NOFD)	Binds to the active site of FIH1, therefore preventing its hydroxylase activity (McDonough et al., 2005). Accumulated HIF protein is protected from hydroxylation at Asn803 (Chan et al., 2016)	Tool compound, preliminary use in cell culture models, investigations of transcriptional regulation only.
PHD active site blockers	Enarodustat (JTZ-951)	Blocks the active site of PHD, preventing proline hydroxylation, leading to HIF accumulation (Ogoshi et al., 2017)	Phase 3 clinical trials for anaemia in chronic kidney disease (NCT04027517)
	TP0463518	Blocks PHD active site preventing proline hydroxylation of HIF Hamada et al. (2018); Kato et al. (2018)	Utilised in preclinical and cell culture models. Induces EPO production in the liver (Kato et al., 2019). Phase 1 trials in healthy humans and anaemic chronic kidney disease patients (Shinfuku et al., 2018)
	PHD-1-IN-1	Binds active site Fe2+ ion and induces the formation of an “Arg367-out” pocket preventing hydroxylation and therefore leads to HIF accumulation	Used in preclinical and cell culture models (Ahmed et al., 2017)
	Vadadustat (AKB-6548)	Binds the PHD active site and prevents proline hydroxylation of HIF	Approved for the treatment of anaemia associated with chronic kidney disease, Japan, 2020 (Markham, 2020)

Continued on next page

Table 1.2 – continued from previous page

Compound Class	Compound	Method of Action	Current Usage
	Roxadustat (FG-4592)	Binds the PHD active site and prevents proline hydroxylation of HIF	Approved for the treatment of anaemia associated with chronic kidney disease, China , 2018 (Dhillon, 2019)
	GSK360A	Binds PHD in the alpha ketogluterate site, preventing HIF prolyl hydroxylation (Bao et al., 2010)	Utilised in cell culture and pre clinical models.
	Daprodustat (GSK1278863)	Blocks the HIF binding site of PHD enzymes leading to HIF accumulation(Ariazi et al., 2017)	Approved for the treatment of anaemia associated with chronic kidney disease, Japan, 2020 (Dhillon, 2020)

1.9 General project aims

The work described in this thesis aimed to investigate the role of FIH1 in the cardiovascular responses to hypoxia. To this end, both mouse and cell culture experimental models were used to evaluate the effects of a loss of FIH1 function. Specifically, a mouse with a global deletion of the HIF1AN gene (encoding FIH1) was studied in chapter 3 and 4, and in chapter five the effects of a small molecule FIH1 inhibitor were evaluated. The specific questions addressed in each chapter are outlined below.

Mitochondrial consequences of FIH1 loss

Metabolic remodelling, particularly of mitochondrial metabolism is a core response to hypoxia. It is not known how the loss of FIH1 effects the mitochondrial and oxidative characteristics of the heart. The effect of a loss of FIH1 protein upon oxidative metabolism in the heart was studied using hearts isolated from FIH1$^{-/-}$ hearts. Rates of fatty acid oxidation were assessed in isolated perfused hearts, as well as several markers of mitochondrial content and function. Additionally, the interaction with FIH1 loss with exposure to chronic hypoxia was evaluated.

Effect of FIH1 loss on ischaemia reperfusion injury and glucose metabolism

There is substantial evidence that alterations in the activity of the HIF signalling system affect the outcome of cardiac ischaemia reperfusion injury. It is not known, however, how the loss of FIH1 affects ischaemia reperfusion in the heart. An ex vivo ischaemia reperfusion model was developed and hearts from WT and FIH1$^{-/-}$ mice studied. Furthermore, the effect of FIH1 deletion on glucose metabolism, and its interaction with the recovery from ischaemia was investigated.

Effect of FIH1 inhibition upon angiogenic signalling in hypoxia

Angiogenesis is a key response to hypoxia which is promoted by HIF signalling. In the heart, following myocardial infarction, there is evidence of hypoxia, and also evidence that promoting HIF signalling can be beneficial. It is not known, however, if inhibiting FIH1 can potentiate the angiogenic response to hypoxia. To address this, novel bioluminescent techniques were developed and the effect of acute chemical inhibition of FIH1 upon VEGF-A production in hypoxic endothelial cells was studied.

Chapter 2

General Methods

The work presented in this thesis utilising animals was performed in accordance with the Home Office Guidance and the relevant legislation of The Animals (Scientific Procedures) Act, 1986. Furthermore all work was conducted according to The University of Nottingham institutional guidelines.

2.1 Generation of mice with a constitutive deletion of FIH1

To study the effects of FIH1 in-vivo mice were generated with a constitutive deletion of the Hif1an gene. Genetic deletion was performed as previously described (Zhang et al., 2010), with mice bred on a C57/BL6J background. Mice were group housed in standard laboratory conditions (humidity 40-60%, temperature 22-24 °C, 12 hour light-dark cycle) with ad libitum access to water and standard laboratory chow.

2.1.1 Confirmation of genotype

The genotype of FIH1 mice was determined by polymerase chain reaction (PCR) from an ear notch tissue biopsy in pups. For each animal used in an experiment a tail tip biopsy was taken post mortem to confirm the genotype.

Tissue biopsies were digested in a lysis buffer (0.1 M Tris (pH 8.5), 5 mM EDTA, 0.2% SDS, 0.2 M NaCl, 0.05% proteinase K) at 55°C overnight. Genomic DNA was precipitated by the addition of an equal volume of isopropanol, and washed with 70% ethanol. Genomic DNA was amplified via multiplex PCR with primers listed in table 2.1.

Table 2.1 Primers used for genotyping of FIH1 mice

Primer	Sequence
LOX1	5'-GACTGCTGCCAAACCCTTC-3'
SDL2	5'-CGTTTCACACTGGTGAGACCCTG-3'
3'NEO 2	5'-CCAAACAGAACCGCACAATG-3'

Multiplex PCR was performed in a 10 μl reaction volume containing 0.5 μl diluted gDNA, 1 μl Dream Taq buffer (Thermo Scientific, Loughborough, UK) 0.05 μl Taq polymerase (Thermo Scientific, Loughborough, UK), 100 μM dNTPs, 2 μM LOX1, SDL2 and 3'NEO 2 primers. The PCR reaction consisted of 3 minutes at 95 °C followed by 35 cycles of 30 seconds at 95 °C, 30 seconds at 60 °C, and 30 seconds at 72 °C, followed by a final extension step of 3 minutes at 72 °C. PCR products were separated on a 3% Agarose gel containing ethidium bromide. Gels were imaged under U.V. light.

Deletion of the FIH1 target region included the binding site for the SDL2 primer and exons 1 and 2. Therefore, for wild type alleles, there was amplification of the region covered by the LOX1 forward and SDL2 reverse primer, a 259 base pair product. For FIH1 null alleles, deletion of the target region brought the 3'NEO 2 sequence to within 430 base pairs of the LOX1 region, thus a PCR

product of 430 base pairs. As such, on the agarose gels, biopsies from WT animals showed a single band at 259 base pairs, KO animals a single band at 430 base pairs, and heterozygous animals two bands of equal intensity at 259 and 430 base pairs. Figure 2.1 shows an example agarose gel image from genotyping.

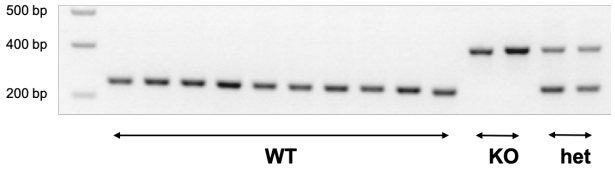


Fig. 2.1 Example agarose gel from genotyping of FIH1 mice. WTs display a single band at 259 base pairs (lanes 1-10), KOs single band at 430 base pairs (lanes 11-12), heterozygotes a band at both 259 and 430 base pairs (lanes13-14).

2.2 Chronic hypoxic housing

To study the effects of chronic hypoxia upon murine physiology a protocol of progressive chronic hypoxic exposure was employed. This protocol is well characterised and has been previously used to study the responses of both rats (Heather et al., 2012; Mansor et al., 2016) and mice (Cole et al., 2016; Handzlik et al., 2018) to hypoxia.

Animals were housed on a 12-hour light-dark cycle, with water and standard laboratory chow provided *ad libitum* at all times. Normal mice home cages were placed in a flexible film isolator, with a through flow of filtered air. Hypoxia was generated within the chamber by removal of O_2 content in the incoming air via a hypoxic generator (Hypoxico, New York, USA). The O_2 and CO_2 concentrations within the chamber were monitored continuously via an online sensor system (Normocap Oxy, Datex Engstrom, Finland) with CO_2 not exceeding 0.1%. Hypoxia was gradually introduced over the first 7 days of hypoxic housing, with continuous exposure to 11% O_2 over the subsequent two weeks as described in figure 2.2. In order to monitor animals adaptation to, and tolerance of the

hypoxic conditions, body weight was measured daily, within the hypoxic chamber. Animals were also assessed for any adverse behavioural responses during daily monitoring.

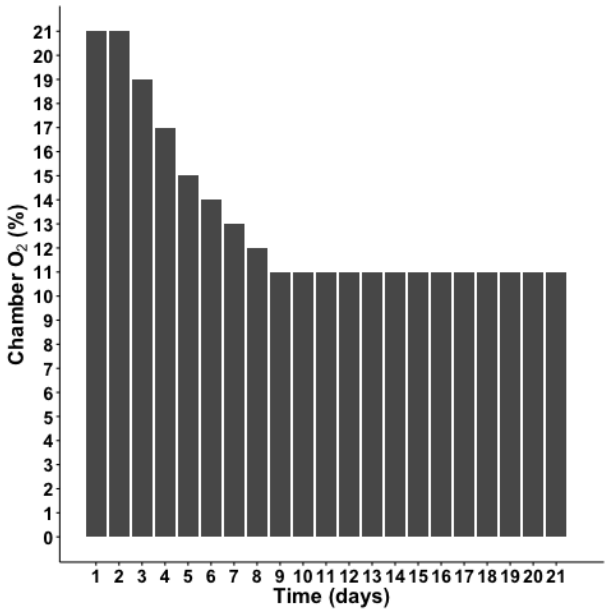


Fig. 2.2 Schematic representation of hypoxic housing protocol

Control animals were housed in normoxia throughout. Normoxic and hypoxic animals were housed in the same room, ensuring exposure to equivalent temperature, humidity, and light-dark cycle conditions. Humidity and temperature in the chamber were maintained at an ambient level of 40-60% and 22-24 °C respectively.

Following chronic hypoxic housing, all animals were exposed to room (normoxic) air for 1 hour. Subsequently, they were euthanised with a sodium pentobarbitone intraperitoneal injection (0.1-0.15 ml of 200 μg/ml).

2.3 Blood Haemoglobin

Immediately following heart excision around 10 μl blood was sampled in duplicate from the chest cavity for the determination of haemoglobin concentration.

Samples were measured using the HemoCue Analyser (HemoCue 201^{+}; Angelholm, Sweden). The measurement is made by the blood being haemolysed by sodium deoxycholate to release haemoglobin. Released haemoglobin is converted to methaemoglobin by sodium nitrite, which reacts with sodium azide to give azide methemoglobin. The absorbance of the sample is then measured at 570 nm and 880 nm, to negate the effect of turbidity, and haemoglobin calculated.

2.4 Isolated heart perfusion

2.4.1 Heart excision

Animals were terminally anaesthetised with an intraperitoneal injection of sodium pentobarbitone (0.1-0.15 ml of 200μg/ml). Upon withdrawal of the pedal reflex an incision was made beneath the sternum and two further incisions made towards the animals head, allowing the rib cage to be folded back over the animals head and the thoracic cavity exposed. The beating heart was quickly excised and arrested in ice cold Krebs-Henseleit buffer. The heart was trimmed of all undesired surrounding tissue and weighed. The ascending aorta was located and cannulated with a 16 gauge cannula.

2.4.2 Langendorff isolated heart perfusion protocol

Upon successful cannulation hearts were transferred to a Langendorff perfusion rig. The hearts were perfused with 150 ml of recirculating buffer at a constant pressure of 80 mmHg. The perfusion buffer was a modified Krebs-Henseleit solution containing (in mM): 118 NaCl, 4.7 KCl, 1.2 $MgSO_4$, 2.25 $CaCl_2$, 0.5 Na_2EDTA, 11 glucose, 25 $NaHCO_3$, 1.2 KH_2PO_4 and 0.4 palmitate pre-bound to bovine serum albumin ((BSA), 3%), heated to 37 °C and gassed with mixture of 95% O_2 and 5% CO_2. Prior to perfusion, the iCa^{++} concentration of the perfusion

buffer was assessed using a portable blood gas and electrolyte analyser (EPOC, Epocal Inc., Ottawa, Canada), and adjusted to 1.8 mM.

Coronary flow was monitored continuously with an inline flow meter connected to a PowerLab 16/35 (ADInstruments, New Zealand). Cardiac function was continually monitored via a polyethylene balloon inserted into the left ventricular lumen of the heart. The balloon was filled with distilled water and inflated to give an EDP of 4-8 mmHg. The contraction of the left ventricle was measured via a pressure transducer connected to a PowerLab 16/25 (ADInstruments, New Zealand) and recorded at 2 kHz using Lab Chart Pro software (version 8, ADInstruments, New Zealand). Functional indices for each heart were derived from the LV pressure traces as described in figure 2.3. Left ventricular developed pressure (DP) was calculated as the difference between peak systolic pressure (PSP) and end diastolic pressure (EDP). The rate pressure product (RPP) was calculated as the product of heart rate and left ventricular developed pressure, expressed in terms of mmHg min^{-1}.

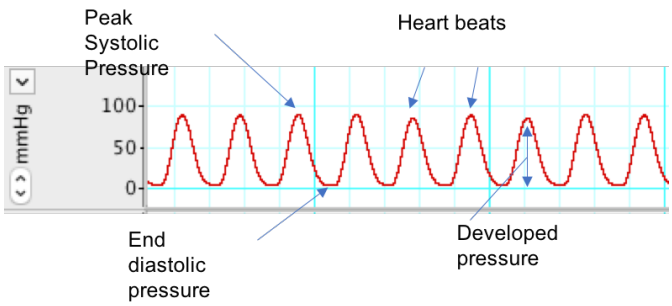


Fig. 2.3 Example pressure trace from a Langendorff perfused heart, showing left ventricular pressure (mmHg) over time.

Ischaemia reperfusion

The Langendorff perfusion procedure was manipulated to allow modelling of ischaemia reperfusion injury ex-vivo. Hearts were excised, cannulated, and perfused in Langendorff mode as described above. Following a 30 minutes

baseline period of perfusion, hearts were subjected to low-flow ischaemia, with coronary flow reduced to a rate of 0.5 ml/minute/g wet weight of tissue, controlled by a peristaltic pump (IPC-N, Ismatec, Switzerland). Following 30 minutes of low flow ischaemia, the restriction to coronary flow was removed and hearts were re perfused for 30 minutes at a constant pressure of 80 mmHg.

Modelling ischaemia reperfusion injury utilising a low flow model has several advantages over often used zero flow models. In patients there is clear evidence of the importance of collateral vessel blood flow during ischaemia, on the post ischaemic function of the heart (Sabia et al., 1992). As such, preclinical ex vivo animal models utilising low flow protocols (Cave et al., 2000) can better reflect the residual flow seen in patient hearts during ischaemia (Milavetz et al., 1998). Furthermore, use of a low flow model allows more relevant and externally valid investigation of metabolism during and following reperfusion (Zuurbier et al., 2020).

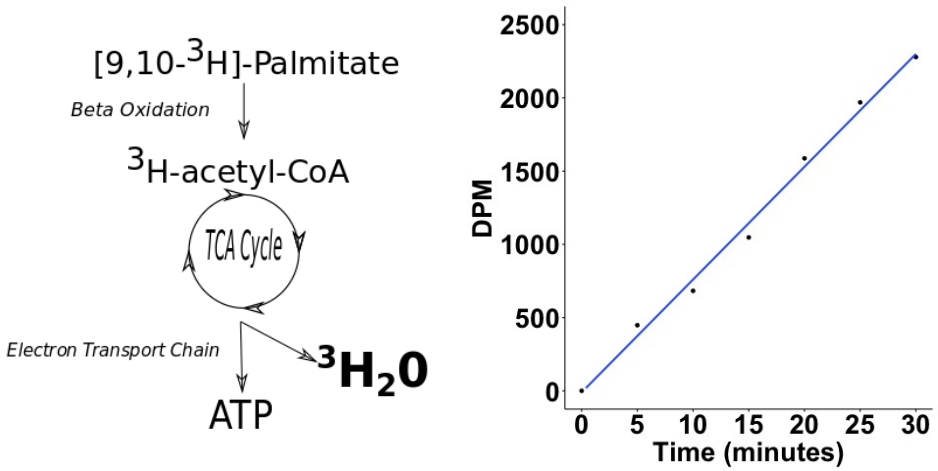
2.4.3 Measurement of metabolic flux in the isolated beating heart

The perfusion buffer for isolated Langendorff perfused hearts was spiked with ^{3}H radioisotope tracers in order to facilitate the measurement of metabolic fluxes. Techniques used were adaptations of those previously described for use with isolated working rat hearts (Lopaschuk and Barr, 1997).

2.4.4 Measurement of palmitate oxidation

Palmitate oxidation in perfused hearts was measured using [9, 10-^{3}H]-palmitate. Measurements of palmitate oxidation were made based on the principle that [9, 10-^{3}H]-palmitate will produce $^{3}H_2O$ upon oxidation, as described in figure 2.4.

Hearts were perfused as described, with 150 ml of recirculating buffer containing 20 μl [9, 10-^{3}H]-palmitate. Two 0.5 ml aliquots of recirculating buffer were sampled from the perfusion apparatus at 5 minute intervals throughout the perfusion procedure. Perfusate samples were processed with a modified Folch extraction (Lopaschuk and Barr, 1997). 1.88 ml of a chloroform:methanol mixture (1:2, v/v), 0.625 ml chloroform, and 0.625 ml 2 M KCL: 0.4 M HCl were added to each sample in turn, and mixed for 10 minutes on a blood tube rotator and centrifuged for 10 minutes at 2000 g. The top aqueous layer of the separated mixture was removed with a pasteur pipette and combined with 1 ml chloroform, 1 ml methanol 0.9 ml KCL: 0.4 M HCl. The second mixture was mixed for 15 minutes and centrifuged at 2000 g for 10 minutes. 0.5 ml of the aqueous phase of the second mixture was combined with 10 ml scintillation fluid and counted to determine ^3H_2O accumulation. The rate of palmitate oxidation in the heart was expressed as μmol/minute/g wet weight, calculated from the linear increase in ^3H_2O over time.



(a) Schematic representation of ^3H_2O production in the heart

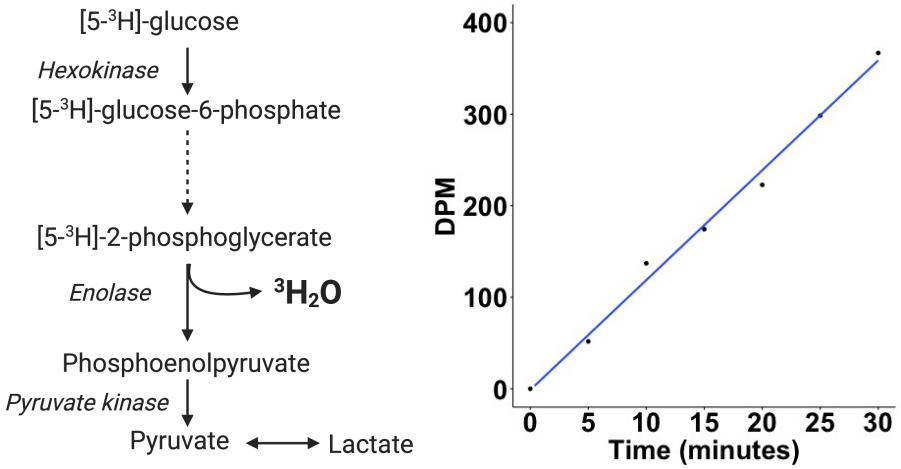
(b) Example of ^3H_2O accumulation over time in perfusate

Fig. 2.4 Method of fatty acid oxidation in the isolated Langendorff perfused heart. 2.4a Shows the process of ^3H_2O from [9, 10-3H]-palmitate oxidation. 2.4b shows an example of ^3H_2O accumulation over time in the perfusate. The rate of fatty acid oxidation is calculated from the gradient of the straight line.

2.4.5 Measurement of Glycolytic flux

Glycolytic flux was measured in perfused hearts using [5-^{3}H] glucose. Measurement of glycolytic flux was based on the principle that ^3H_2O is released by the conversion of 2-phosphoglycerate to phosphoenolpyruvate, catalysed by enolase, as described in figure 2.5.

Hearts were perfused as described, with 150 ml of recirculating buffer containing 20 μl [5-^{3}H] glucose (specific activity 15 Ci/mmol). Two 0.5 ml aliquots of recirculating buffer were sampled from the perfusion apparatus at 5 minute intervals throughout the perfusion procedure. Perfusate samples were processed as previously described (Lopaschuk and Barr, 1997). Dowex (1 x 4-200, anion exchange resin) was cleaned by washing in a solution of 1.25 M sodium hydroxide, 1.6 M boric acid. Glass screening columns were filled with the cleaned Dowex solution and washed with distilled water. A volume of 200 μl of perfusate sample was added to each column and allowed to flow through for 15 minutes and then the column washed with 8 x 200 μl volumes of water. 10 ml of scintillation cocktail was added to the flow through and liquid scintillation counting performed. The linear increase in ^3H_2O over time was used to calculate the rate of glycolytic flux, which was expressed as μmol/min/g wet weight (figure 2.5).



(a) Schematic representation of ^3H_2O production in the heart

(b) Example of ^3H_2O accumulation over time in perfusate

Fig. 2.5 Method of glycolytic flux measurement in the isolated Langendorff perfused heart. 2.5a Shows the process of ^3H_2O production from [5-^{3}] glucose. 2.5b shows an example of ^3H_2O accumulation over time in the perfusate. The rate of glycolytic flux is calculated from the gradient of the straight line.

2.4.6 Measurement of net lactate efflux

The net lactate efflux from perfused hearts was determined in the buffer samples taken for the measurement of glycolysis, described above. A 96-well plate based spectrophotometric assay was used to determine lactate concentrations in the buffer samples, based on previously published protocols (Lundholm et al., 1963). 50 μl of sample, blank, or standard (0-400 μM sodium l-lactate) were added to 150 μl of assay buffer (0.2 M Tris, 10 μM EDTA, 5% hydrazine hydrate, pH 9.5). The plate was read at 340 nm to determine baseline NADH absorbance. The conversion of NAD^+ to NADH was followed to determine lactate formation (reaction 1). Following the addition of lactate dehydrogenase and 30 minutes incubation at 30°C plates were measured again at 340 nm to determine the increase in NADH absorbance. The presence of hydrazine hydrate in the reaction buffer ensured that the reaction ran to completion (Lundholm et al., 1963). Perfusate lactate concentration was determined and the net lactate efflux for each heart expressed as μmol/min/g wet weight.

$$\text{Lactate} + \text{NAD}^{+} \xrightarrow{\text{Lactate Dehydrogenase}} \text{Pyruvate} + \text{NADH} \qquad \{1\}$$

2.5 Western blotting

2.5.1 Protein Extraction

Whole heart tissue was crushed under liquid nitrogen in a modified metal mortar and pestle device (Biomedical Engineering Unit, Nottingham University, UK). Around 30 mg of heart tissue was homogenised for one minute in an ice cold RIPA buffer containing: 150 mM NaCl, 25 mM Tris-HCl, 1% Triton-X 100, 1% Sodium deoxycholate, 0.1% SDS, and a protease inhibitor cocktail (cOmplete, Mini, EDTA-free Protease Inhibitor Cocktail, Roche, UK). The solution was centrifuged at 4 °C for 10 minutes at 13,000 g. The supernatant was removed and stored at -80 °C.

2.5.2 Protein Quantification

Protein concentrations were quantified using a Pierce BCA Protein Assay Kit (Thermo Scientific, UK), according to manufacturers instructions. An aliquot of each protein sample was diluted with distilled water and 10 μl added to 200 μl working reagent on a 96 well assay plate. A standard curve of was produced by adding 10 μl of known protein standards to 200 μl working reagent. The plate was mixed and incubated at 37 °C for 30 minutes, cooled to room temperature and absorbance measured at 562 nm using a spectrophotometric microplate reader (Sunrise, Tecan, Switzerland).

2.5.3 Electrophoresis and Protein Transfer

Protein concentration was normalised between lysate samples, and an aliquot of each sample mixed with 6x Laemmli loading buffer containing: 12% SDS, 0.06% bromophenol blue, 60 mM Tris-HCl pH 6.8, 47% glycerol, and 9.3% DTT. Protein samples were denatured by boiling for 5 minutes at 95 °C. Equal quantities of protein were loaded to 10% polyacrylamide gels and run for 70 minutes at 100 V. Subsequently gels were placed on top of a nitrocellulose membrane inside a blotting cassette (Bio-RAD Laboratories, USA). Protein was transferred from gel to nitrocellulose in an ice cooled buffer containing: 25 mM Tris, 192 mM glycine, and 20% methanol at 100 V for one hour.

2.5.4 Antibody Detection of Proteins

Following protein transfer, membranes were stained with Ponceau-S stain to ensure successful and equal protein transfer. Membranes were washed for 5 minutes in Tris buffered saline-Tween (TBS-T; 50 mM Tris, 150 mM NaCl, 0.1% Tween 20 (Sigma, UK)). Membranes were then blocked for one hour at room temperature in TBS-T containing 5% skimmed milk powder or BSA, depending upon the protein being assessed. Primary antibodies against the protein of interest were diluted in 5 ml of TBS-T containing 5% skimmed milk powder or BSA according to manufactures directions. Membranes were incubated in the primary antibody solution overnight (~16 hours). Following primary antibody incubation, membranes were washed for 6 x 5 minutes in TBS-T. Horse radish peroxidase (HRP) conjugated secondary antibodies, were diluted in TBS-T containing 5% skimmed milk powder (Marvel, UK) or BSA (Lampire Biological Laboratories, USA). Membranes were incubated in secondary antibody solution for 1 hour at room temperature with constant agitation, then washed for 6 x 5 minutes in TBS-T.

Blots were incubated with enhanced chemiluminescence (ECL) detection solution (Amersham, GE Healthcare, UK) and a digital image obtained using a chemiluminescent camera (LAS-3000 Mini Fujifilm; Japan), with exposure times dependent upon the protein being examined.

Protein expression was quantified with Image J software (NIH, USA), using standard densitometry. The expression of proteins of interest was normalised to a loading control protein, allowing for comparisons to be made between experimental conditions.

2.6 Mitochondrial copy number quantification

Mitochondrial copy number was quantified in tissues using real time PCR according to the protocol of Quiros et al. (2017). This allows for the comparison of mitochondrial to nuclear DNA content, as a marker of mitochondrial content in a given tissue.

Total DNA extraction

Tissues samples were initially crushed under liquid nitrogen. Total DNA extraction was performed using an EZNA DNA isolation kit (Omega Bio-Tek Inc., Norcross, GA USA), according to manufacturers instructions. 20-30 mg of tissue was suspended in 200 μl of lysis buffer containing proteinase K, and incubated overnight at 55 °C, after which samples were treated with RNase A (Thermo Scientific, Loughborough, UK). Subsequently, 220 μl of BL buffer was added to the tissue lysate and incubated at 70 °C for 10 minutes. 220 μl of 100% Ethanol were added and the whole lysate added to a Hi.Bind DNA mini column, and centrifuged for 1 minute at 20,000 g for 1 minute and the flow through discarded. 500 μl of HBC buffer was added to the column, spun at 20,000 g for 30 seconds and the flow through discarded. The column was washed twice and dried. Total

DNA was subsequently eluted in 200 μl of elution buffer, heated to 70 °C. The concentration of DNA in each sample was quantified using a NanoDrop One (ThermoFischer Scientific) at 260 nm.

Real time PCR

DNA samples were normalised to a concentration of 5 ng/μl and real time PCR was performed for two mitochondrial (16S rRNA & ND1), and one nuclear (HK2) targets. Primer sequences can be found in table 2.2, and the relative position of the primers in the mitochondrial genome seen in figure 2.6. Both the ND1 and 16S primers cover regions of mitochondrial DNA that is stable and not prone to deletions (Tanhauser and Laipis, 1995). The HK2 primer pair covers an intron region, therefore limiting the influence of RNA contamination. Primer efficiency was initially assessed using a 12 point standard curve and found to be equivalent, at approximately 100% in each primer pair.

Each PCR reaction was performed in triplicate in a volume of 20 μl containing: 10 μl GoTaq qPCR SYBR green master mix (Promega, Maddison, Wisconsin, USA), 10 ng DNA, 1 μM forward primer, 1 μM reverse primer, and 300 nM CXR reference dye. The PCR reaction was performed on a 7900 ht PCR machine (Applied Biosystems) and consisted of initial step of 5 minutes at 95 °C, 45 cycles of 10 seconds at 95 °C, 10 seconds at 60 °C, 20 seconds at 72 °C, followed by dissociation curve analysis. A no template control (water) reaction was included in triplicate for each target. Mitochondrial DNA content was normalised to nuclear using the $2^{-\Delta\Delta Ct}$ (Livak and Schmittgen, 2001). The inclusion of template free controls as well as the inclusion of dissociation curves demonstrated that each primer pair generated a single product, with the absence of primer dimers.

Table 2.2 Primer pairs for analysis of mitochondrial copy number

Target	Primer Sequence
HK2	Forward 5'-GCCAGCCTCTCCTGATTTTAGTGT-3'
	Reverse 5'-GGGAACACAAAAGACCTCTTCTGG-3'
16s rRNA	Forward 5'-CCGCAAGGGAAAGATGAAAGAC-3'
	Reverse 5'-TCGTTTGGTTTCGGGGTTTC-3'
ND1	Forward 5'-CTAGCAGAAACAAACCGGGC-3'
	Reverse 5'-CCGGCTGCGTATTCTACGTT-3'

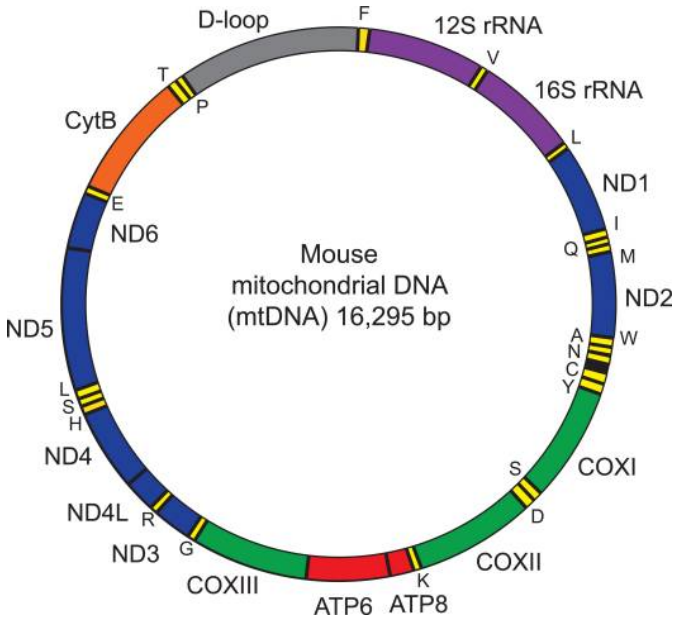


Fig. 2.6 Mouse mitochondrial DNA, from Quiros et al. (2017). The mitochondrial DNA is comprised of an inner light strand (L-strand) and an outer heavy strand (H strand) each encoding different genes. Genes are annotated in a position to reflect where they are encoded. Colours reflect different gene categories: rRNAs (purple), tRNAs (yellow), proteins that constitute oxidative phosphorylation complexes I (blue), II (green), IV (orange), V (red).

2.7 Enzyme activity assays

Enzyme activities were assessed in frozen tissue samples.

2.7.1 Citrate Synthase

Citrate synthase activity was assessed in heart tissue according to the method of Srere (1969). The assay is based upon the formation of citrate from Acetyl-CoA and oxaloacetate (reaction 2). The rate of the reaction can be monitored by assessing the rate of the colorimetric reaction forming 5-thio-2-nitrobenzoic acid (TNB) (reaction 3).

$$\mathrm{Acetyl\,CoA} + \mathrm{Oxaloacetate} \xrightarrow{\mathrm{Citrate\,Synthase}} \mathrm{Citrate} + \mathrm{CoA{-}SH} + \mathrm{H^+} + \mathrm{H_2O} \quad \{2\}$$

$$\mathrm{CoA{-}SH} + \mathrm{DTNB} \longrightarrow \mathrm{TNB} + \mathrm{CoA{-}S{-}S{-}TNB} \quad \{3\}$$

Tissue (10-15 mg) was homogenised in 1 ml of an ice cold buffer (100 mM imidazole, 1 mM EGTA, 5 mM $MgCl_26H_2O$, and 0.1% Triton X-100). The homogenate was centrifuged at 500 g for 10 minutes at 4 °C and the supernatant saved. The reaction was performed in a 1 ml cuvette, containing: 100 μl assay buffer (1M Tris-HCL (ph8.1), 1 mM DTNB (5,5-dithio-bis(2- nitrobenzoic acid)), 50 μl 10 mM Acetyl-CoA, 750 μl H_2O and tissue homogenate. The reaction was performed at 30 °C and initiated by the addition of 50 μl 10 mM oxaloacetate. Absorption was measured at 412 nm for 2 minutes, with one reading taken per second. Citrate synthase activity was calculated from the first 30 second linear period of the reaction, utilising the molar absorption coefficient for TNB at 412 nm of 13.6 $.mM^{-1}cm^{-1}$. An example of the change in absorption over the course of the measurement can be seen in figure 2.7. The protein concentration was

measured in the homogenate using the Pierce BCA assay (described above), and the rate of Citrate synthase activity expressed relative to protein (μmol.min^{-1}.mg protein^{-1}).

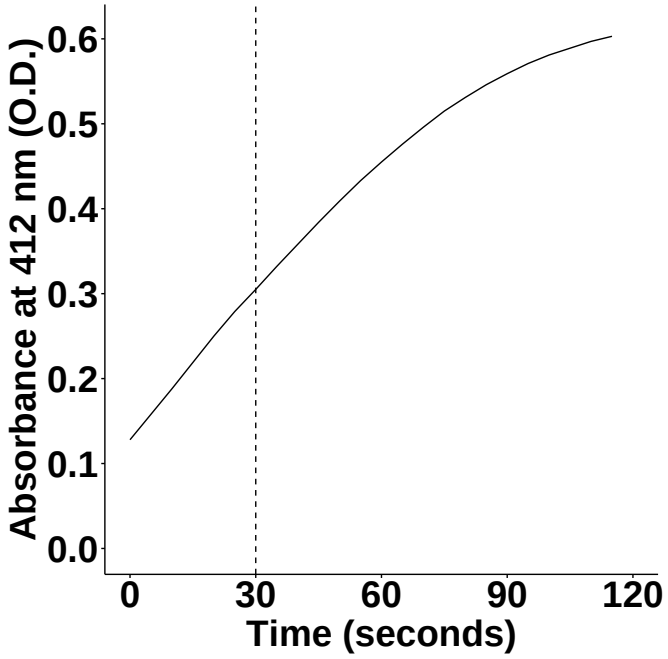


Fig. 2.7 Example plot of absorbance at 412 nm during a citrate synthase activity assay The activity of citrate synthase in the sample was calculated from the linear period of absorbance change during the first 30 seconds following oxaloacetate addition. Rates were normalised to sample protein content.

2.8 Tissue metabolites

Metabolite concentrations were determined in snap frozen tissue samples. Tissue samples were freeze dried and then subsequently powdered at room temperature using fine forceps and a scalpel. Any visible connective tissue was removed, thus ensuring metabolites were measured in a pure muscle sample.

2.8.1 Perchloric acid metabolite extract

Metabolites were extracted from powdered tissue with perchloric acid (PCA) using the method of Harris et al. (1974). To every 12.5 mg of freeze dried powdered tissue, 1 ml of 0.5 M PCA, 1 mM EDTA solution was added. The mixture was incubated on ice for 10 minutes, with periodic vortex mixing. Samples were then centrifuged at 2000 g for 3 minutes, at 4 °C. The supernatant was recovered and neutralised by the addition of one quarter volume of 2.2 M $KHCO_3$. The mixture was again centrifuged at 2000 g for 3 minutes, at 4 °C, the supernatant was removed, and stored at -80 °C until subsequent analysis. In order to calculate metabolite concentrations relative to the dry mass of tissue in the PCA extract, the extraction factor was calculated as described in equation 2.1.

$$\text{Extraction factor} = \frac{V_{PCA}(V_{supt} + V_{KHCO3})}{V_{supt} \text{ x Tissue weight}} \tag{2.1}$$

Where:

V_{PCA} = the initial volume of PCA added (μl)

V_{supt} = the volume of the recovered supernatant (μl)

V_{KHCO3} = the volume of $KHCO_3$ added (μl)

Tissue weight = the mass of powdered dry tissue (mg).

2.8.2 Glucose-6-phosphate, Phosphocreatine, and ATP

Glucose-6-phosphate, PCr, and ATP were measured sequentially using a spectrophotometric assay (Harris et al., 1974) utilising the PCA tissue extract. The three-step assay followed changes of NADPH absorbance, measured at 340 nm using a spectrophotometer (Spectra Max 190, Molecular Devices Ltd, Wokingham, UK). On a 96 well plate 25 μl of PCA tissue extract, standard, or blank

were added to 225 μl of triethanolamine hydrochloride buffer (100 mM, pH 7.5) containing 40 μM ADP, 5 mM glucose and 1 mM $NADP^+$.

The plate was initially mixed and incubated at 30 °C for five minutes and absorbance measured at 340 nm (A1). 4 μl of glucose-6-phosphate dehydrogenase (0.25 units) were added to each well, the plate mixed and incubated at 30 °C for 20 minutes and the absorbance read at 340 nm (A2 (reaction 4)).

$$\text{G}-6\text{-P} + \text{NAD}^+ \xrightarrow{\text{G}-6\text{-P dehydrogenase}} 6\text{-P}-\text{gluconolactone} + \text{NADPH} \qquad \{4\}$$

4 μl of hexokinase (1.5 units) were added to each well, the plate mixed and incubated at 30 °C for 20 minutes and the absorbance read at 340 nm (A3 (reaction 5)).

$$\text{ATP} + \text{glucose} \xrightarrow{\text{Hexokinase}} \text{ADP} + \text{glucose}-6\text{-phosphate} \qquad \{5\}$$

4 μl of creatine kinase (1.3 units, dissolved in 0.5% NaHCO3 + 0.05% BSA) were added to each well, the plate mixed and incubated at 30 °C for 20 minutes and the absorbance read at 340 nm (A4 (reaction 6)).

$$\text{PCr} + \text{ADP} \xrightarrow{\text{Creatine kinase}} \text{Cr} + \text{ATP} \qquad \{6\}$$

The metabolite concentrations were calculated based on equations 2.2,2.3, and 2.4, and expressed in terms of μmol / g dm (grams dry mass of tissue).

$$\text{G6P } (\mu\text{mol/ g dm}) = \frac{[(V2(A2sample - A2blank)]x[V1(A1sample - A1blank)]xEF}{SVx6.22} \qquad (2.2)$$

$$\text{ATP } (\mu\text{mol/ g dm}) = \frac{[(V3(A3sample - A3blank)]x[V2(A2sample - A2blank)]xEF}{SVx6.22} \tag{2.3}$$

$$\text{PCr } (\mu\text{mol/ g dm}) = \frac{[(V4(A4sample - A4blank)]x[V3(A3sample - A3blank)]xEF}{SVx6.22} \tag{2.4}$$

Where:

V1 = initial reaction volume (μl)

V2 = volume following glucose-6-phosphate dehydrogenase addition (μl)

V3 = volume following hexokinase addition (μl)

V4 = volume following creatine kinase addition (μl)

A1 = initial absorbance of sample (or blank) at 340 nm

A2 = absorbance of sample (or blank) at 340 nm

A3 = absorbance of sample (or blank) at 340 nm

A4 = absorbance of sample (or blank) at 340 nm

EF = PCA extraction factor (equation 2.1)

SV = the initial volume of PCA extract added (μl)

6.22 = molar extinction coefficient of NADPH at 340 nm ($cm^2.\mu mol^{-1}$).

2.8.3 Pyruvate, ADP, and AMP

Pyruvate, ADP, and AMP were measured sequentially in a spectrophotometric assay using the PCA tissue extract (Harris et al., 1974). The assay follows the change of NADH absorbance at 340 nm in a series of three reactions. Two hundred μl of PCA metabolite extract, standard, or blank was added to 50 μl

triethanolamine hydrochloride buffer (100 mM pH 7.5) containing 40 μM ADP, 5 mM glucose, 1 mM $NADP^+$ on a 96 well plate.

The plate was initially mixed and incubated at 30 °C for five minutes and absorbance measured at 340 nm (A1). 4 μl of lactate dehydrogenase (3 units) were added to each well, the plate mixed and incubated at 30 °C for 20 minutes and absorbance read again at 340 nm (A2,(reaction 7)).

$$\text{Pyruvate} + \text{NADH} \xrightarrow{\text{Lactate dehydrogenase}} \text{Lactate} + \text{NAD}^+ \qquad \{7\}$$

4 μl of pyruvate kinase (0.34 units) were added to each well and the plate mixed and incubated at 30 °C for 20 minutes and absorbance measured at 340 nm (A3 (reaction 8)).

$$\text{ADP} + \text{PEP} \xrightarrow{\text{Pyruvate Kinase}} \text{ATP} + \text{Pyruvate} \qquad \{8\}$$

Finally, 4 μl of myokinase (0.8 units) were added to each well, the plate shaken and incubated at 30 °C for 20 minutes and absorbance measured at 340 nm (A4 (reaction 9)).

$$\frac{1}{2}\text{AMP} + \frac{1}{2}\text{ATP} \xrightarrow{\text{Myokinase}} \text{ADP} \qquad \{9\}$$

The concentration of metabolites were calculated according to equations 2.5, 2.6, and 2.7 and expressed as μmol/ g dm.

$$\text{Pyruvate } (\mu\text{mol/ g dm}) = \frac{[(V2(A2sample - A2blank)]x[V1(A1sample - A1blank)]xEF}{SVx6.22} \qquad (2.5)$$

$$\text{ADP } (\mu\text{mol/ g dm}) = \frac{[(V3(A3sample - A3blank)]x[V2(A2sample - A2blank)]xEF}{SVx6.22} \tag{2.6}$$

$$\text{AMP } (\mu\text{mol/ g dm}) = \frac{[(V4(A4sample - A4blank)]x[V3(A3sample - A3blank)]xEF}{SVx6.22} \tag{2.7}$$

Where:

V1 = initial reaction volume (μl)

V2 = volume following lactate dehydrogenase addition (μl)

V3 = volume following pyruvate kinase addition (μl)

V4 = volume following myokinase addition (μl)

A1 = initial absorbance of sample (or blank) at 340 nm

A2 = absorbance of sample (or blank) at 340 nm

A3 = absorbance of sample (or blank) at 340 nm

A4 = absorbance of sample (or blank) at 340 nm

EF = PCA extraction factor (equation 2.1)

SV = the initial volume of PCA extract added (μl)

6.22 = molar extinction coefficient of NADPH at 340 nm ($cm^2.\mu mol^{-1}$).

Total adenine nucleotide (TAN) pool and energy charge

The total adenine nucleotide (TAN) pool was calculated as the sum of ATP, ADP, and AMP concentrations. The energy charge of the heart was calculated according to the method of Atkinson and Walton (1967), described in equation 2.8.

$$\text{Energy charge} = \frac{[ATP] + [\frac{1}{2}ADP]}{[ATP] + [ADP] + [AMP]} \tag{2.8}$$

2.8.4 Free creatine

Free creatine content was measured in PCA metabolite extract utilising the previously described spectrophotometric method (Harris et al., 1974). On a 96 well plate 20 μl of sample, standard, or blank were added to 300 μl of 100 mM glycine (pH 9.1) containing 30 mM KCL, 1.5 mM ATP, 1 mM PEP, 0.161 mM NADH, 2.5 units PK and 1.25 units lactate dehydrogenase (LDH). The plate was incubated at 30 °C for five minutes and the baseline absorbance read at 340 nm. 10 μl creatine kinase (dissolved 10 mg/ml in 0.5% $NaHCO_3$, 0.05% BSA) was added to each well to initiate the coupled reactions described below (reactions 10,11,12). The plate was mixed and incubated at 30 °C for 30 minutes and the absorbance read again at 340 nm.

$$\text{Cr} + \text{ATP} \xrightarrow{\text{Creatine kinase}} \text{PCr} + \text{ADP} \tag{10}$$

$$\text{ADP} + \text{PEP} \xrightarrow{\text{Pyruvate Kinase}} \text{ATP} + \text{Pyruvate} \tag{11}$$

$$\text{Pyruvate} + \text{NADH} \xrightarrow{\text{Lactate dehydrogenase}} \text{Lactate} + \text{NAD}^{+} \tag{12}$$

Free creatine was calculated as described in equation (2.9) and expressed in terms of μmol/ g dm. The total creatine content was calculated as the sum of free creatine and phosphocreatine, expressed in terms of μmol/ g dm.

$$\text{Free Creatine } (\mu\text{mol/ g dm}) = \frac{[(V2(A2sample - A2blank)]x[V1(A1sample - A1blank)]xEF}{SVx6.22} \quad (2.9)$$

Where:

V1 = initial reaction volume (μl)

V2 = volume following creatine kinase addition (μl)

A1 = initial absorbance of sample (or blank) at 340 nm

A2 = absorbance of sample (or blank) at 340 nm

EF = PCA extraction factor (equation 2.1)

SV = the initial volume of PCA extract added (μl)

6.22 = molar extinction coefficient of NADH at 340 nm ($cm^2.\mu mol^{-1}$).

2.8.5 Glycogen

Tissue glycogen content was determined using a previously established protocol with slight modification (Harris et al., 1974). One to two mg of freeze dried, powdered tissue was weighed, dissolved in 100 μl of 100 mM NaOH and incubated at 80 °C for 10 minutes. The solution was neutralised by the addition of 400 μl neutralisation buffer (1 part 100 mM HCl: 2 parts citrate buffer (200 mM citric acid + 200 mM Na_2HPO_4). Tissue glycogen was hydrolysed to glycosyl units via the addition of 15 μl Amyloglucosidase (AGDase, 200 mg/ml dissolved in citrate buffer). Samples were incubated at room temperature for 1 hour and centrifuged at 20,000 g for 2 minutes. The resultant supernatant was taken for analysis. The extraction factor of the sample was calculated as described in equation 2.10.

$$\text{Extraction factor} = \frac{\text{Vol}_{\text{NaOH}} + \text{Vol}_{\text{HCL:Citrate}} + \text{Volume}_{\text{AGDase}}}{\text{Tissue weight}} \quad (2.10)$$

Where:

V_{NaOH} = the initial volume of NaOH added (μl)

$V_{HCL:Citrate}$ = the volume of HCl:Citrate buffer added (μl)

V_{AGDase} = the volume of AGDase added (μl)

Tissue weight = the mass of powdered dry tissue (mg).

Samples were assayed in 96 well reaction plates. 25 μl of either sample, blank, or standard were added to 250 μl of assay buffer (100 mM triethanolamine hydrochloride, 40 mM KOH, 30 mM magnesium acetate tetrahydrate, 1 mM EDTA, 0.75 mM ATP, 1 mM DTT, 1 NAD, pH 8.2). Absorbance was measured at 366 nm (A1), and subsequently Glucose-6-phosphate-dehydrogenase and hexokinase (4 μl total volume) were added to each well and the plate incubated at room temperature for 20 minutes. The assay is based upon tracking the formation of NADH from the derived glycosyl units as described in reactions 13 and 14.

$$\text{ATP} + \text{Glucose} \xrightarrow{\text{Hexokinase}} \text{ADP} + \text{Glucose}-\text{6-P} \quad \{13\}$$

$$\text{G}-\text{6-P} + \text{NAD}^{+} \xrightarrow{\text{G}-\text{6-P dehydrogenase}} \text{6-P}-\text{gluconolactone} + \text{NADH} \quad \{14\}$$

Absorbance was measured again at 366 nm (A2) and the glycogen content of each sample, expressed in μmol/ g dry mass, calculated as described in equation 2.11.

$$\text{Glycosyl units } (\mu\text{mol/ g dm}) = \frac{[(V2(A2sample - A2blank)]x[V1(A1sample - A1blank)]xEF}{SVx3.4} \quad (2.11)$$

Where:

V1 is the initial reaction volume (μl)

V2 is the reaction volume following the addition of enzymes (μl)

A1 is the initial measured absorbance at 340 nm

A2 is the absorbance following the addition of enzymes

EF represents the extraction factor calculated in equation 2.10

SV is the sample volume in (μl)

3.4 represents the millimolar extinction coefficient of NADH at 366 nm (cm^2/μmol).

2.8.6 Tissue lactate

Tissue lactate concentration was determined in the PCA extract, utilising the method described above, based on equation 1. The lactate concentration was normalised to the PCA extraction factor, and tissue lactate expressed as μmol/g dm.

2.9 Cell culture

In order to study the effects of FIH1 inhibition on acute signalling events cell culture models were employed.

2.9.1 Cell lines utilised

HeLa cells with a 33 base pair HiBiT tag inserted into the C terminus of the HIF-1α gene were obtained from Promega. The generation of this cell line has

been described by Schwinn et al. (2018). The HiBiT tag on the C terminus of HIF-1α of these cells facilitates the monitoring of HIF-1α protein abundance when combined with LgBiT as a full length NanoLuciferase is formed (Schwinn et al., 2018). As such, these cells can be readily utilised to monitor HIF-1α induction. HeLa cells were used up to passage 12.

Human umbilical vein endothelial cells (HUVECs) were obtained from a single male donor (COO35C; Thermo Fischer Scientific, UK). HUVECs were used for experiments between passages 3 and 6.

Human embryonic kidney 293T cells (HEK293T) were obtained from a female donor (CRL-3216, ATTC, Virginia, USA). HEK293T cells were used up to passage 30.

2.9.2 General cell culture conditions

Both HeLa and HEK293T cells were routinely cultured in Dulbecco's Modified Eagle's Medium (DMEM, D6429 Sigma,UK), containing 2 mM L-glutamine and supplemented with 10% foetal bovine serum (FBS, F2442, Sigma, UK). HUVECS were cultured in M200 (M200500, Gibco, UK) + 2% Gibco Large Vessel Endothelial Supplement (LVES) (A1460801, Gibco, UK). All cell lines were routinely cultured in T75 culture vessels. Passaging of cells was performed when they were 70-80% confluent. Cells were washed with phosphate buffered saline (PBS), and detached from the culture vessel using trypsin-EDTA (0.5 g/L trypsin, 0.2 g/L EDTA). Following dissociation, trypsin was neutralised by the addition of growth media in a 10 fold excess, and cells removed and pelleted by centrifugation at 150 g for 5 minutes. Cell pellets were resuspended in growth media, and seeded into new culture vessels at the desired density.

2.9.3 Hypoxic Cell culture

To study cell function in hypoxia cell cultures were incubated in an hypoxic glove box tissue culture incubator (O_2 Control InVitro Glove Box, Coy Lab Products, Grass Lake, MI, USA). This allowed for the oxygen concentration in the air that the cultures were incubated in to be accurately manipulated. The air within the chamber was diluted with nitrogen via a continuous gas sensor-flow control unit. Additionally, CO_2 was controlled in the same manner and maintained at 5%. Within the glove box humidified cabinets contained the culture vessels and the whole glove box was maintained at 37 °C. The sleeved working space in the glove box, and ability to introduce or remove items through an air purged port, allowed samples to be taken or processed within the hypoxic environment without any fluctuations in the oxygen concentration. Furthermore, when experiments required lysis of hypoxic cells this was performed within the hypoxia chamber to ensure that there was no reoxygenation of cultures. This is particularly relevant when determining HIF-1α expression, due to its short half life upon reoxygenation (Schwinn et al., 2018).

2.10 Hypoxia response element (HRE) reporter assay

In order to study HIF-1α transcriptional activity in cultured cells a luciferase reporter assay was employed. The HRE-luciferase plasmid was a gift from Navdeep Chandel (Addgene plasmid # 26731 ; http://n2t.net/addgene:26731 ; RRID:Addgene_26731) and was originally described by Emerling et al. (2008). The plasmid contains a firefly luciferase enzyme under the control of a promoter containing three hypoxia response elements, cloned from the phosphoglycerate kinase 1 gene, in a pGL2 vector backbone (figure 2.8).

The plasmid was received as a bacterial stab and streaked out onto an agar plate containing 100 µg/ml ampicillin. Following overnight growth at 37 °C, single bacterial colonies were picked from the plate with a sterile pipette tip, and grown in 10 ml of LB broth (Sigma), containing 100 µg/ml ampicillin in a sterile universal tube for 8 hours with orbital shaking. The resultant bacterial growth was sub-cultured in 200 ml of LB broth, containing 100 µg/ml ampicillin, and grown overnight at 37 °C with orbital shaking.

Plasmid DNA was extracted using the Promega PureYield Plasmid Maxiprep System (Promega, Wisconsin, USA), according to the manufacturer's instructions. Briefly, 200 ml of bacterial culture was subjected to centrifugation at 5,000 g for 10 minutes to pellet the bacterial cells. The cell pellet was resuspended in 12 ml of resuspension buffer by vortex mixing. Twelve ml of cell lysis solution was added, and the solution mixed by inversion and incubated at room temperature for 3 minutes. Following this, 12 ml of neutralization solution was added and mixed by inverting 15 times before centrifugation for 20 minutes 14,000 x g.

The pure yield clearing and binding columns were assembled together and attached to a vacuum manifold. The bacterial lysate was added in two successive aliquots to the column and the vacuum released once all the lysate had cleared the column. The clearing column was removed and discarded, and 5 ml of endotoxin removal wash solution added to the binding column and vacuum reapplied. The column was then washed with 20 ml of wash solution and dried completely by maintaining the vacuum for a further five minutes following the flow through of the wash solution. For elution of the plasmid DNA, the binding column was placed over a 1.5 ml tube, using an elution connector and 1.5 ml of nuclease water added and left to saturate the membrane for 5 minutes, before elution via vacuum.

The concentration and quality of the resultant plasmid DNA was assessed using a NanoDrop spectrophotometer. The DNA concentration determined from the absorbance at 260 nm and the ratio of absorbance at 260 nm to that at

280 nm used as a marker of DNA quality, with ~1.8 considered pure plasmid DNA. To validate the prepared plasmid DNA, aliquots were sequenced by the University of Nottingham sequencing service, using the forward primer 5'-GTCCGAGGTCCACTTCGCATATTAAG. Sequencing results were aligned to the reference sequence using NCBI blast.

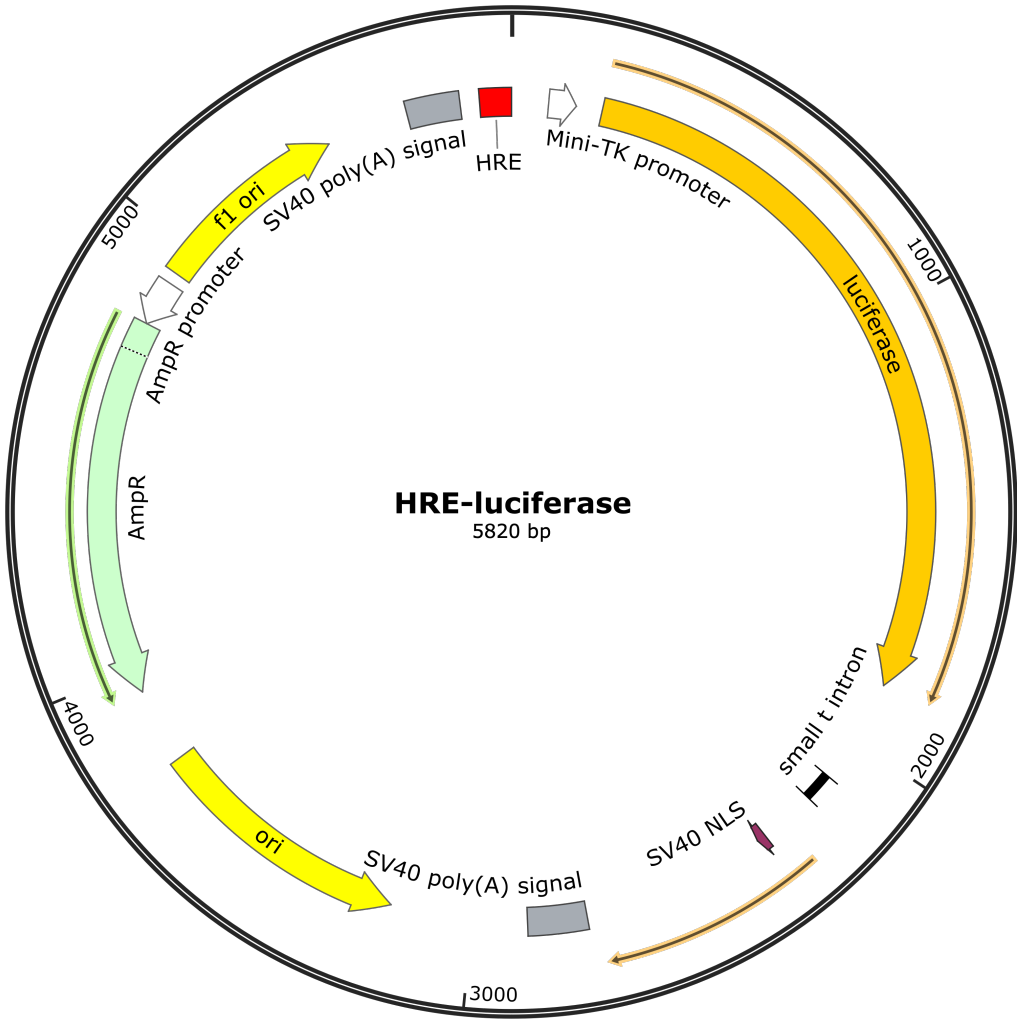


Fig. 2.8 Map of hypoxia response element (HRE) luciferase plasmid. HRE (red) denotes 3 x hypoxia response element sequences, cloned from PGK-1, upstream of firefly luciferase. Mini-TK promoter - minimal herpes simplex virus (HSV) thymidine kinase promoter, small t intron - SV40 (simian virus 40) small t antigen intron, SV40 NLS - nuclear localization signal of SV40 (simian virus 40) large T antigen, SV40 poly(A) signal - SV40 polyadenylation signal, ori - high-copy-number ColE1/pMB1/pBR322/pUC origin of replication, AmpR - ampicillin resistance gene β-lactamase, AmpR promoter - ampicillin resistance gene promoter, f1 ori - f1 bacteriophage origin of replication, SV40 poly(A) signal - SV40 polyadenylation signal.

2.10.1 Transfection of HRE reporter

Transient transfection of cells was performed using FuGENE HD reagent (Promega, Wisconsin, USA). Cells were washed trypsinised from growth vessels and seeded in 6 well plates at a concentration of 1 x10^5/well in 2 ml of DMEM with 10% FBS. Following approximately 8 hours incubation to allow cell attachment, transfection was performed. In the transfection mixture, FuGENE HD reagent was used at a ratio of 3:1 (μl reagent: μg DNA), all diluted in Opti-MEM (ThermoFischer Scientific, Loughborough, UK) to a final volume of 100 μl. The transfection mixture was incubated at room temperature for 5 minutes, then 100 μl, containing 0.5 μg of DNA added to each well of the 6 well plate.

Following 16 hours incubation with the transfection mixture, cells were washed and removed from 6-well plates with trypsin-EDTA, pooled, and cells counted. Transfected cells were then plated into white 96-well plates (655098, Greiner BioOne, Kremmunster, Austria) at a density of 10 x 10^3 cells per well and allowed to attach for 6 hours. Subsequently media was replaced and treatments begun.

2.10.2 Measurement of HRE-Luciferase activity

Following treatments cells were supplemented with 500 μM D-Luciferin (APExBio, Houston, Texas, USA) and allowed to equilibrate for five minutes. Luminescence was then measured using a TopCount platereader (Perkin Elmer, UK), with an adhesive white plate back on the bottom of plates to avoid signal loss. For each experiment data were normalised to the values of the normoxic control condition, and expressed as fold increase in HRE signalling.

2.11 CRISPR Cas9 HiBiT protein tagging

In order to utilise NanoBit split luciferase techniques (Dixon et al., 2016) to determine VEGF-A protein expression, CRISPR techniques were employed to append the HiBiT sequence to desired locations at the 3' end of the VEGF-A gene via homology directed repair (HDR).

2.11.1 Design of CRISPR components

CRISPR components were designed according to the protocol of Ran et al. (2013). The coding sequence, complete with the 3'untranslated region, for the VEGF-A gene was exported from the human genome 38 database (https://genome.ucsc.edu). Appropriate protospacer adjacent motif (PAM) sites immediately to the 5'of the stop codons for exon 8a and 8b were located and guide RNA (gRNA) sequences generated using the CRISPOR program (http://crispor.tefor.net; Concordet and Haeussler (2018)). Single-stranded donor oligonucleotide (ssODN) repair templates were designed to have approximately 60-80 nucleotide homology arms to both the 5'and the 3'of the PAM site, with the inclusion of the 33 nucleotides encoding the HiBiT sequence immediately to the 5'of the stop codon. Additionally, silent mutations of the PAM sites were introduced into the ssODN to avoid repeat cutting of edited DNA. Sequences of gRNAs and ssODN are shown in AppendixA, table A.1. All gRNAs and ssODNs were custom synthesised to order (IDT; Coralville, Iowa; USA)

2.11.2 Assessment of suitability of selected CRISPR editing sites

In order to determine the suitability of the selected sites for CRISPR mediated gene editing, genomic DNA was extracted from HUVECs (as described in 2.6).

Genomic DNA was amplified via PCR, utilising the primers in table 2.3, which target a 399 base pair (bp) region of the VEGF-A gene, including the desired editing sites. Three 50 μl PCR reactions were pooled and purified using the Wizard SV Gel and PCR clean-up system (Promega, Maddison, Wisconsin, USA), and eluted in 50 μl nuclease free water. The purified PCR product was sequenced by the University of Nottingham sequencing service, utilising the same primers as for the PCR reaction and aligned to the reference genome using NCBI blast. The sequence was assessed for any polymorphisms in the PAM sites that would effect CRISPR editing efficiency.

Table 2.3 Primers used for HUVEC VEGF-A exon eight amplification and sequencing

Primer	Sequence
Forward	5'-ACCCCAGCCTTTGTTTTCCA-3'
Reverse	5'-GTGGGTGGGTGTGTCTACAG-3'

2.11.3 Preparation of Ribonucleoprotein complexes

Ribonucleoprotein (RNP) complexes were formed between desired gRNA, generic trans activating CRISPR RNA (tracrRNA; Alt-R® CRISPR-Cas9 tracrRNA, IDT; Coralville, Iowa; USA) and engineered Cas9 nuclease (Alt-R® S.p. Cas9 Nuclease V3, IDT, Coralville, Iowa; USA). Initially, 5 μl of tracrRNA (100 μM) was combined with 5 μl of gRNA (100 μM) and heated to 95 °C for five minutes, then allowed to cool to room temperature, over a period of 15 minutes. RNP complexes were aliquoted and stored at -20 °C until required.

RNP complexes were formed immediately prior to introduction into cells. 1.2 μl of tracrRNA:gRNA complex was combined with 1.2 μl Cas9 protein (100 μM), and 0.8 μl PBS and mixed via gentle pipetting. The solution was left at room temperature for 20 minutes to allow nucleotide-protein complex formation.

2.11.4 Delivery of CRISPR components to HUVECs

RNP complexes were combined with 4 μl of ssODN (100 μM) and 4 μl of Alt-R® Cas9 Electroporation Enhancer (IDT; Coralville, USA). HUVECs were washed with PBS and detached from growth vessels with trypsin. Cells were counted and 3 x10^5 cells were resuspended in 100 μl of Mirus ingenio electroporation solution (Mirus Bio, (Cat # MIR50114)). The CRISPR components were added to the cell suspension and transferred into a 0.2 cm electroporation cuvette with a small cell dropper. The cuvette was inserted into an Amaxa Nucleofactor 2 device and electroporation performed using program V-001. Following electroporation, cells were immediately transferred into 1 ml of culture media and mixed gently. The electroporated cells were then seeded in culture vessels at the required density.

2.11.5 Assessment of CRISPR editing

In order to assess the efficacy of the incorporation of the HiBiT sequence into the VEGF-A gene, genomic DNA was extracted from pools of edited cells and PCR performed as described in 2.11.2. PCR products were separated on 3% agarose gels and visualised under U.V. light. Successful incorporation of the HiBiT sequence was demonstrated by an increase in PCR product size of 33 bp. An additional confirmatory PCR reaction was performed, where the forward primer was exchanged for a primer relating to the final 22 nucleotides of the HiBiT sequence (5'- GCGGCTGTTCAAGAAGATTAGC -3'). The reverse primer remained the same (2.3). PCR was performed and PCR products separated on a 3% agarose gel. Successful addition of HiBiT to exon 8a generated a product of 372 bp and addition to exon 8b generated a product of 317 bp.

2.12 Bioluminescent measurements of HiBiT tagged proteins

The quantification of the expression of HiBiT tagged proteins was performed as previously described (Schwinn et al., 2018), with some minor modifications. All bioluminescent assays were performed in white 96-well plates (655098, Greiner BioOne, Kremmunster, Austria), with an adhesive white plate back in place to avoid signal loss.

Lytic assays of intracellular protein

To determine the expression of intracellular HiBiT tagged proteins, an equal volume of Nano-Glo HiBiT lytic buffer (N247A, Promega) was added to culture media, supplemented with Furimazine and LgBiT polypeptide to give final concentrations of 10 μM and 100 nM respectively. Plates were incubated at 37°C for 10 minutes and then luminescence read on a PHERAstar FS plate reader (BMG Labtech, Ayelsbury, Bucks, UK), with a gain setting of 3600.

Assays of HiBiT tagged protein secreted into media

To determine the secretion of HiBiT tagged proteins into culture media, 30 μl of media samples were plated into white 96-well plates. 10 μl of HEPES buffered salt solution (HBSS; 10 mM HEPES, 10 mM glucose, 145 mM NaCl, 5 mM KCl, 1 mM $MgSO_4$, 2mM sodium pyruvate, 1.3mM $CaCl_2$,; pH 7.45), was added containing LgBiT protein to give a final concentration of 100 nM. The plate was incubated at 37 °C for 20 minutes to facilitate complementation of HiBiT with LgBiT. Subsequently, a further 10 μl of HBSS was added containing furimazine to give a final concentration of 10 μM. Plates were incubated at 37 °C for a further 5 minutes and luminescence read on a PHERAstar FS plate reader (BMG

Labtech, Ayelsbury, Bucks, UK), with a gain setting of 3600 and filter settings to measure emissions between 475-505 nm.

2.13 Evaluation of HiBiT tagged protein binding to receptor

In order to determine if the HiBiT tagged VEGF-A protein secreted from CRISPR edited HUVECs was capable of successfully binding to its canonical receptors, VEGFR2 and NRP1, assays were performed using LgBiT tagged receptors expressed in HEK293T cells and binding assessed via luminescent production.

2.13.1 Expression of LgBiT tagged VEGFR2 and NRP1 in HEK293T cells

Plasmids encoding NRP1 and VEGFR2 with a LgBiT tag on the N-terminus were previously generated and described by Peach et al. (2021). HEK293T cells were seeded at a density of 3 x10^5/well in 6 well plates in 2 ml of growth media. Following 24 hours of growth, cells were transfected with 1 μg plasmid DNA with 3 μl FuGENE HD reagent, diluted in a final volume of 100 μl Opti-MEM, prepared as described above. After 24 hours of transfection, cells were washed and trypsinised then seeded into white 96-well plates (655098, Greiner BioOne, Kremmunster, Austria) pre coated with 0.1 mg/ml poly-d-lysine, at a density of 30 x10^3/well.

2.13.2 Conditioned media treatment

Twenty-four hours after seeding LgBiT-NRP1 and LgBiT-VEGFR2 transfected HEK293T cells were treated with CRISPR edited HUVEC conditioned media.

Growth media was first aspirated and cells washed with PBS. Cells were treated with either unconditioned HUVEC media (control), CRISPR edited HUVEC conditioned media, or control media supplemented with 100 pM purified HiBiT peptide (Promega). Additionally, to determine if binding could be displaced, the NRP1 experiment also included a condition of CRISPR edited HUVEC conditioned media supplemented with 100 nM recombinant VEGF 165a (R&D Systems, Abingdon, UK). Cells were incubated with experimental media for 1 hour at 37 °C.

2.13.3 Bioluminescence determination

Following conditioned media treatment, cells were supplemented with 10 μM furimazine and an adhesive plate back was applied to the plate. Bioluminescence was immediately read using a PHERAstar FS plate reader (BMG Labtech, Aylesbury, Bucks, UK), with a gain setting of 3600 and filter settings to measure emissions between 475-505 nm.

2.14 Immunocytochemistry

Staining

Immunocytochemistry was performed upon cells cultured in black 96 well tissue culture plates (655090, Greiner BioOne, Kremmunster, Austria). Cells were stained for the endothelial cell marker CD31 (PECAM-1) (Müller et al., 2002). Following desired experimental treatments culture media was aspirated and cells immediately fixed with 3% paraformaldehyde in PBS for 10 minutes at room temperature. Post fixation, cells were washed three times for five minutes with PBS and subsequently permeabalised by incubation with 0.025% Triton X-100 (Sigma) in PBS for 10 minutes. Cells were again washed with PBS (3 x 5 minute

washes), and then blocked by incubation with PBS containing 3% BSA and 1% glycine for 30 minutes at room temperature. Cells were again washed (three five minute washes with PBS) and blocked again by incubation with 10% chicken serum in PBS for 30 minutes at room temperature. Blocking solution was removed and cells incubated with primary antibody (Rabbit monoclonal anti-CD31, MA5-33063, Invitrogen) diluted 1:1500 in 10% chicken serum PBS overnight at 4 °C. The following day, the antibody solution was removed and the cells washed (PBS, 3 x 5 minute washes). Cells were then incubated with secondary antibody (Chicken anti rabbit Alexa Fluor 488, A-21441, Invitrogen) diluted 1:500 in 10% chicken serum PBS, for 1 hour at room temperature in the dark. Cells were again washed (PBS, 3 x 5 minute washes) then incubated for 10 minutes with 2 mg/ml bisBenzimide H33342 trihydrochloride (B2241; Sigma-Aldrich) in PBS, to stain nuclei. Cells were washed for a final time, 3 five minute washes with PBS, and stored covered with PBS at 4 °C in the dark until imaging.

Image capture

Plates were imaged using a ImageXpress Micro widefield platereader (Molecular Devices, USA) fitted with an extra long working distance 20X objective. Images were taken at 4 sites pre well with a FITC (excitation 482/35 nm, emission 536/40 nm) and a DAPI filter (excitation 377/50 nm, emission 447/60 nm) for CD31 and nuclei respectively. Exposure times were 500 ms for the FITC filter and 25 ms for the DAPI filter.

2.15 Statistical Analysis

All statistical analysis was performed using R Version 3.6.3 and Prism Version 9.1.0. Data are reported as mean ± standard error (SEM) in all instances, unless

otherwise stated. Statistical significance was deemed to have been met when statistical tests returned a p value of 0.05 or less.

Differences between independent experimental groups were assessed via independent two-tailed t.tests (e.g. WT vs FIH1$^{-/-}$ mice). When relevant, two-way ANOVA was utilised to assess for significant main effects, followed with post-hoc testing to locate specific differences between groups/time points, with corrections made for multiple comparisons to control the type I error rate. Two way ANOVA with repeated measures was utilised when serial measurements were made within the same groups. Where significant main effects were observed specific differences were again located via post-hoc testing with control of the type I error rate. In instances where three or more groups were compared with one independent variable, a one-way ANOVA was performed, particularly relevant to chapter 5. In such cases, post hoc testing was performed to locate specific differences between groups.

In chapter five, due to the variability of CRISPR mediated gene editing, non-parametric statistical methods were employed, with data reported as median and individual data points shown. Differences due to treatment were assessed via a Wilcoxon matched-pairs signed rank test (figure 5.8).

Statistical methods employed are further described in each experimental chapter, and denoted within figure legends where appropriate.

Chapter 3

The effect of FIH1 loss on indices of cardiac mitochondrial content and function, and interaction with chronic hypoxic exposure

3.1 Abstract

Background Adaptation to hypoxic exposure is regulated in a large part by the HIF signalling pathway. The activity of the HIF system is constrained by proline hydoxylases and the asparaginyl hydroxylase FIH1. One of the core responses to hypoxia the HIF system directs is the modulation of metabolism. The present chapter sought to understand the role of FIH1 in controlling mitochondrial metabolism in the heart.

Methods Mice with a systemic deletion of the FIH1 gene were studied in comparison to wild type littermate controls. Fatty acid oxidation rates were determined in isolated perfused hearts using ^{3}H palmitate. Mitochondrial content and function were assessed on the level of enzyme activity, protein, and DNA content. A further cohort of mice were studied in response to three weeks hypoxic exposure (11% O_2) and changes in mitochondrial content assessed in the heart and skeletal muscle.

Results Rates of fatty acid oxidation were not different between hearts from WT and FIH1$^{-/-}$ mice (0.24 ± 0.030 vs 0.23 ± 0.031 μmol/minute/g wet weight respectively). Similarly, there was no difference in citrate synthase activity, or mitochondrial content between WT and FIH1$^{-/-}$ hearts. Blood haemoglobin was equivalent between WT and FIH1$^{-/-}$ mice, and hypoxia led to an approximate 1.3 fold increase in both genotypes. Hypoxia did not lead to any changes in mitochondrial content in either WT or FIH1$^{-/-}$ heart or skeletal muscle.

Conclusion The present investigation found no evidence of altered fatty acid metabolism or mitochondrial content due to the loss of FIH1 in the heart. Furthermore there was no evidence of polycythaemia associated with reduced activity of HIF proline hydroxylases.

3.2 Introduction

Modulation of metabolism is an essential response to hypoxia in order to promote cell survival, HIF-1 is central to this and there are an array of metabolic HIF-1 targets (Semenza, 2012). Mitochondria are a central node in metabolism, providing the site of oxidative metabolism and thus the site of the majority of ATP production in the heart (Stanley et al., 2005). Furthermore, they are therefore the fundamental site of O_2 consumption, and as such susceptible to changes in oxygen availability, such as in hypoxia.

As well as being involved in the upregulation of glycolytic enzymes (Iyer et al., 1998; Semenza et al., 1994), HIF-1α is also involved in the regulation of mitochondrial content and metabolism. Deletion of PHD2 in the heart leads to stabilisation of HIF-1α and to mitochondrial loss and structural abnormalities (Moslehi et al., 2010). Similarly, loss of PHD1 in skeletal muscle leads to reduction in mitochondrial oxygen consumption (Aragonés et al., 2008). Conversely cardiac specific deletion of HIF-1α increases mitochondrial content (mtDNA and mitochondrial volume) and approximately doubles citrate synthase activity. Furthermore, HIF-1$\alpha^{-/-}$ hearts also have increased expression of genes involved in beta oxidation and mitochondrial fatty acid import (Krishnan et al., 2009). Collectively, there is substantial evidence that HIF-1α signalling acts to regulate mitochondrial function and metabolism.

Mitophagy is an important component of the metabolic response and adaptation to hypoxia, under the control of HIF-1α-BNIP3 signalling (Zhang et al., 2008). Upon exposure of mouse embryonic fibroblasts (MEF), to 1% O_2 for 48 hours, there is an approximate 5 fold reduction in mitochondrial DNA content, and associated reduction in O_2 consumption. This effect however is lost in HIF-1$\alpha^{-/-}$ MEFs (Zhang et al., 2008). These data highlight the role of HIF-1α in the mitochondrial response to hypoxia, and suggest that elevated HIF-1α signalling may

promote further reductions in mitochondrial mass upon hypoxic exposure. This intimates that enhanced HIF-1 signalling under hypoxia, such as through FIH1 inhibition, may further reduce mitochondrial content and oxygen consumption. With the high degree of expression of FIH1 in skeletal muscle this provides a valuable tissue to study the effects of FIH1 manipulation. Short term hypoxic exposure (5 hours of 12% O_2) of FIH1 muscle specific KO mice reduces oxygen consumption during exercise to a greater degree than WT controls, therefore demonstrating an accelerated adaptation to acutely reduced oxygen availability (Sim et al., 2018). It is not known, however, how the loss of FIH1 may interact with more chronic exposure to hypoxia.

The present chapter aimed to understand how modulation of FIH1 affects oxidative metabolism, and mitochondrial content and function. Specifically whether the loss of FIH1 alters fatty acid oxidation and mitochondrial content and function in the heart. Furthermore, how the loss of FIH1 interacts with chronic hypoxia to regulate mitochondrial content will be assessed.

3.3 Methods

3.3.1 Animals

FIH1$^{-/-}$ and littermate WT control animals were bred and genotyped as described in the general methods chapter. Mice were housed under standard laboratory conditions on a 12 hour light/dark cycle with ad libitum access to standard chow diet and studied at 10- 12 months of age. All animal experimentation was performed in accordance with the Home Office guidelines (The Animals (Scientific Procedures) Act, 1986) and local university of Nottingham guidelines and procedural requirements.

3.3.2 Cardiac fatty acid oxidation

Hearts were excised from terminally anaesthetised WT and FIH1$^{-/-}$ mice and Langendorff perfused as described in the general methods. To determine the rate of palmitate oxidation the perfusion buffer contained [9,10-^{3}H]-palmitate. Timed perfusate samples were taken throughout the perfusion period, and $^{3}H_2O$ separated as described in the general methods chapter. The rate of fatty acid oxidation was calculated from the rate of $^{3}H_2O$ accumulation and expressed relative to heart weight.

3.3.3 Chronic hypoxic housing

In order to study the interaction between FIH1 deletion and hypoxia in vivo, WT and FIH1$^{-/-}$ mice were housed in normobaric hypoxia for a period of three weeks. Oxygen availability was reduced in a graded manner over the first seven days, and maintained at 11% for the 14 days. Hypoxically housed animals were monitored daily, and their body weight recorded at the same time each day. Normoxic control animals were housed in the same room as hypoxic animals, and exposed

to standard room air. The hypoxic housing protocol is described in detail in the general methods.

3.3.4 Tissue analysis

Tissues were snap frozen using Wollenberger clamps cooled to the temperature of liquid nitrogen, and stored at -80°C until further processing and analysis. In the case of heart tissue this was at the end of Langendorff perfusion. Skeletal muscle (gastrocnemius) was excised from the limb and immediately frozen.

Citrate synthase activity

Citrate synthase activity was measured according to the method of Srere (1969), and normalised to protein content, as described in general methods.

Mitochondrial copy number

Total DNA was extracted from tissues and quantified. DNA concentration was normalised between samples, and qPCR performed for HK2, ND1, and 16SrRNA. The abundance of each of the latter two mitochondrial genes was normalised to nuclear DNA (HK2), utilising the $2^{-\Delta\Delta ct}$ method (Livak and Schmittgen, 2001; Quiros et al., 2017). This protocol is described in full in the general methods.

Western blotting

Western blotting was performed on snap frozen heart tissue from WT and FIH1$^{-/-}$ heart tissue as described in the general methods. The expression of mitochondrial complexes I-V was determined using Total OXPHOS Rodent Antibody Cocktail (ab110413, Abcam, UK), and actin utilising rabbit anti-actin polyclonal antibody (A2066, Sigma, UK). Secondary antibodies used were goat anti mouse, and goat anti rabbit, respectively (HAF007 and HAF008, R & D Systems, USA).

3.4 Statistical analysis

Data are reported as mean ± standard error, unless otherwise stated. Comparisons between WT and FIH1$^{-/-}$ mice were made using unpaired t.tests in the case of single measurements. In the case of hypoxic experiments where there were four groups of animals analysis was made using two-way ANOVA, with repeated measures as appropriate. In all cases results were considered to be statistically significant with $p \leq 0.05$. Data analysis was performed using R version 3.6.3.

3.5 Results

3.5.1 Fatty acid oxidation in FIH1$^{-/-}$ hearts

Both heart and body weight were significantly reduced in FIH1$^{-/-}$ mice relative to WT controls (both 0.8 fold lower, p = 0.001 & 0.018 for body weight and heart respectively, table 3.1)). The heart to body weight ratio was not different between genotypes.

Table 3.1 Morphological characteristics of wild type and FIH$^{-/-}$ mice utilised for measurement of Fatty acid oxidation, mean ± standard error

	WT	**FIH1$^{-/-}$**	**p.value**
Body weight (g)	37.5 ± 1.16	28.8 ± 1.99	0.001
Heart weight (mg)	233 ± 7.75	191 ± 15.44	0.018
HW/BW ratio (mg/g)	6.25 ± 0.355	6.73 ± 0.547	0.388

Values represent mean ± standard error (n = 7 WT and 6 KO). P values calculated by unpaired Student's t.test between genotypes.

Fatty acid oxidation

Indices of cardiac function of isolated perfused hearts were not different between those from WT and FIH1$^{-/-}$ mice (table 3.2). Absolute rates of coronary flow were not different between genotypes, however, when expressed relative to heart weight, FIH1$^{-/-}$ hearts had significantly greater flow rates. Fatty acid oxidation rates in these hearts were not different between WT and FIH1$^{-/-}$ mice (figure 3.1).

Table 3.2 Cardiac function of WT and FIH$^{-/-}$ hearts utilised for measurement of Fatty acid oxidation, mean ± standard error

	WT	**FIH1$^{-/-}$**	**p.value**
Heart rate (bpm)	212 ± 19.5	210 ± 21.2	0.96
Developed pressure (mmHg)	62.5 ± 8.09	71.0 ± 3.07	0.36
RPP (HR x DP)	13454 ± 2403	14905 ± 1817	0.64
Coronary flow (ml/min)	2.13 ± 0.106	2.27 ± 0.191	0.56
Coronary flow (ml/min/gww)	9.23 ± 0.569	12.03 ± 0.873	0.03

Values represent mean ± standard error (n = 7 WT and 6 KO). P values calculated by unpaired students t.test between genotypes.

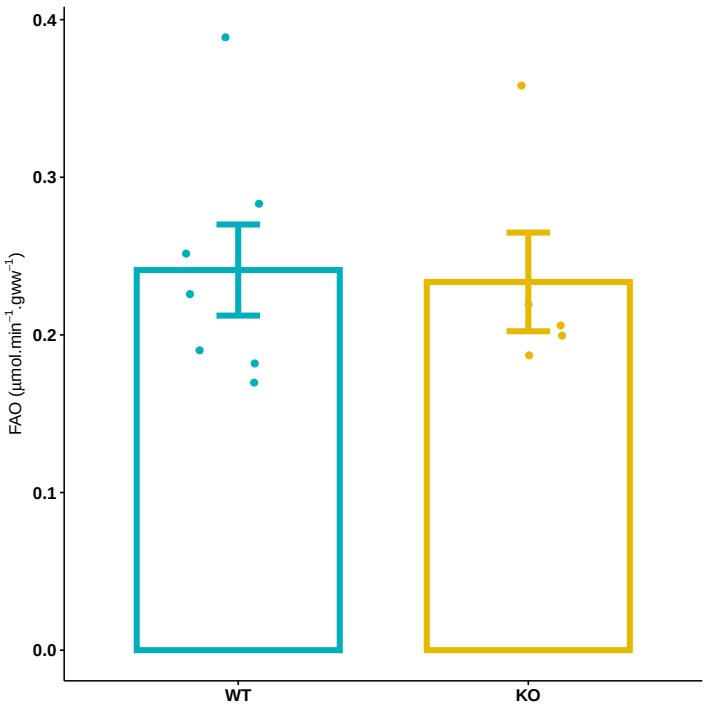


Fig. 3.1 Fatty acid oxidation in WT and FIH1$^{-/-}$ hearts. Bars represent mean ± standard error, no significant difference between genotypes.

Citrate Synthase Activity

Citrate synthase activity was not altered in between ventricular tissue from WT and FIH1$^{-/-}$ hearts (1.01 $\pm$ 0.026 vs 0.96 $\pm$ 0.039, p = 0.36, figure 3.2).

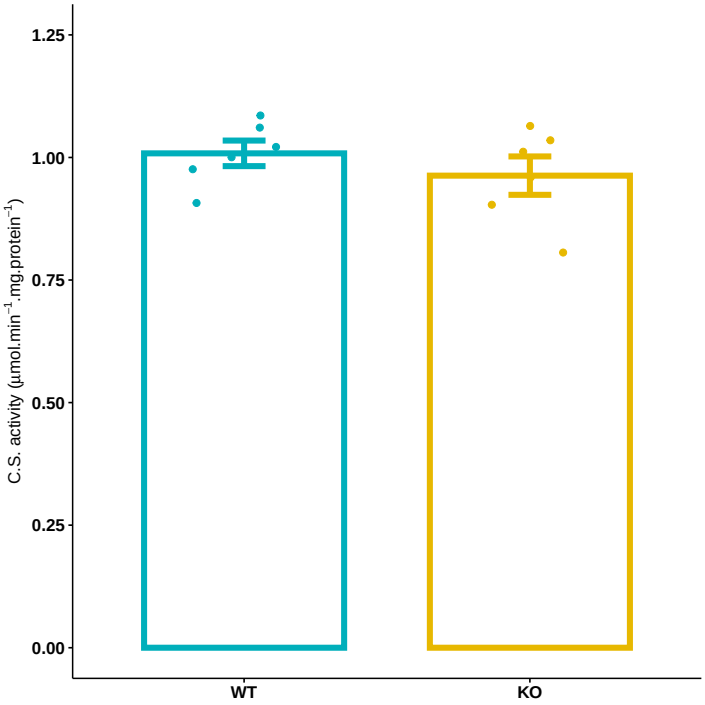
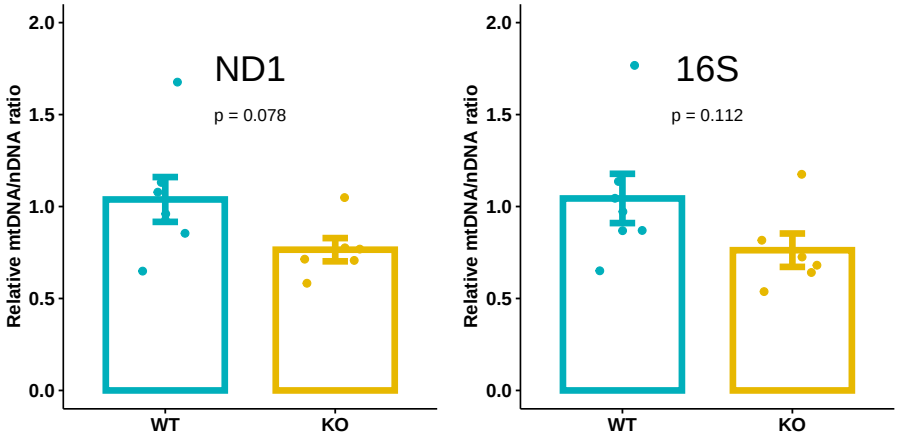


Fig. 3.2 Citrate synthase activity in WT and FIH1$^{-/-}$ hearts. Bars represent mean $\pm$ standard error, no significant difference between genotypes.

Mitochondrial content

The mitochondrial copy number in the heart, assessed by mitochondrial to nuclear DNA ratio, in WT and FIH1$^{-/-}$ is shown in figure 3.3. Although the values for FIH1$^{-/-}$ mice were 0.74 and 0.73 fold of wild types, for ND1 and 16S respectively, this did not meet the threshold of statistical significance (p = 0.078 and 0.112 respectively). The protein expression of each of the mitochondrial complexes (I - V) were shown to be no different between WT and FIH1$^{-/-}$ hearts (figure 3.4).



(a) (b)

Fig. 3.3 Mitochondrial/nuclear DNA ratio of WT and FIH1$^{-/-}$ hearts. Bars represent mean ± standard error. The ratio of mitochondrial ND1 DNA to nuclear DNA is plotted in (a), and the ratio of 16s mitochondrial DNA to nuclear DNA (b).

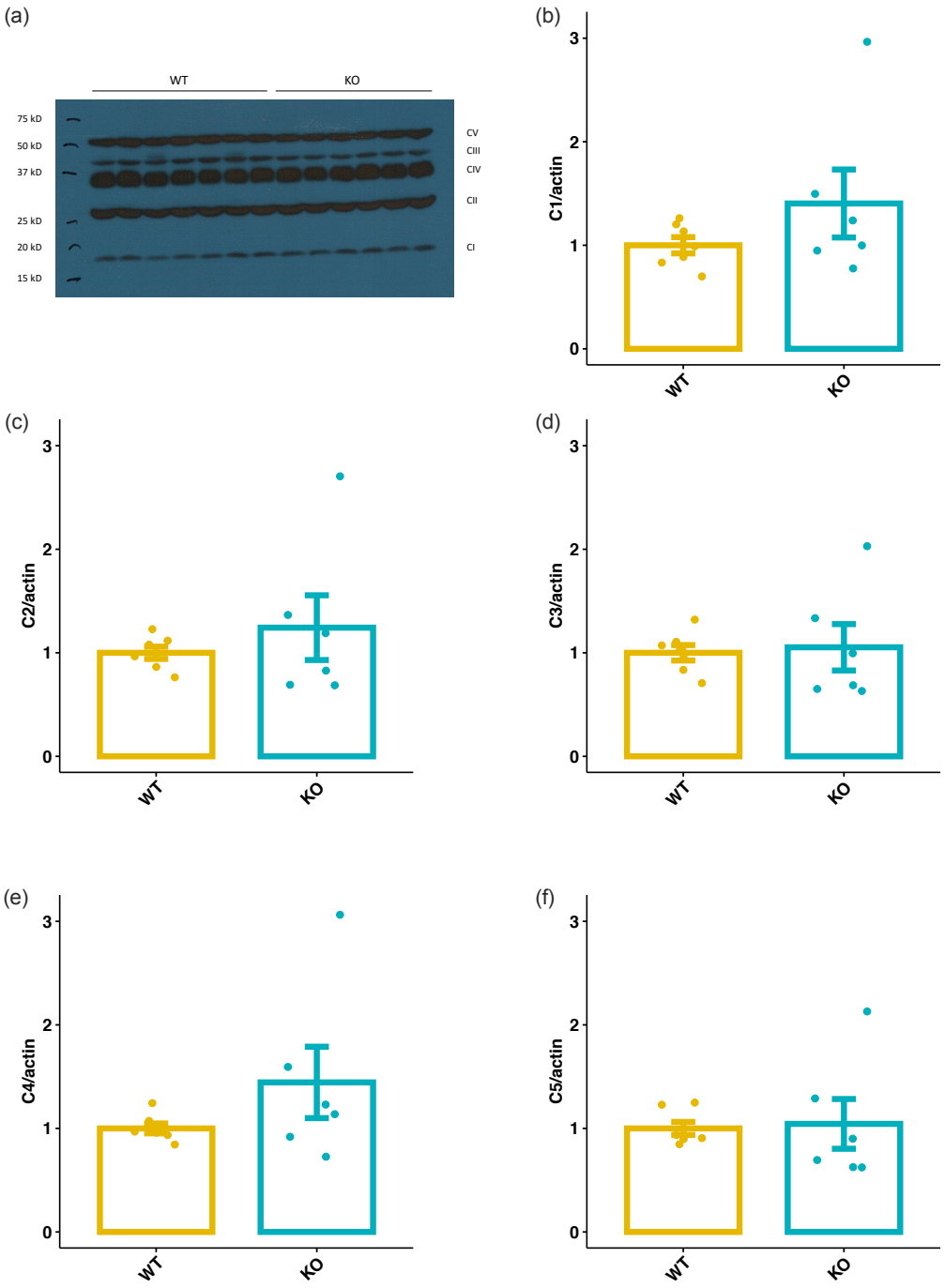
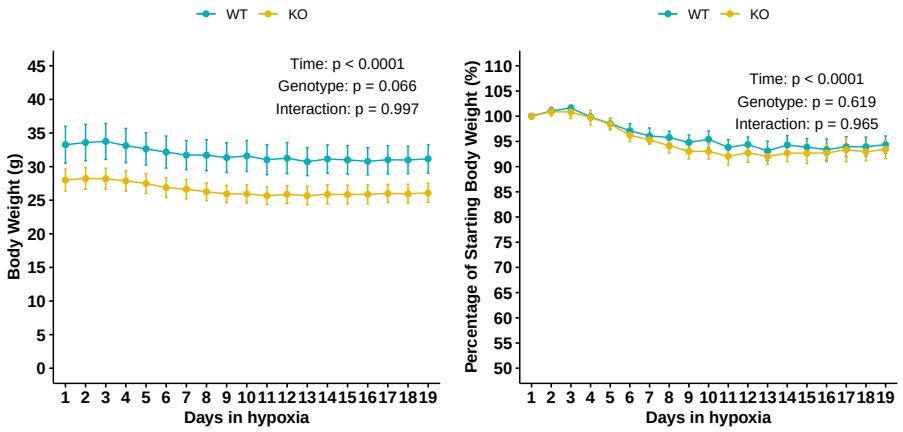


Fig. 3.4 Protein expression of mitochondrial complexes in WT and FIH1$^{-/-}$ heart. Example blot (a), expression of each complex (b-f), bars represent mean ± standard error. No significant difference in expression of any of the complexes.

3.5.2 The mitochondrial consequences of the interaction of chronic hypoxia and FIH1 deletion in cardiac and skeletal muscle

Chronic hypoxic housing led to a modest reduction in body weight. This effect was seen across both WT and FIH1$^{-/-}$ mice (figure 3.5a), and there was no evidence of an interaction effect between hypoxia and FIH1 deletion upon body weight. Furthermore, when expressed relative to starting body weight, there is a clear absence of any genotype effect, and the magnitude of body weight loss is the same between genotypes (figure 3.5b).



(a) (b)

Fig. 3.5 Body weight responses of WT and FIH1$^{-/-}$ mice during chronic hypoxia. Absolute body weights are displayed in (a), and relative to starting body weight in (b). Points represent mean ± standard error, for WT (n=7) and FIH1 KO (n=8). Results of two way repeated measures ANOVA are shown for each figure.

When housed in normoxia, there was no difference in blood haemoglobin between WT and FIH1$^{-/-}$ mice (15.0 ± 0.69 vs 14.6 ± 0.481, figure 3.6). Mice housed in hypoxia had a 1.3 fold higher blood haemoglobin concentration than control animals of the same genotype housed in normoxia. This was true of both WT and FIH1$^{-/-}$ mice, and there were no effects of genotype or genotype-hypoxia interactions. Mitochondrial/nuclear DNA ratio was not different between

WT and FIH1$^{-/-}$ mice in either skeletal muscle (figure 3.7) or heart (figure 3.8). Furthermore, there was no change in mitochondrial/nuclear DNA ratio in response to chronic hypoxic housing, in either tissue or genotype.

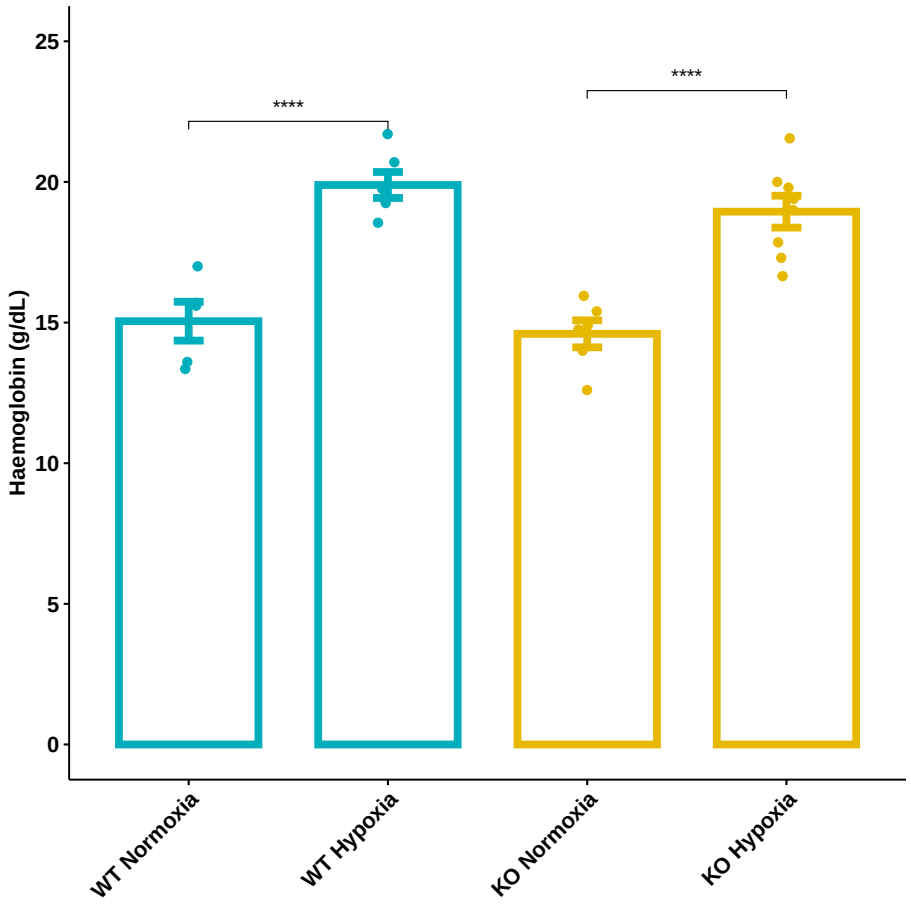
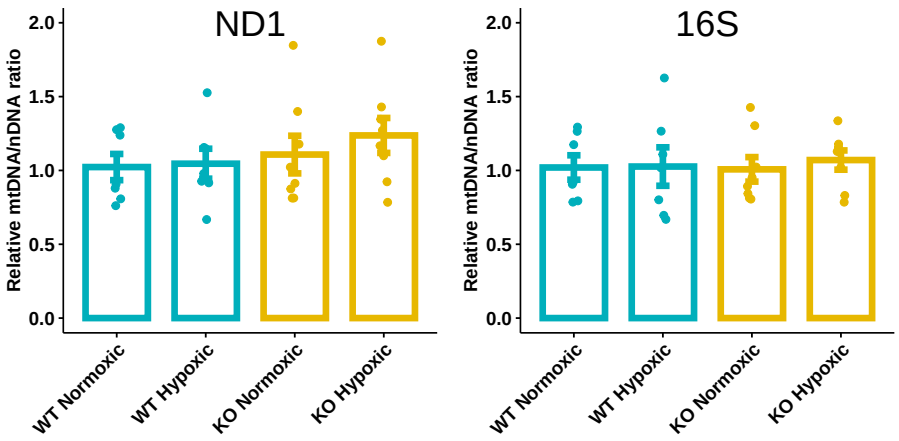
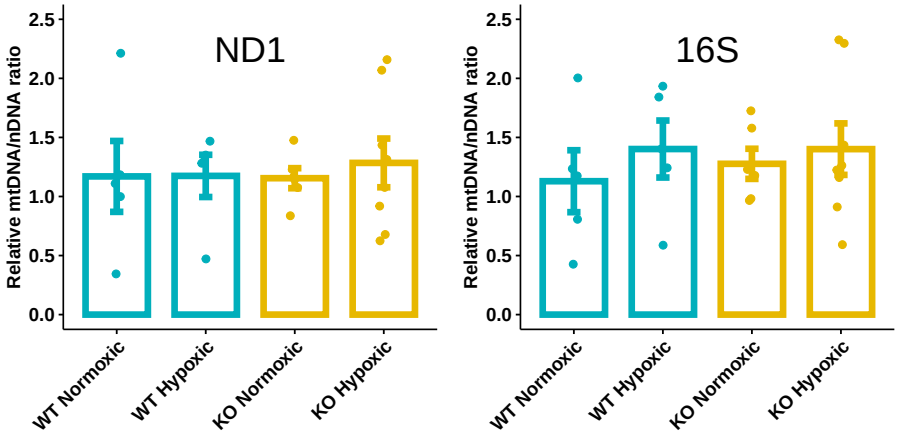


Fig. 3.6 Blood haemoglobin in WT and FIH1$^{-/-}$ mice housed in either normoxia or chronic hypoxia. Bars represent mean ± standard error, **** represents p<0.0001. No significant effect of genotype or genotype-hypoxia interaction.



(a) (b)

Fig. 3.7 Mitochondrial/nuclear DNA ratio of WT and FIH1$^{-/-}$ skeletal muscle, from mice housed in normoxia or hypoxia . Bars represent mean ± standard error. The ratio of mitochondrial ND1 DNA to nuclear DNA is plotted in (a), and the ratio of 16s mitochondrial DNA to nuclear DNA (b).Two way ANOVA revealed no significant effect of hypoxia, no significant effect of genotype, and no hypoxia-genotype interaction.



(a) (b)

Fig. 3.8 Mitochondrial/nuclear DNA ratio of WT and FIH1$^{-/-}$ hearts, from mice housed in normoxia or hypoxia . Bars represent mean ± standard error. The ratio of mitochondrial ND1 DNA to nuclear DNA is plotted in (a), and the ratio of 16s mitochondrial DNA to nuclear DNA (b). Two way ANOVA revealed no significant effect of hypoxia, no significant effect of genotype, and no hypoxia-genotype interaction.

3.6 Discussion

The present chapter aimed to understand mitochondrial regulation by FIH1 in the heart, and how this interacts with chronic hypoxia. The principal finding, therefore, is that the loss of FIH1 in the heart does not lead to differences in key markers of mitochondrial and oxidative capacity.

Cardiac mitochondrial function is not effected by FIH1 loss.

The present investigation provides no evidence of altered mitochondrial function due to FIH1 loss in the heart. The equivalence in the rate of cardiac fatty acid oxidation in hearts from mice with FIH1 deletion (figure 3.1) is in contrast to the effects of exposure to chronic hypoxia. In both rat (Mansor et al., 2016) and mouse (Cole et al., 2016) hearts, exposure to 21 days chronic hypoxia reduced the rate of ex vivo fatty acid oxidation by approximately 20% and 26% respectively.

Studies of mice carrying the Chuvash polycythaemia point mutation in the VHL gene, a model of moderate upregulation of HIF signalling, found no depression of cardiac fatty acid oxidation rates (Slingo et al., 2016). This in keeping with the present investigation where FIH1 loss, which causes a moderate upregulation in HIF signalling (Zhang et al., 2010), did not lead to reduction in fatty acid metabolism. Together, this suggests, that the changes in cardiac fatty acid metabolism seen in the environmental hypoxia models described above are dependent on more than a moderate upregulation of HIF signalling alone.

The equivalence in FAO between WT and FIH1$^{-/-}$ mice is supported by finding of equivalent citrate synthase activity (figure 3.2), mitochondrial DNA content (figure 3.3), and expression of mitochondrial complex proteins (figure 3.4). Similar to changes in fatty acid oxidation, hypoxic exposure has been shown to reduce these indices, e.g. reduction in citrate synthase activity (Mansor et al., 2016), and reduced complex 1 protein expression (Heather et al., 2012) in the

chronically hypoxic rat heart. This further underlines the difference in phenotype between the chronic hypoxia and FIH1$^{-/-}$ heart.

Chronic hypoxia induces similar haematological changes, but no detected mitochondrial changes in WT and FIH1$^{-/-}$ mice

The equivalence in blood haemoglobin in normoxically housed mice (figure 3.6) is in contrast to mice with other genetic mutations that enhance HIF signalling. Mice carrying the Chuvash polycythaemia mutation (chronic up-regulation of HIF signalling) have a 1.14 fold increase in blood haemoglobin, relative to WT controls (Slingo et al., 2016). This is a much more minor up-regulation than that seen with inducible deletion of PHD2 in mice, which results in an approximate 1.6 fold increase in blood haemoglobin, and leads to heart failure likely due to increased cardiac demand of hyperviscosity of the blood (Minamishima et al., 2008). Collectively these findings suggest that the degree of polycythaemia and increase in blood haemoglobin is relative to the degree of increase in HIF signalling, and that changes in HIF signalling due to FIH1 deletion are insufficient to stimulate this.

Hypoxic housing in the present study led to increases in blood haemoglobin equivalent to previous investigations utilising comparable hypoxia exposure protocol (Cole et al., 2016; Handzlik et al., 2018; Mansor et al., 2016). There was no effect of FIH1 deletion upon the haemoglobin response to hypoxia, with both WT and FIH1$^{-/-}$ increasing to equivalent levels. It should be stressed, however, that this single time point measurement following three weeks of hypoxia may mask potential differences in the dynamics of the change in blood haemoglobin. Previous investigations have shown that the FIH1$^{-/-}$ mouse has a blunted erythropoietic response when exposed to hypoxia (9% O_2) for 10 hours, in terms of both plasma erythropoietin (EPO) and renal EPO mRNA expression Zhang

et al. (2010). The present investigation could be expanded, therefore, by taking serial measurements upon exposure to hypoxia to understand the dynamics of the erythropoetic response.

Hypoxia induced reductions in body weight are associated with reductions in energy intake and associated with modulated appetite signalling in humans (Debevec, 2017; Lippl et al., 2010). Hypoxia induced body weight reductions in rodents are not consistently reported, likely due to differences in the degree of hypoxic exposure, and also the age of the animals studied. With body weight increases due to growth in juvenile animals masking effects of weight loss due to hypoxia. The modest degree of body weight loss seen in the present investigation was consistent between WT and FIH1$^{-/-}$ mice. This likely represents a reduction in food intake, as when normoxic control mice are pair-fed the weight loss due to extreme hypoxia is matched (Nakada et al., 2017). However, as neither food intake nor energy expenditure were quantified in the present investigation, different mechanisms of body weight regulation under hypoxia between the genotypes cannot be ruled out.

In skeletal muscle biopsies of sea level dwellers ascending to Everest base camp (5300 m), with two weeks spent over 4000 m, there was no reduction in the mitochondrial content. In an additional studied cohort, however, whom ascended to higher altitudes (> 8000 m) over a longer time frame, there were substantial reductions in skeletal muscle mitochondrial content (Levett et al., 2012). With reference to the present investigation, the absence of any reduction in mitochondrial content of the skeletal muscle may be due to the degree of hypoxic exposure. Similarly, with respect to mitochondrial content in the heart, exposure of mice to greater reductions in oxygen availability (7% O_2) led to a significant reduction in cardiac mitochondrial DNA content and cristae number (Nakada et al., 2017). With reference to the present investigation, therefore, it seems intuitive that the absence of any effect of hypoxic exposure upon mitochondrial

content is due to the degree of hypoxia mice were subjected too. Exposure to a greater degree of hypoxia would likely have led to a decrease in mitochondrial content, which may have exposed differences between WT and FIH1$^{-/-}$ mice.

Limitations

The present investigation aimed to understand the regulation of mitochondria in the heart by a loss of function model. There are several areas of investigation that could be addressed to further expand the scope of the present investigation and its finding. Although the majority of cardiac ATP production is via mitochondrial oxidation of lipids (Stanley et al., 2005), the role of carbohydrate is still significant and was not addressed in the present investigation. Utilisation of a ^{13}C glucose tracer, in addition to the ^{3}H would have allowed simultaneous measurement of glucose oxidation (Lopaschuk and Barr, 1997). Furthermore, although effort was made to evaluate mitochondrial characteristics via a number of techniques, study of the respiration of isolated mitochondria utilising different substrates would add strength to the current investigation.

The heart contains two distinct subpopulations of mitochondria, subsarcolemmal and interfibrillar (Palmer et al., 1977). Previous investigations of the cardiac mitochondrial responses to hypoxia have demonstrated some differences in response between these two populations (Heather et al., 2012). With reference to the present investigation, therefore, it may be that changes in mitochondrial characteristics have been missed, by studying whole tissue samples alone.

Furthermore, due to limited sample availability, the investigation of the interaction between FIH1 loss and chronic hypoxia was restricted to assessment of mitochondrial DNA alone. This could be further developed by further in vivo and ex vivo characterisation.

Conclusion

The present investigation found no evidence of regulation of fatty acid metabolism or mitochondrial characteristics by FIH1 in the heart. Collectively these data suggest that the FIH1$^{-/-}$ does not phenocopy all of the characteristics of the chronically hypoxic heart.

Chapter 4

The effect of FIH1 loss on cardiac ischaemia reperfusion injury and glucose metabolism

4.1 Abstract

Background Potentiated HIF signalling via prolyl hydroxylase (PHD) inhibition has previously been demonstrated to be cardioprotective in ischaemia reperfusion injury. Furthermore, in conditions of reduced or impaired HIF signalling, ischaemia reperfusion injury is exacerbated. In addition to negative regulation by PHD enzymes HIF signalling is negatively regulated by FIH1. It is not known, however, if enhancing HIF signalling via reducing FIH1 activity could serve as a method of reducing ischaemia reperfusion injury in the heart. The present study aimed to assess the effect of FIH1 loss on cardiac ischaemia reperfusion injury, with particular examination on the role of glucose metabolism.

Methods Hearts from WT and FIH1$^{-/-}$ mice were isolated and Langendorff perfused. The perfused hearts underwent ischaemia (0.5 ml/min/gww) and subsequent reperfusion. Cardiac function was assessed throughout via left ventricular balloon. Cardiac metabolism was assessed in the perfused hearts using ^{3}H glucose tracer. A subset of hearts were perfused to the end of ischaemia only. Metabolite concentrations in the myocardium were assessed both post ischaemia only and post ischaemia reperfusion.

Results Functional recovery was greater in hearts from FIH1$^{-/-}$ than WT controls (76.9% vs 51.1%; $p < 0.05$). Additionally, glycolysis was elevated in FIH1$^{-/-}$ hearts during baseline and reperfusion (1.3 and 1.6 fold respectively; $p < 0.05$). The accumulation of lactate within the heart during ischaemia was 1.5 fold greater in KO than WT hearts ($p < 0.05$). The PCr content and energy charge of hearts showed significant depression post ischaemia relative to post reperfusion, but no genotype effects were observed.

Conclusion The FIH1$^{-/-}$ heart exhibits enhanced recovery from ischaemia reperfusion injury relative to WT controls. This enhanced functional recovery is associated with elevated glycolytic flux in the FIH1$^{-/-}$ heart and increased lactate

accumulation during ischaemia. Collectively these data suggest that FIH1 loss of function in the heart may provide a therapeutic target to protect the heart from ischaemic injury.

4.2 Introduction

In myocardial infarction rapid reperfusion of the area deprived of blood flow is desired in order to limit myocardial damage and preserve heart function and viability. The process of reperfusion itself can, however, induce cardiomyocyte death (Hausenloy and Yellon, 2013). This process is known as ischaemia reperfusion (IR) injury.

There is a body of evidence that suggests that the degree of cardiac HIF signalling can influence the degree of ischaemic injury. Table 4.1 outlines studies that have investigated the impact of different manipulations of the HIF signalling pathway upon ischaemia reperfusion injury. Hearts from mice with a cardiac specific HIF-1α deletion (Cre-recombinase under the control of α -myosin heavy chain promoter) experience a significantly greater degree of infarction following ischaemia reperfusion injury (Nanayakkara et al., 2015). Conversely, there is a breadth of evidence, from a range of experimental models, that enhanced HIF signalling is protective in the face of ischaemia reperfusion injury.

Table 4.1 Summary of in and ex-vivo investigations of altered HIF signalling in ischaemia reperfusion injury

Intervention	**Species**	**Outcome**	**Reference**
Pretreatment with $CoCl_2$ (30 mg/kg $CoCl_2$ 24 hours prior to ischaemia reperfusion)	Mouse	Significantly reduced infarct size	Xi et al. (2004)
Pretreatment with DMOG (20 mg/kg 24 hours preceding ischaemia reperfusion)	Rabbit	Significantly reduced infarct size	Ockaili et al. (2005)
Pretreatment with $CoCl_2$ (20 mg/kg $CoCl_2$ 24 hours prior to ischaemia reperfusion)	Neonatal-piglets	Significantly reduced cardiomyocyte apoptosis	Kerendi et al. (2006)
Cardiac HIF-1α overexpression (HIF-1α overexpression, under control of α myosin heavy chain promoter)	Mouse	Significantly reduced infarct size and improved cardiac function 4 weeks post ischaemia reperfusion injury	Kido et al. (2005)
Acute PHD2 depletion via siRNA	Mouse	Significantly reduced infarct size; improved recovery of RPP	Natarajan et al. (2006)
Acute administration of DMOG (1 mg, 2 hours prior to ischaemia)	Mouse	Significantly reduced infarct size	Eckle et al. (2008)
Acute administration of siRNA against PHD2	Mouse	Significant reduction in infarct size	Eckle et al. (2008)
Partial genetic HIF-1α ablation (HIF-1$\alpha^{-/+}$)	Mouse	Complete loss of ischaemic preconditioning	Cai et al. (2008)
Genetically engineered reduction in PHD2 expression (8% of WT mRNA in heart)	Mouse	Significantly greater recovery of RPP	Hyvärinen et al. (2010)

Continued on next page

Table 4.1 – continued from previous page

Intervention	Species	Outcome	Reference
Cardiac specific PHD2 deletion	Mouse	Significantly reduced infarct size at 6 hours post reperfusion; Improved fractional shortening at 3 weeks	Hölscher et al. (2011)
Genetic PHD1 deletion	Mouse	Significantly reduced infarct size; significant reduction in degree of cardiomyocyte apoptosis	Adluri et al. (2011)
Pretreatment with DMOG (40 mg/kg 24 hours prior to ischaemia)	Rat	Significantly improved LV developed pressure	Poynter et al. (2011)
Genetically engineered reduction in PHD2 expression	Mouse	Significantly improved ejection fraction; significant reduction in apoptosis (both assessed 24 hours post reperfusion)	Kerkelä et al. (2013)
Pretreatment with G3K36OA (30 mg/kg 4 hours prior to ischaemia)	Rat	Significant reduction in infarct size	Ong et al. (2014a)
Cardiac specific inducible VHL deletion	Mouse	Significant reduction in infarct size	Ong et al. (2014a)
Cardiac specific HIF-1α deletion	Mouse	Significant increase in infarct size	Nanayakkara et al. (2015)
Cardiac specific inducible PHD3 deletion	Mouse	Significant reduction in infarct size three days post reperfusion	Xie et al. (2015)

Genetic deletion or reduction in PHD1 (Adluri et al., 2011), PHD2 (Eckle et al., 2008; Hölscher et al., 2011; Hyvärinen et al., 2010; Kerkelä et al., 2013; Natarajan et al., 2006), and PHD3 (Xie et al., 2015) have all been shown to be cardioprotective in ischaemia reperfusion injury. Similarly the inducible deletion of VHL in the heart is protective against IR injury, giving further support to the concept that increased HIF signalling is cardioprotective (Ong et al., 2014b). Furthermore, pretreatment of animals with both pan hydroxylase (Eckle et al., 2008; Kerendi et al., 2006; Ockaili et al., 2005; Poynter et al., 2011; Xi et al., 2004), and PHD specific (Ong et al., 2014b) inhibitors also confers protection from cardiac ischaemic injury.

In addition to the control of HIF accumulation via PHD activity (Ivan et al., 2001; Jaakkola et al., 2001; Masson et al., 2001), the transcriptional activity of HIF-1 is under the control of FIH1 (Mahon et al., 2001). FIH1 acts to negatively regulate HIF signalling. It is not known if reduced FIH1 function influences the degree of IR injury in the heart.

Evidence that a reduction of FIH1 function may be beneficial in the face of ischaemia reperfusion comes from the finding that miR-335 overexpression is cardioprotective in rat hearts undergoing ischaemia reperfusion injury (Wu et al., 2018). FIH1 is a target of miR-335, and overexpression of miR-335 in H9c2 cardiomyocytes reduces FIH1 mRNA, protein, and activity, whilst increasing HIF-1α transcriptional activity (Wu et al., 2018). This suggests that the miR-335 induced cardioprotection may be mediated, at least in part, by a reduction in FIH1 activity. Embryonic fibroblasts isolated from FIH1$^{-/-}$ mice exhibit elevated intracellular ATP, an enhanced glycolytic reserve, and an elevated rate of lactate production when exposed to hypoxia (Sim et al., 2018; Zhang et al., 2010), characteristics likely to be beneficial in the face of ischaemia reperfusion if they are recapitulated in the heart (Zuurbier et al., 2020).

The present study aimed to investigate the potential of FIH1 as a modulator of cardiac function following ischaemia reperfusion injury, utilising a FIH1 loss of function model. In the context of cardioprotection seen by loss of PHD function and pan-hydroxylase inhibition, it was anticipated that the loss of FIH1 function in the heart may provide protection, i.e. enhanced recovery of cardiac function following ischaemia reperfusion injury. Furthermore, due to the metabolic effects seen due to elevated HIF signalling, and indeed alterations in whole body metabolism seen in FIH1$^{-/-}$ mice and in cells derived from them, it was anticipated that glucose metabolism in the heart would be altered with FIH1 loss, and in particular the rate of glycolysis would be elevated.

4.3 Methods

Animals

FIH1$^{-/-}$ and littermate WT control animals were bred and genotyped as described in the general methods chapter. Mice were housed under standard laboratory conditions on a 12 hour light/dark cycle with ad libitum access to standard chow diet and studied at 10- 12 months of age. All animal experimentation was performed in accordance with the Home Office guidelines (The Animals (Scientific Procedures) Act, 1986) and local university of Nottingham guidelines and procedural requirements.

Isolated heart perfusion

Hearts were excised and cannulated as described in the general methods. Hearts were Langendorff perfused for 30 minutes, after which they were subjected to 30 minutes of low flow ischaemia (0.5 ml/minute/gww). Full flow was then restored and hearts reperfused for 30 minutes. Hearts were freeze clamped in Wollenberger tongs cooled to the temperature of liquid nitrogen at the end of the perfusion protocol. Hearts were then submerged in liquid nitrogen and stored at -80°C until further analysis. A further group of hearts were perfused as described until the end of ischaemia and freeze clamped. A schematic description of the study design is shown in figure 4.1.

Cardiac function was recorded throughout the perfusion protocols utilising a left ventricular balloon. Functional indices were calculated from the left ventricular pressure trace, and cardiac function was expressed in terms of rate pressure product ((RPP), the product of heart rate and developed pressure). Functional recovery from ischaemia reperfusion injury was determined as the proportion of the RPP at the end of reperfusion of the baseline RPP and expressed as a percentage.

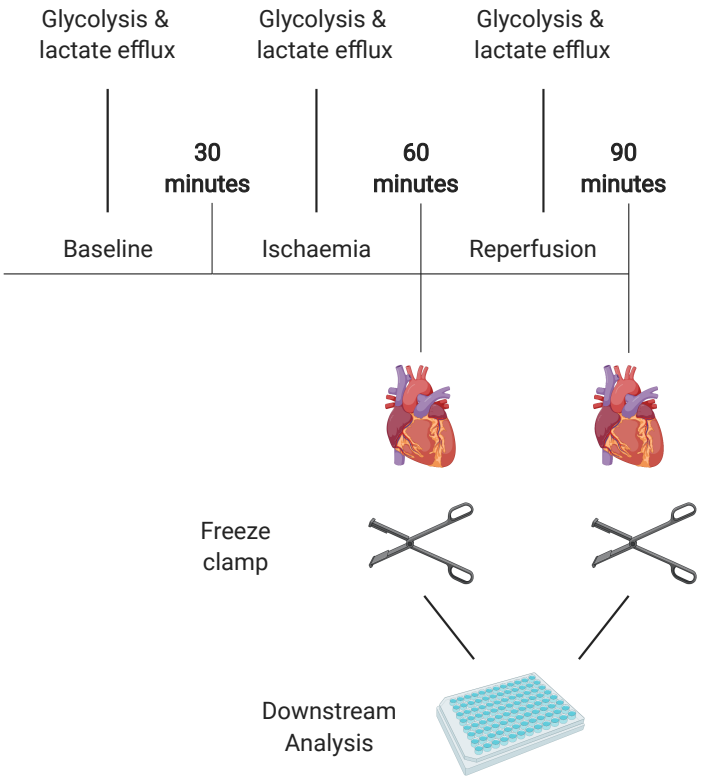


Fig. 4.1 Schematic representation of ischaemia reperfusion study design. FIH1$^{-/-}$ and WT hearts were Langendorff perfused and subjected to low flow ischaemia (0.5 ml/min/gww). Glycolytic flux and net lactate efflux were measured during baseline, ischaemia, and reperfusion as indicated. Cardiac function was assessed throughout via left ventricular balloon. Hearts were freeze clamped at the end of ischaemia, or the end of reperfusion as indicated.

Glycolytic flux

The rate of glycolysis was determined in the isolated hearts throughout perfusion. [5-^{3}H] glucose was utilised, and the rate of glycolysis was determined from the conversion of the labelled substrate into $^{3}H_2O$ in timed perfusate samples, as described in the general methods chapter.

Lactate efflux

The rate of net lactate efflux from the heart was determined by performing lactate assays, as described in the general methods, on the timed perfusate samples taken for determination of glycolytic flux. The rate of efflux was calculated using linear regression.

Cardiac tissue metabolite assays

A portion of ventricular tissue from the freeze clamped hearts was freeze dried overnight, and subsequently powdered and any connective tissue removed. Metabolites were extracted from this tissue using PCA. This metabolite extract was then utilised to assess the abundance of ATP, ADP, AMP, PCr, and free creatine. The total TAN pool and the energy charge of the heart were calculated as described in the general methods chapter. A separate portion of freeze dried tissue was utilised for the determination of glycogen, as described in the general methods chapter.

Statistical analysis

All data are reported as mean $\pm$ standard error. In all statistical analyses, results were considered to be statistically significant with $p \leq 0.05$. Comparisons between morphological characteristics of WT and FIH1$^{-/-}$ mice were made using unpaired two tailed t.tests.

All other data were analysed using a two-way ANOVA, with repeated measures where appropriate. In cases where significant main effects were observed, post hoc analysis was performed with Sidak correction for multiple comparisons. Data analysis were performed using R version 3.6.3.

4.4 Results

Morphological characteristics

Anthropometric details of the mice are described in table 4.2. There were no statistically significant differences between genotypes.

Table 4.2 Morphological characteristics of wild type and FIH1$^{-/-}$ mice, mean ± standard error

	WT	FIH1$^{-/-}$	p.value
Body weight (g)	31.6 ± 1.45	28.0 ± 1.14	0.062
Heart weight (mg)	208 ± 7.92	194 ± 9.15	0.243
HW/BW ratio (mg/g)	6.77 ± 0.355	7.00 ± 9.15	0.626

Values represent mean ± standard error (n = 17 WT and 16 KO). P values calculated by unpaired Student's t.test between genotypes.

Coronary flow

Hearts from FIH1$^{-/-}$ mice did not display any differences in coronary flow relative to controls. The coronary flow of hearts undergoing ischaemia reperfusion is shown in table 4.3, expressed in absolute terms and relative to heart weight. Coronary flow during ischaemia relative to baseline was 5.1% ± 0.31 in WT hearts and 4.7% ± 0.49 in FIH1$^{-/-}$ hearts (no difference between genotypes, p = 0.58). As such coronary flow during ischaemia represented an equivalent reduction in flow between genotypes, both relative to heart weight and baseline perfusion.

Hearts from FIH1 KO mice are protected from ischaemia reperfusion injury

Hearts from FIH1$^{-/-}$ mice display a degree of cardiac protection relative to WT controls.

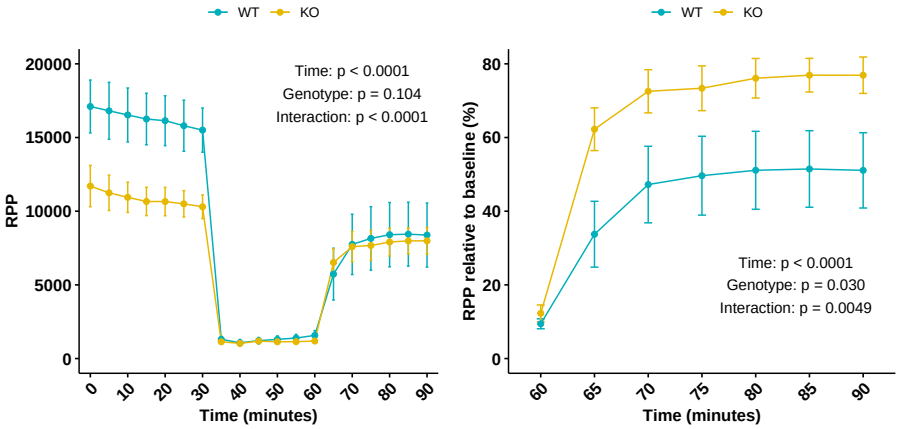
Table 4.3 Coronary flow of hearts from FIH$^{-/-}$ mice during baseline, ischaemia, and reperfusion

	WT	**FIH1$^{-/-}$**
Baseline (ml/min)	2.36 ± 0.194	2.32 ± 0.405
Baseline (ml/min/gww)	10.3 ± 0.733	11.7 ± 1.39
Ischaemia (ml/min)	0.115 ± 0.004	0.099 ± 0.007
Ischaemia (ml/min/gww)	0.500 ± 0.000	0.500 ± 0.000
Reperfusion (ml/min)	2.36 ± 0.241	2.20 ± 0.434
Reperfusion (ml/min/gww)	10.4 ± 0.925	11.0 ± 1.49

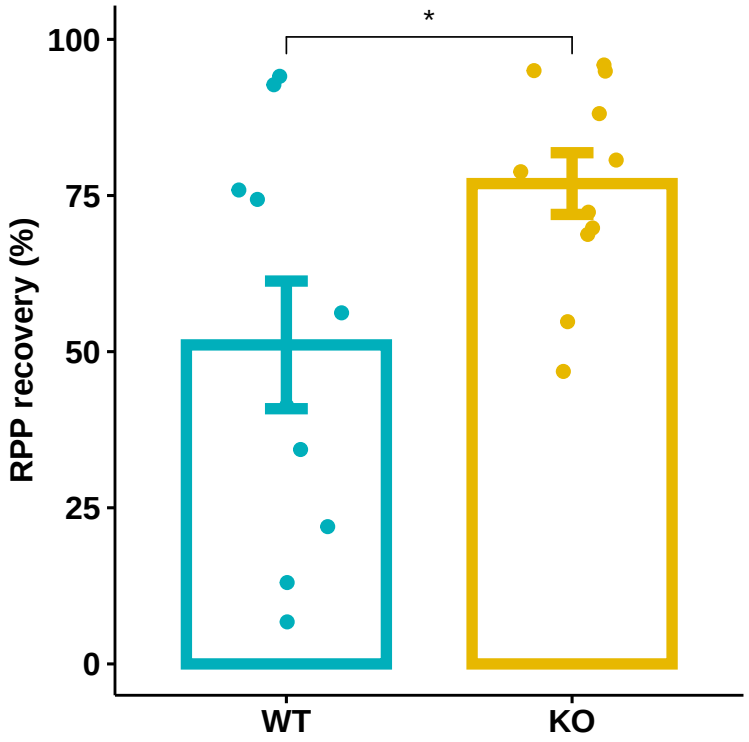
Values represent mean ± standard error expressed both in terms of ml/min and ml/min/gww (n = 10 WT and 11 KO). Two way ANOVA with repeated measures revealed significant main effect of time period, but no main effect of genotype or genotype:time period interaction.

Functional indices of hearts undergoing ischaemia reperfusion injury are displayed in figure 4.2. There was a clear abolishment of function during the ischaemic period (30-60 minutes 4.2a). The baseline function (RPP) was significantly greater in WT than KO hearts (RPP 15503 ± 1498 vs 10299 ± 804 ; $p < 0.01$). This modest impairment in baseline cardiac function is driven by a deficit in developed pressure, rather than heart rate (figure 4.3). The relative recovery of function of each heart was determined by expressing the RPP at the end of recovery to the RPP at the end during baseline perfusion (expressed as a %, figure 4.2b). The final proportion of baseline function was 1.5 fold greater in KO that WT hearts ($p < 0.05$, figure 4.2c).

The enhanced recovery of function seen in FIH1$^{-/-}$ hearts is driven by a greater proportional recovery of developed pressure. The heart rate response to ischaemia reperfusion injury is similar in FIH1$^{-/-}$ and WT mice (figure 4.3a). Developed pressure during reperfusion, although approximately equal in absolute terms (figure 4.3c), is proportionally greater in FIH1$^{-/-}$ than WT hearts (figure 4.3d).



(a) (b)



(c)

Fig. 4.2 Cardiac function in WT and FIH1$^{-/-}$ hearts during ischaemia and reperfusion. 4.2a displays the RPP for WT and hearts during baseline (0-30 minutes) ischaemia (30-60 minutes) and reperfusion (60-90) minutes. 4.2b displays the function during reperfusion relative to baseline function (percentage RPP). 4.2c displays final function relative to baseline function. All data are mean $\pm$ standard error, * signifies $p < 0.05$, independent t.test (n = 10 WT and 11 KO).

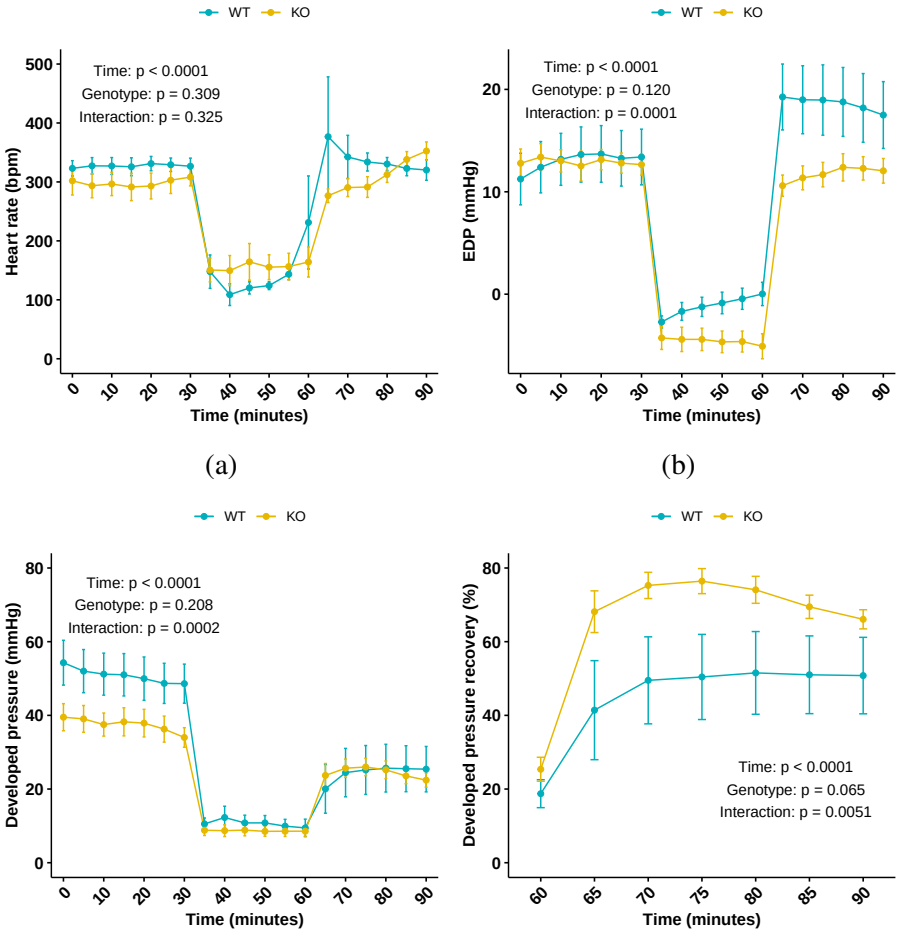


Fig. 4.3 Heart rate, end diastolic pressure, and developed pressure in WT and FIH1$^{-/-}$ hearts during ischaemia and reperfusion. Developed pressure in reperfusion relative to baseline was greater in FIH1$^{-/-}$ hearts (d). All data are mean $\pm$ standard error (n = 10 WT and 11 KO).

Hearts from FIH1 KO mice have accelerated glycolytic flux

Glycolytic flux was elevated in FIH1$^{-/-}$ hearts relative to WT controls (figure 4.4). In FIH1$^{-/-}$ hearts glycolytic flux was 1.3 and 1.6 fold greater than WT hearts in baseline and reperfusion respectively (both $p < 0.05$). FIH1$^{-/-}$ hearts also showed evidence of increased lactate production (figure 4.5). There was a significant main effect of genotype on the rate of net lactate efflux ($p < 0.05$), and a significant main effect of time period ($p < 0.001$), but no significant genotype-time interaction. Post hoc analysis did not reveal significant differences in net lactate efflux between genotypes at any individual time point. The total net lactate production of the heart (relative to heart weight) across the whole perfusion protocol was greater in FIH1$^{-/-}$ hearts than WT (figure 4.5b, 11.0 ± 0.99 vs 8.1 ± 0.51 μmol/gww, $p = 0.026$) .

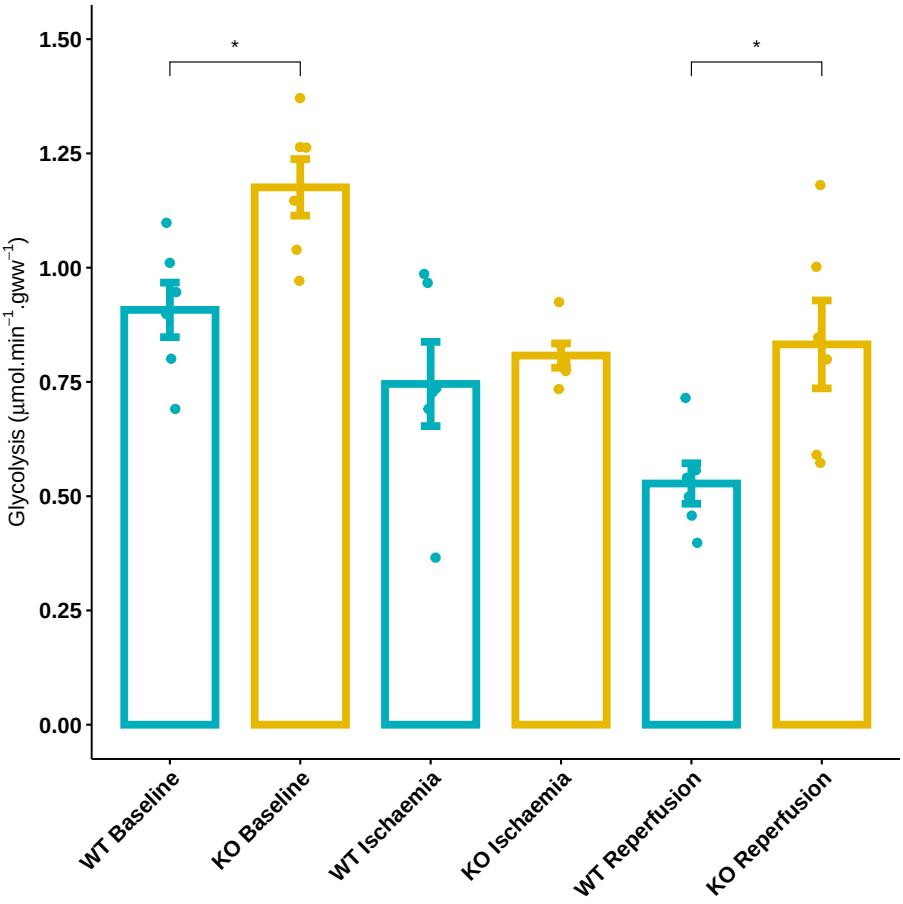
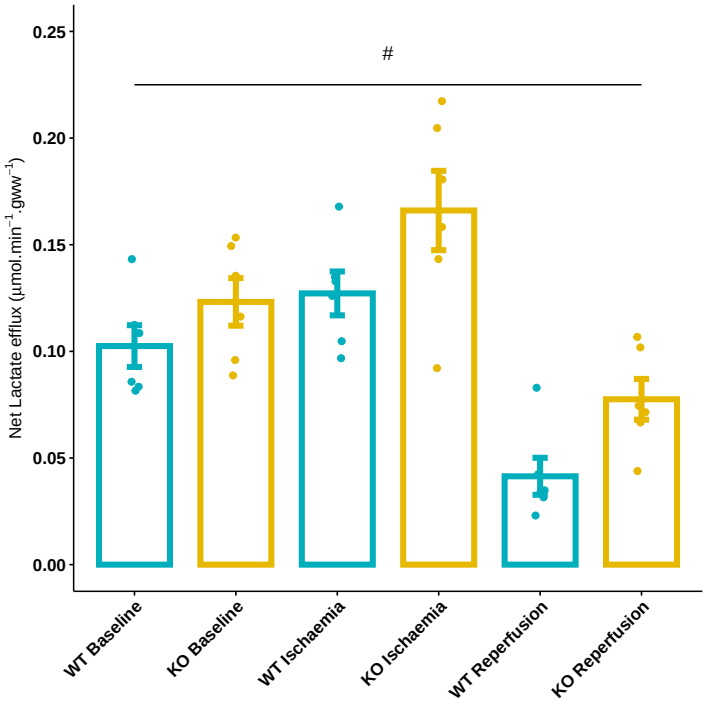
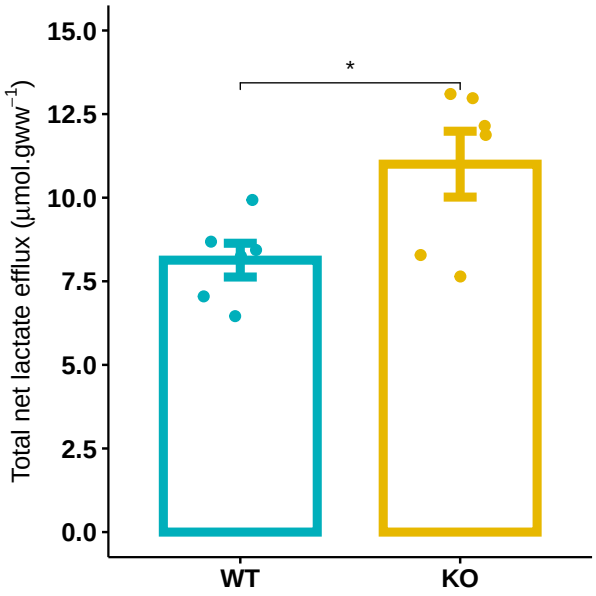


Fig. 4.4 Glycolytic flux in FIH1$^{-/-}$ and WT hearts during baseline, ischaemia, and reperfusion. All data are mean ± standard error, * represents significant difference between genotypes at given time point ($p < 0.05$).



(a)



(b)

Fig. 4.5 Net lactate efflux from FIH1$^{-/-}$ and WT hearts during baseline, ischaemia, and reperfusion. ANOVA revealed significant main effect of genotype and time period, adjusted p.values from post hoc analysis did not reveal a significant effect of genotype at any individual time point, (4.5a). The total net lactate efflux over the 90 minute perfusion protocol (4.5b) was significantly greater in KO than WT hearts. All data are mean $\pm$ standard error, # signifies a significant main effect of genotype, * signifies $p < 0.05$, independent t.test.

4.4.1 Tissue metabolites

Glycogen

Glycogen stores were significantly reduced in ischaemic hearts in comparison to hearts that also underwent reperfusion. This effect was present in both WT ($p < 0.001$) and FIH1 $^{-/-}$ ($p < 0.0001$) hearts. There was, however, no significant effect of genotype, or genotype - time point interaction effect upon tissue glycogen (figure 4.6).

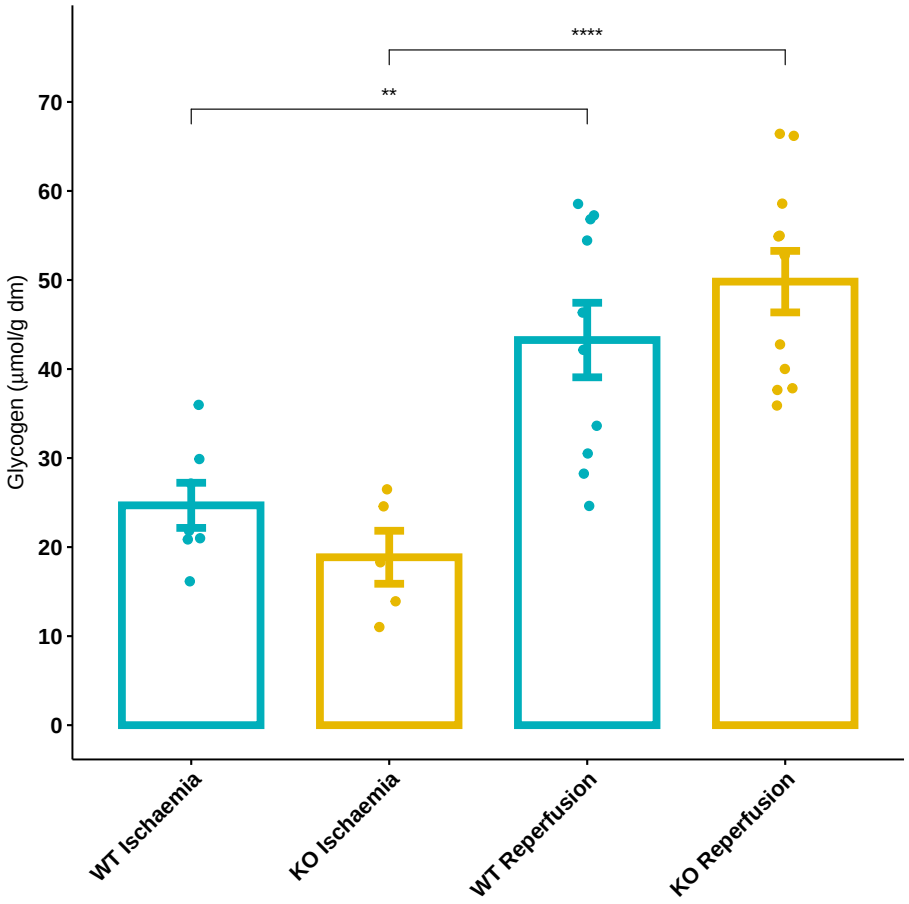
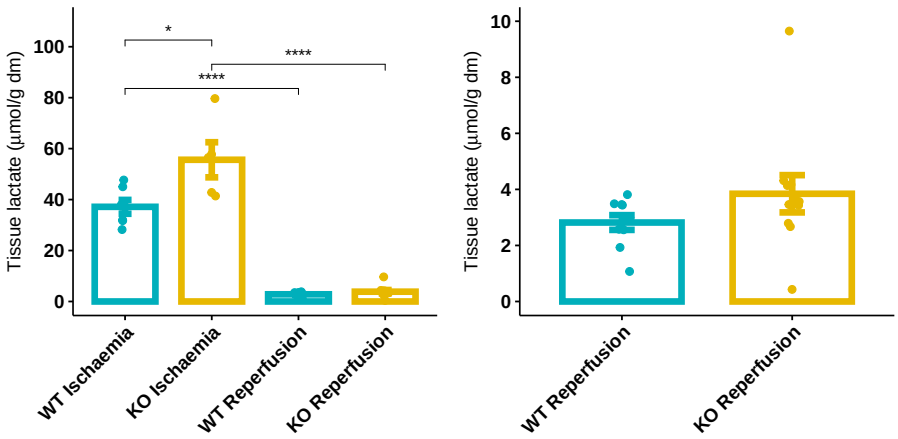


Fig. 4.6 Glycogen content of WT and FIH1$^{-/-}$ hearts following ischaemia or ischaemia-reperfusion. Bars represent mean ± standard error,** represents $p < 0.01$, and **** represents $p < 0.0001$ relative to the same genotype. ANOVA revealed no significant effect of genotype and no significant genotype-condition interaction.

Tissue Lactate

The degree of lactate accumulation in the ventricular tissue was far greater in hearts frozen at the end of ischaemia relative to those that underwent reperfusion (approximately 13 fold in WT and 15 fold in FIH1$^{-/-}$ hearts, both $p < 0.0001$). Furthermore, the degree of lactate accumulation in ischaemic FIH1$^{-/-}$ hearts was greater than ischaemic WT hearts ($p < 0.05$, figure 4.7a). There was no significant difference in tissue lactate between genotypes in reperfused hearts 4.7b.



(a) (b)

Fig. 4.7 Lactate content of WT and FIH1$^{-/-}$ hearts following ischaemia or ischaemia-reperfusion. Bars represent mean ± standard error, ** represents $p < 0.01$, and **** represents $p < 0.0001$ relative to the same genotype. All hearts are displayed in (a) and hearts that underwent reperfusion are plotted again in (b) on an appropriate scale.

High energy phosphate metabolites

There were substantial differences in high energy metabolites and energy status of hearts that had been perfused to the end of ischaemia in comparison to those that also underwent subsequent reperfusion (figures 4.8 and 4.9). In all cases, however, although significant differences within genotypes between the two time points were present, there were no significant main effects of genotype, or genotype- time point interactions. The ATP concentration in hearts did not

differ significantly between ischaemic and reperfused hearts of either genotype. However, due to differences in ADP and AMP concentrations (data not shown), there was significantly greater energy charge in reperfused hearts relative to ischaemic hearts of the same genotype (figure 4.8). This was despite a reduction in the total TAN pool in reperfused hearts relative to those that did not undergo reperfusion (4.8c).

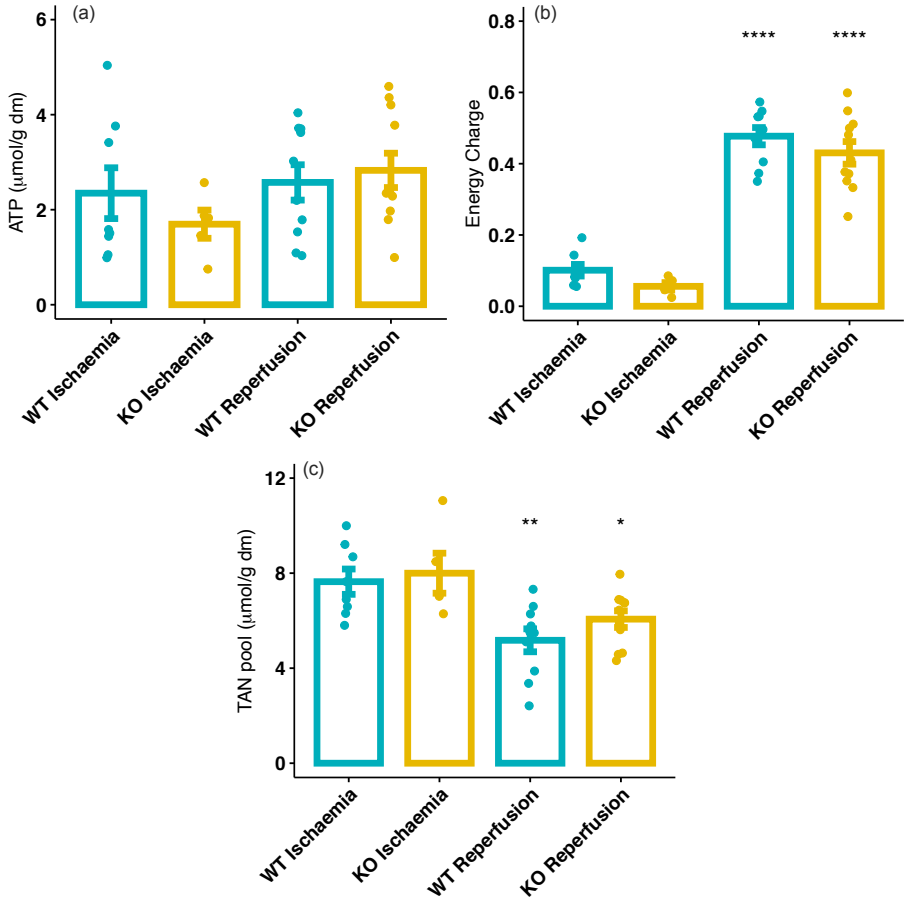


Fig. 4.8 ATP content (a), energy charge (b) and total TAN pool (c) of WT and FIH1$^{-/-}$ hearts following ischaemia and ischaemia reperfusion. Bars represent mean ± standard error, * represents $p < 0.05$, ** represents $p < 0.01$, and **** represents $p < 0.0001$ all relative to the ischaemic time point for the same genotype. ANOVA revealed no significant effect of genotype and no significant genotype-condition interaction.

PCr was significantly greater in reperfused hearts, relative to ischaemic (figure 4.9a). Free creatine concentration shows the inverse relationship, with reperfused

values lower in the reperfused state (figure 4.9b). The total creatine pool was significantly lower in reperfused WT hearts in comparison to hearts of the same genotype that did not go reperfusion. This was not seen, however, in FIH1$^{-/-}$ hearts (figure 4.9c).

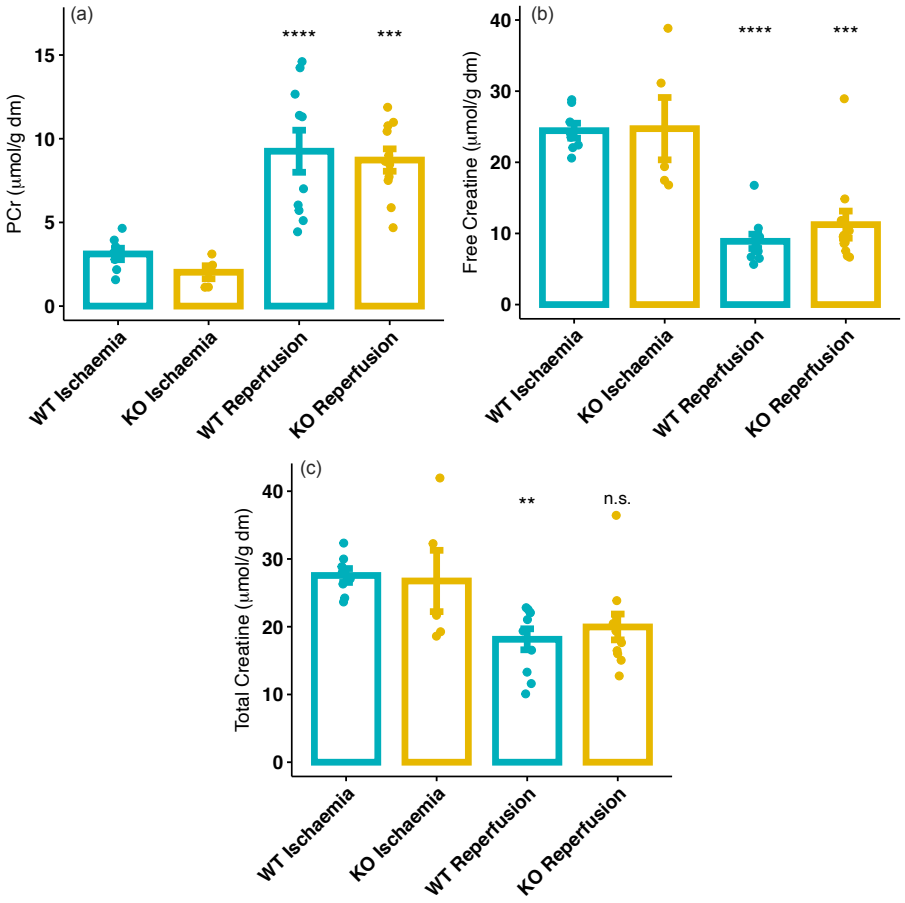


Fig. 4.9 PCr (a), free (b), and total creatine content (c) of WT and FIH1$^{-/-}$ hearts following ischaemia and ischaemia reperfusion. Bars represent mean ± standard error, ** represents $p < 0.01$, and **** represents $p < 0.0001$ all relative to the ischaemic time point for the same genotype (n.s. = no sig. difference). ANOVA revealed no significant effect of genotype and no significant genotype-condition interaction.

4.5 Discussion

There is substantial evidence that promoting HIF-1α signalling can promote recovery in cardiac ischaemia reperfusion injury (table 4.1). It was not previously known, however, if cardioprotection could be achieved through loss of FIH1 function. The principle aim of the present investigation was to evaluate the loss of FIH1 function during cardiac ischaemia reperfusion injury. As such, the main finding is that the FIH1$^{-/-}$ heart had a greater degree of functional recovery following ischaemia reperfusion. This was in parallel to metabolic differences between FIH1$^{-/-}$ and WT control hearts. This is the first report of cardioprotection in ischaemia reperfusion injury due to FIH1 loss of function. This finding is in agreement with findings that manipulation of the HIF system via modulation of PHD function can affect the degree of ischaemia reperfusion injury in the heart (Hyvärinen et al., 2010; Ong et al., 2014a; Xie et al., 2015).

Functional performance of FIH1$^{-/-}$ hearts

The modest reduction in baseline function in FIH1$^{-/-}$ hearts (figure 4.2a) was driven predominantly by a reduction in developed pressure (figure 4.3c) . There was no difference in heart rate in FIH1$^{-/-}$ hearts. Equivalence in HR is in contrast to the modest tachycardia that has been reported in vivo (Zhang et al., 2010), suggesting, therefore, that elevation in heart rate reported in vivo with FIH1 loss is due to differences other than the intrinsic pace making of heart.

The finding of enhanced recovery of cardiac function in FIH1$^{-/-}$ hearts is novel and has not previously been studied. Several reports have provided evidence that pan-hydroxylase inhibition (e.g. DMOG) is cardioprotective in ischaemia reperfusion (Eckle et al., 2008; Ockaili et al., 2005; Poynter et al., 2011). This has predominantly been attributed to increased HIF-1 stabilisation due to inhibition of PHD enzymes. Indeed, both genetic (Adluri et al., 2011; Hölscher

et al., 2011; Hyvärinen et al., 2010; Kerkelä et al., 2013; Xie et al., 2015) and targeted pharmacological (Ong et al., 2014b) PHD specific inhibition have shown to be cardioprotective in the context of ischaemia reperfusion injury. The present investigation now provides evidence that loss of FIH1 function alone is cardioprotective.

Whether the loss of FIH1 function may provided additive effects above specific PHD inhibition cannot be determined from the present investigation, and would require studies utilising a combination of loss of function models to explore. The finding that FIH1 is active to lower oxygen tensions than PHD enzymes (Tian et al., 2011) and inhibition of FIH1 promotes expression of a subset of genes not induced by the inhibition of PHD enzymes alone (Chan et al., 2016), might suggest that there may be an additive effect. If that were the case, with a view to clinical translation, there may be a case for providing specific PHD inhibitors in parallel with FIH1 inhibition, this would have the benefit of being able to better titrate dosage, and also avoid off target effects associated with pan hydroxylase inhibition.

Metabolic flux

Although previous reports have highlighted metabolic perturbations in whole body (Sim et al., 2018; Zhang et al., 2010) and MEF (Sim et al., 2018) metabolism with FIH1 loss, prior to the results presented in this thesis, the specific effects in the heart were unknown. The robust increase in cardiac glycolytic flux seen in the FIH1$^{-/-}$ heart is a novel finding in this investigation (figure 4.4). This is in agreement with the increased glycolytic capacity seen in FIH1$^{-/-}$ MEFs (Sim et al., 2018), but is not associated with alterations in fatty acid metabolism (chapter 3- figure 3.1). This finding of accelerated glycolysis is also in agreement with PHD2 loss of function in the heart, which results in increased glycolytic gene

expression and increased lactate production (Hyvärinen et al., 2010), and also a mouse model of Chuvash polycythemia, a modest increase in HIF signalling, that causes accelerated glycolysis, but unaltered fatty acid metabolism in the heart (Slingo et al., 2016).

During ischaemia the lack of increase in glycolytic flux relative to baseline (figure 4.4) likely represents some degree of inhibition due to the large degree of lactate accumulation (figure 4.7) . The accumulation of lactate has an inhibitory affect on glycolysis in the heart (Rovetto et al., 1975). Nevertheless, the contribution of glycolysis to ischaemic energy production is substantial. Measurements of myocardial oxygen consumption in isolated mouse hearts prior to and during arrest by K^+ overload demonstrates that contraction accounts for approximately 72% of oxygen consumption (Boardman et al., 2009). Therefore, in the present study, where contractile function was essentially reduced to zero during ischaemia, the energy requirements of the heart can be assumed to be greatly reduced. As such, the rates of glycolytic flux, although in absolute terms not elevated, likely represent a greatly increased proportion of ATP synthesis occurring.

The increased cardiac functional recovery in the present study (figure 4.2) was concurrent with elevated glycolysis during reperfusion (figure 4.4). The elevated glycolysis in $FIH1^{-/-}$ hearts likely facilitated the greater degree of recovery. Glycolytic flux in early reperfusion is a requisite for functional recovery of the heart, and supports the restoration of ionic homeostasis (Jeremy et al., 1993).

Tissue metabolites

Ischaemia and subsequent reperfusion clearly elicited a large metabolic stress on the heart. The energy charge in hearts at the end of ischaemia is greatly depressed relative to reperfusion (figure 4.8). This occurred without any significant reduction in ATP concentration in ischaemic relative to reperfused hearts, and

was driven by changes in ADP and AMP concentrations. In agreement with this, results from previous investigations utilising ^{31}P nuclear magnetic resonance spectroscopy to assess ATP concentrations throughout low flow ischaemia reperfusion, show that ATP is lost during low flow ischaemia relative to baseline, and not recovered during reperfusion (Luptak et al., 2007). The dynamics of the creatine pool suggest that PCr was utilised to maintain ATP concentrations during ischaemia (a depletion of PCr and accumulation of free creatine figure 4.9). In the reperfused hearts there is substantial elevation of PCr, with reciprocal reduction in free creatine concentration. Although these data demonstrate that the heart undergoes an energy crisis during ischaemia, which is to some degree resolved upon reperfusion, they do not provide mechanistic insight into the enhanced functional recovery in the FIH1$^{-/-}$ heart, as no significant differences between genotypes were observed. The significant reduction in the size of the total creatine pool in WT hearts that underwent reperfusion, relative to ischaemic only hearts suggest a loss of creatine due to reperfusion (figure 4.9C). This may be due to loss of membrane integrity due to reperfusion damage. Indeed a significant effect was not seen in the FIH1$^{-/-}$ hearts, which had improved recovery of function, indicative of reduced damage to the myocardium.

Limitations

The present investigation provides evidence of altered glucose metabolism in the FIH1$^{-/-}$ heart. The use of ^{3}H glucose facilitated the measurement of glycolytic flux but did not allow for further analysis of glucose metabolism. The addition of a second ^{14}C -glucose label would afford concurrent analysis of glucose oxidation in real time. Furthermore, utilisation of stable isotope labelling (e.g. ^{13}C glucose) and subsequent metabolomic analysis may allow exact nodes of metabolic reprogramming to be identified.

A benefit of the isolated heart technique utilised in the present investigation is that cardiac function can be readily assessed without the influence of other physiological cues. However, in order to further explore potential therapeutic utilisation of FIH1 inhibition, assessing the effects using an in vivo model of ischaemia reperfusion would be required.

Conclusions

The present study identifies FIH1 as a modulator of cardiac function following ischaemia reperfusion injury. Furthermore, FIH1 is implicated in the control of cardiac glycolysis, with FIH1 loss accelerating glycolytic flux in the isolated perfused heart. Taken together these results suggest that FIH1 may be a possible target to promote ischaemic protection and glucose metabolism in the heart.

Chapter 5

Development of a CRISPR mediated protein tagging strategy to study the ability of acute chemical FIH1 inhibition to potentiate hypoxia induced angiogenic signalling

5.1 Abstract

Background VEGF-A is of principal importance to angiogenic signalling and a direct HIF-1α target. Augmented HIF signalling in the heart has been shown to be beneficial to recovery following myocardial infarction. FIH1 controls the transcriptional activity of HIF complexes and is active to lower oxygen tensions to PHDs which control the abundance of these complexes. It merits study, therefore, as to whether inhibition of FIH1 can potentiate the HIF/VEGF-A axis to promote angiogenic signalling in hypoxic cells.

Methods Novel bioluminescent techniques were employed to study HIF induced angiogenic signalling. Split Nano luciferase technology (HiBiT- LgBiT) was combined with CRISPR editing to develop bioluminescent assays. Hypoxia response element signalling and HIF-1α protein expression were assessed in HeLa cells with a HiBiT tag on the C terminus of the HIF-1α gene. The VEGF-A gene was tagged with HiBiT in HUVECs in order to study the production of VEGF-A. Cells were treated with FIH1 inhibitor dimethyl N-oxalyl-D-phenylalanine (DM-NOFD) and cultured in either normoxia (room air) or hypoxia (1% O_2).

Results Treatment of HeLa cells with DM-NOFD in hypoxia led to an approximate doubling in HIF signalling activity, with no enhancement of HIF-1α protein expression. DNA of HUVECs could be successfully CRISPR edited to incorporate a HiBiT at the 3' end of VEGF-A exon 8a. This allowed bioluminescent measurements of both intracellular and extracellular VEGF-A to be made. In HUVECs, DM-NOFD treatment did not enhance the production of VEGF-A in hypoxia.

Conclusion The present investigation developed and demonstrated the efficacy of CRISPR mediated protein tagging to monitor the production of VEGF-A. The inhibition of FIH1 did not enhance hypoxic VEGF-A production, despite evidence of enhanced HIF signalling. The methods developed in this chapter

show promise for further investigation of VEGF-A biology and application to other proteins of interest.

5.2 Introduction

Vascular endothelial growth factor A (VEGF-A) is key mediator of angiogenesis and is a direct target of HIF-1α (Semenza, 2010). Cardiac specific deletion of HIF-1α leads to a reduction in both VEGF-A mRNA and decreased vascularity in the the left ventricle (Huang et al., 2004), underlining the importance of the HIF-1α- VEGF-A axis in the heart. Furthermore, angiogenesis is key to recovery of cardiac function following myocardial infarction (Wu et al., 2021a), with activation of the HIF-1α - VEGF-A signalling axis shown to be activated early in the hearts of patients in acute myocardial ischaemia (Lee et al., 2000).

In an experimental myocardial infarction model (permanent left anterior descending artery (LAD) ligation in rats) there is clear induction of HIF-1α in the tissue surrounding the infarcted region (Willam et al., 2006). There are several strands of evidence that suggest augmenting the HIF-1α signal post infarction may prove to be beneficial. In mice housed in hypoxia (7% O_2) for four weeks following LAD ligation there was an increase in cardiac vascularity and enhanced recovery of ejection fraction relative to normoxic controls (Nakada et al., 2017). Support for this effect being HIF mediated is given by the finding that inducible knock down of PHD2 following LAD ligation leads to a substantial improvement in ejection fraction and a reduced infarct size (Jatho et al., 2021).

As HIF signalling is constrained by FIH1 in addition to PHDs, it is important to consider if reduction in FIH1 activity may also be cardio protective post infarction. Injection of shRNA targeting PHD2 in mouse hearts following LAD ligation leads to an enhancement of angiogenic gene expression, and increased left ventricular ejection fraction. Importantly, these effects could be substantially enhanced by co injection with shRNA targeting FIH1 (Huang et al., 2011). These data support a role for FIH1 inhibition in enhancing HIF-1α mediated post infarction cardiac protection. As there is HIF-1α induction in the peri-infarcted region of

hearts (Willam et al., 2006), it is interesting to consider if FIH1 inhibition could enhance the HIF-1α signal to promote angiogenic signalling and improve cardiac performance. With a view to clinical translation, this would have a distinct benefit of augmenting endogenous signalling, thereby reducing the potential for off target effects.

Alternative splicing of VEGF-A can regulate its angiogenic activity (Chapter 1, table 1.1). Consequently, when investigating VEGF-A signalling it is important to consider the expression of different splice variants. Typical methods to investigate VEGF-A expression are limited by sensitivity, and also, in the case of antibody based techniques, can display poor discrimination between splice variants. For example, the commonly used R & D Systems Human VEGF Quantikine ELISA Kit, has a limit of detection of approximately 5 pg/ml (approximately 262 pM) and shows reactivity with recombinant $VEGF_{165}b$. It is imperative, therefore, to have methods that are adequately sensitive and that can differentiate between splice variants.

Alternative approaches to monitor VEGF-A production

Bioluminescent technologies offer an alternative approach to monitor cellular protein expression. NanoLuc is an engineered luciferase, originally isolated from a deep sea shrimp, that is small in size (19 kDa) and emits bioluminescence that is many folds brighter than renilla or firefly luciferase (Hall et al., 2012). Furthermore, two complementing subunits of split NanoLuc can recombine to form a functional, bright luciferase. This system comprises of a small 11-amino acid subunit (HiBiT), and a larger 18- kDa polypeptide (LgBiT), with a very high affinity (Kd ~0.7 nM) (Dixon et al., 2016). In addition to the strength of this split NanoLuc technology in investigating protein-protein interactions, addition of exogenous purified LgBiT to cell systems expressing proteins with a C-terminal

HiBiT tag provides a method to assess protein expression (Schwinn et al., 2018). This technique has the distinct benefit of giving a linear response over 8 orders of magnitude, and detection at very low expression levels (10^{-19}M) (Schwinn et al., 2018; White et al., 2021).

The split NanoLuc bioluminescent techniques have been combined with CRISPR gene editing approaches to monitor protein production in different cell systems. Due to the small size of HiBiT, it has been effectively added to the C-terminus of a range of proteins, allowing for the quantification of their expression Schwinn et al. (2018). In addition to intracellular proteins, this has been performed with secreted proteins such as the chemokine CXCL12, with the HiBiT tag affording the ability to evaluate accumulation in culture media (White et al., 2021). This strategy, therefore, provides an attractive method to quantify the production of VEGF-A in hypoxia, with the possibility of targeting the HiBiT sequence to different exons of the VEGF-A gene to allow the determination of the expression of different splice variants.

Chapter aims

The present chapter aimed to:

1. Determine whether CRISPR mediated HiBiT protein tagging could provide a sensitive assay of hypoxia induced proteins, specifically VEGF-A

2. Evaluate the ability of acute FIH1 inhibition to enhance HIF signalling in hypoxia

3. Utilising the techniques developed in (1), assess the ability of FIH1 inhibition to potentiate hypoxia induced increases in VEGF-A production.

5.3 Results

HiBiT tagged HIF-1α HeLa cells provide a sensitive model to assay HIF-1α protein accumulation

To determine the suitability of HiBiT tagged HIF-1α HeLa cells as a model to investigate HIF-1α stabilisation cells were treated with a range of concentrations of proteasome inhibitor MG132 for either 1,2,3, or 6 hours. At the end of treatments a lytic assay was performed and luminescence read. The assay system demonstrated sensitivity to both increasing concentration, and increasing duration of MG132 treatment upon HIF-1α accumulations (figure 5.1a). An additional concentration response experiment was performed over 6 hours, and the degree of HIF-1α accumulation assessed via Western blot (figure 5.1b), giving further support to the results of the luminescence assay format.

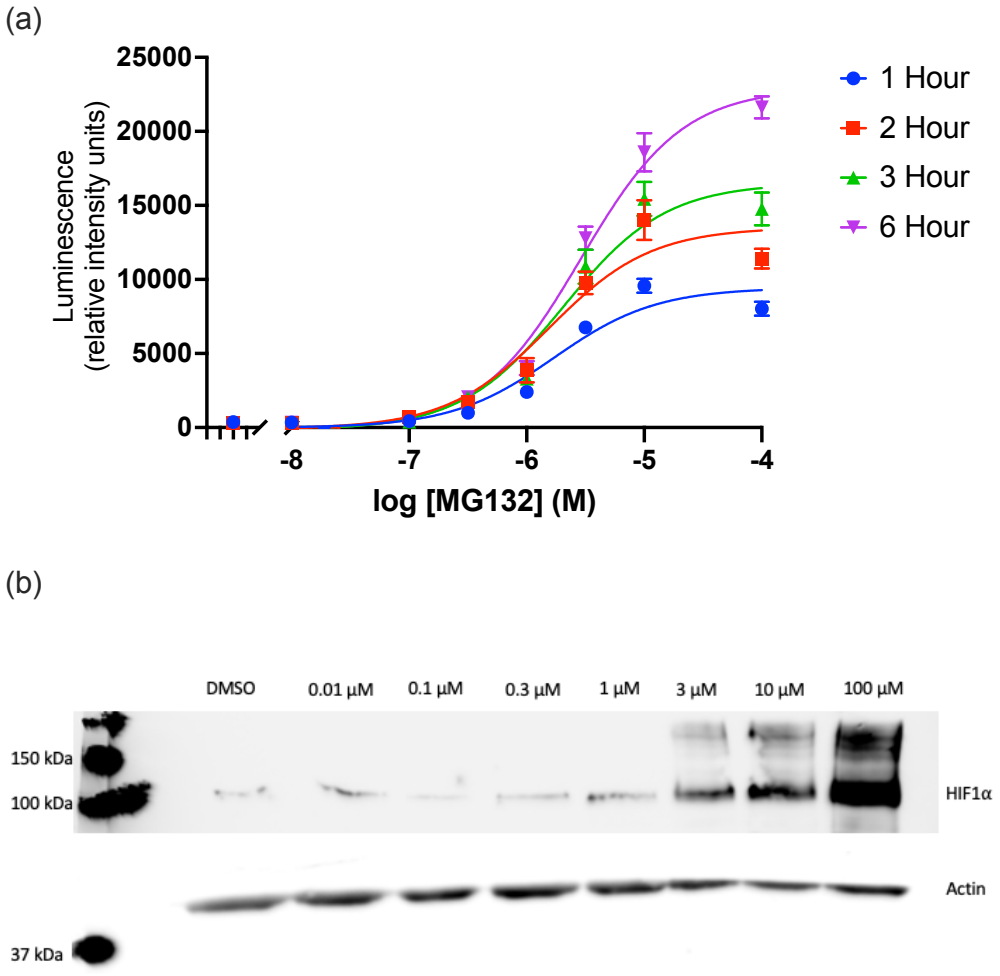


Fig. 5.1 Accumulation of HIF-1α in MG132 treated HeLa HIF-1α HiBiT cells. Cells were treated with proteasome inhibitor MG132 for indicated time periods and HIF-1α accumulation assessed by complementation with LgBiT protein, and addition of Furimazine (a), points represent mean of 6 independent experiments, bars represent standard error of the mean. A representative western blot displaying HIF-1α accumulation following six hours of treatment is shown (b).

DM-NOFD increases HRE signalling in Hypoxia

To evaluate the efficacy of DM-NOFD in enhancing HIF-1α transcriptional activity, hypoxia response element (HRE) signalling assays were performed in HeLa HIF-1α HiBiT cells. Following transfection with HRE Luciferase, cells were cultured in normoxia, or hypoxia (1% O_2) for 16 or 24 hours. Hypoxic culture induced a substantial induction of HRE signalling (figure 5.2a). When cultured in normoxia, DM-NOFD treatment did not cause an induction of HRE signalling (figure 5.2b). In hypoxia, however, DM-NOFD enhanced HRE signalling, with 500 μM treatment leading to 2.1 fold fold greater induction in HRE signalling than vehicle over a 16 h hypoxic period (figure 5.2c). To assess if the DM-NOFD induced increase in HRE signalling in hypoxia was related to any difference in HIF-1α protein accumulation, cells were cultured in hypoxia for 4 hours with or without 500 μM DM-NOFD treatment and lytic assay performed (as in figure 5.1). Culture in hypoxia caused a 5 fold increase in HIF-1α protein, which was not significantly altered by DM-NOFD treatment (figure 5.2d).

Collectively these data suggest that treatment of cells with DM-NOFD can enhance hypoxia response element signalling in cells cultured in 1% O_2. Furthermore the effect is not driven by an enhanced accumulation of HIF-1α protein, suggesting a direct effect upon transcriptional activity and as such a specific inhibitory effect upon FIH1. Based upon these results, a treatment of 500 μM DM-NOFD was utilised in all subsequent experiments.

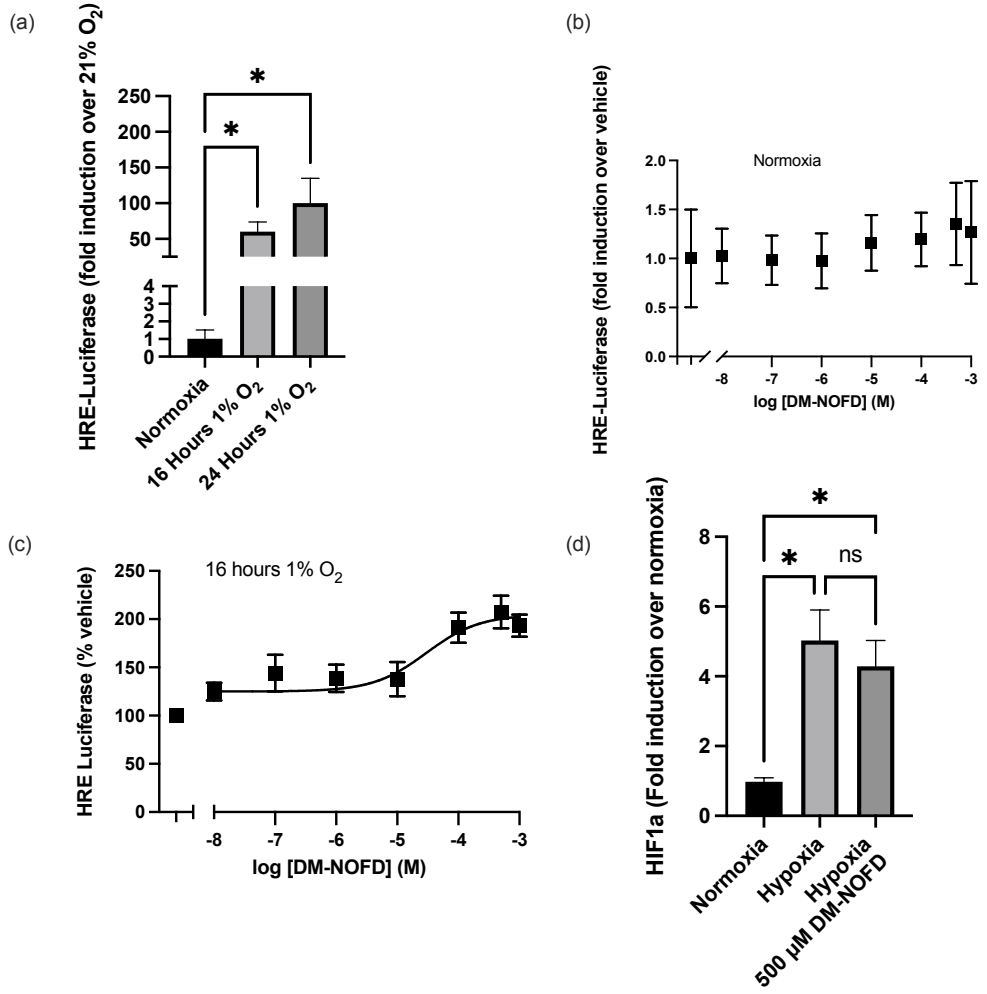


Fig. 5.2 HRE luciferase activity and HIF-1α stabilisation in HeLa HIF-1α HiBiT cells. HeLa HIF-1α HiBiT cells were transfected with HRE-Luciferase reporter and assays of HIF signalling performed (a,b,c). Exposure of cells to hypoxia (1% O_2) led to a substantial up regulation of HRE signalling (a). The treatment of normoxic cells for 16 hours with DM-NOFD did not lead to an induction of HRE signalling (b). Treatment with DM-NOFD during 16 hours hypoxic exposure led to a substantial enhancement of HRE signalling (c). Treatment with DM-NOFD does not alter the HIF-1α protein response to 4 hours incubation in 1% O_2. All data represent the mean $\pm$ standard error from five independent experiments. * represents significant difference ($p < 0.05$) between indicated groups, one way ANOVA with with Tukey post-hoc test.

Development of a CRISPR editing HiBiT tag strategy to monitor VEGF production in HUVECs

In order to monitor VEGF production in HUVECs a CRISPR editing strategy was developed to tag VEGF with HiBiT via homology directed repair (HDR) and therefore allow measurements to be made via luminescence. The desired locations of HiBiT tagging were at the 3' end of exons 8a and 8b (figure 5.3a), therefore allowing for the determination of $VEGF_{xxx}a$ and $VEGF_{xxx}b$ isoforms respectively. To ensure that these sites could be successfully targeted via CRISPR, DNA was extracted from HUVECs and a 399 bp portion of the 3' end of the VEGF-A gene (containing exons 8a and 8b) was amplified via PCR (figure 5.3b). The PCR product was sequenced and aligned to the reference genome. The HUVEC DNA exhibited no single nucleotide polymorphisms (SNPs) and the desired PAM sites were intact (figure 5.3c). Guide RNAs and ssODN were designed to target each of the desired VEGF exons and introduce the 33 nucleotide HiBiT sequence via HDR (figure 5.3d).

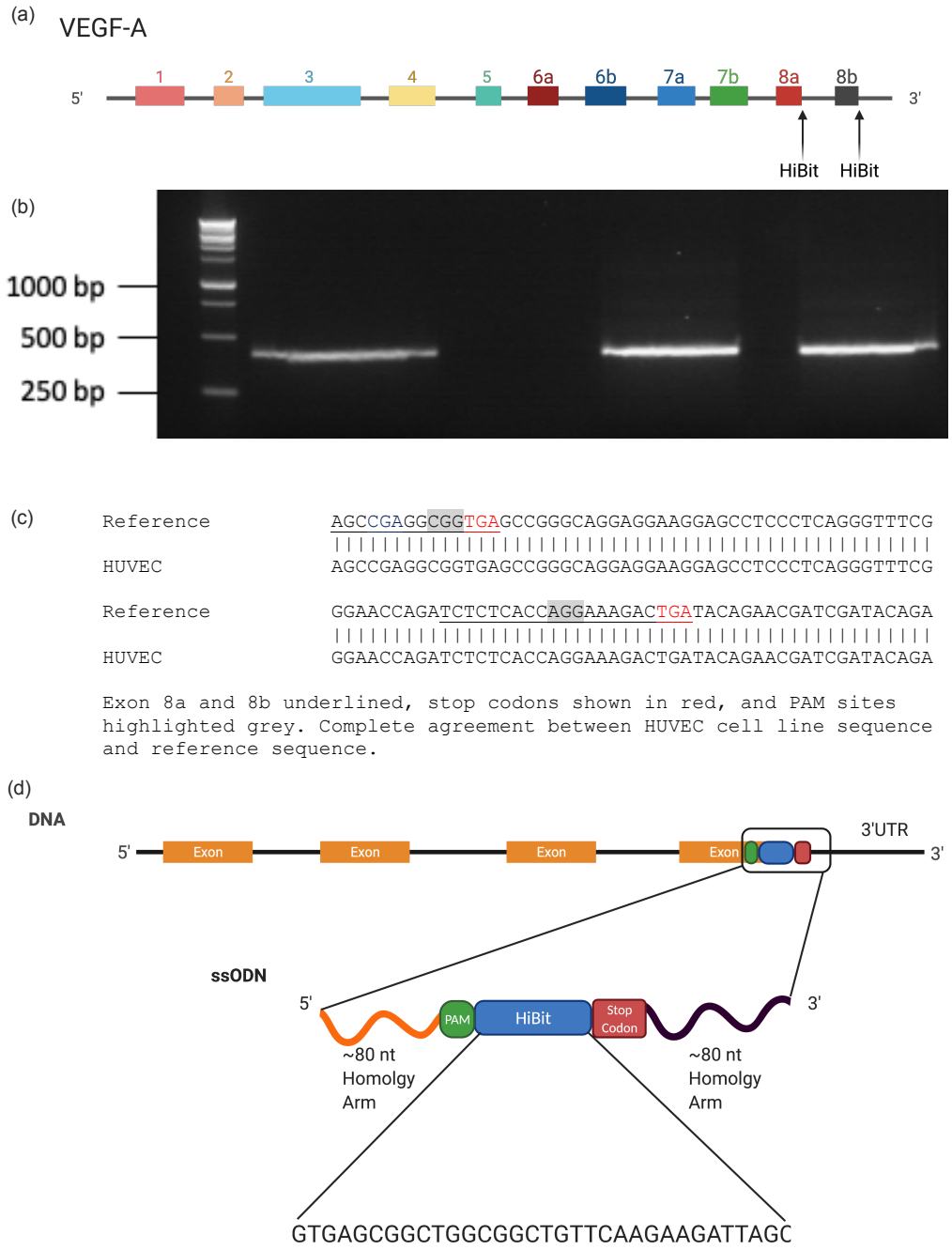


Fig. 5.3 Strategy for CRISPR mediated HiBiT tagging of VEGF-A exons 8a and 8b. VEGF-A gene is represented in (a), showing all exons, and the desired location for HiBiT tagging at the 3' end of exons 8a and 8b. A 399 bp portion of the 3' end of the HUVEC gene (containing exons 8a and 8b) from DNA isolated from HUVECs was amplified via PCR (b). The PCR product was Sanger sequenced and aligned to the reference genome with NCBI blast (c). The sequence is shown with exons 8a and 8b underlined, PAM sites in grey, and stop codons in red, demonstrating an absence of SNPs that would effect CRISPR editing at the desired sites. The general strategy for HDR is shown in (d), with the ssODN containing the HiBiT sequence.

A pilot experiment was performed where the CRISPR reagents were delivered to pools of HUVECs via electroporation, targeting HiBiT addition to either VEGF exon 8a or 8b. Cells were plated in 96 well plates and, following a 24 hour period to allow for cell adherence and CRISPR editing to occur, cultured in either normoxia or hypoxia (1% O_2). Media samples were taken at 24 and 48 hours and secretion of VEGF isoforms assessed via luminescence measurement. There was readily detectable secretion of VEGF-A with HiBiT tagged exon 8a in the media of both normoxic and hypoxic cells (figure 5.4). Signal from cells with the addition of HiBiT to exon 8b could not be readily detected above the signal generated by a media blank. These data suggest that either the 8b isoform is not readily expressed in these cells under the conditions tested, or, alternatively, the CRISPR editing process was unsuccessful in appending the HiBiT sequence to this exon. The signal from the media blank was relatively high in this assay, therefore, on all subsequent experiments a series of non edited cells included and luminescence from experimental conditions corrected by the luminescence given by non edited cells.

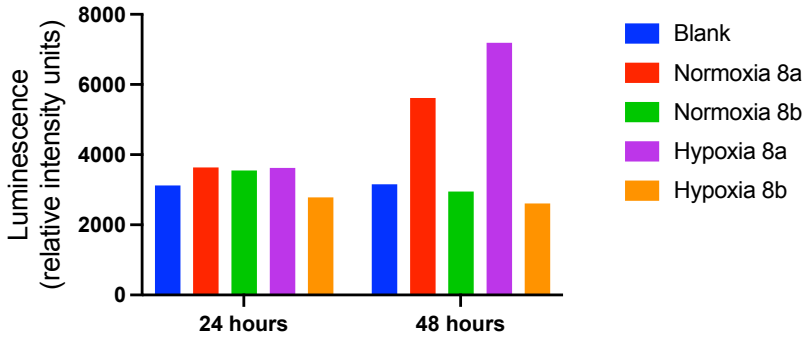


Fig. 5.4 Initial trial experiment of HiBiT tagged VEGF secretion from CRISPR edited HUVECs. Cells were electroporated with CRISPR reagents targeting either the 8a or 8b exon of VEGF-A in order to tag them with the HiBiT sequence. Cells were subsequently seeded in 96 well plates, then exposed to either normoxic or hypoxic (1% O_2) culture for 24 or 48 hours. At each time point, media was collected and subsequently assayed for Luminescence via addition of purified LgBiT protein and furimazine.

In order to determine the presence or absence of HiBiT addition to exon 8b, two pools of cells were electroporated with CRISPR reagents targeting either exon 8a or 8b. Cells were cultured for 5 days in T25 vessels, and then genomic DNA extracted. PCR was performed, targeting the same 399 bp region of the 3' end of the VEGF gene as in figure 5.3. In cells where exon 8a was targeted, a doublet PCR product was present, with the upper band representing a 33 bp shift (the size of the HiBiT insert). In cells where exon 8b was targeted, however, there was no evidence of a secondary PCR product (figure 5.5a).

To ensure the specificity of the double PCR product in the 8a targeted cells, and confirm the absence of such in the 8b targeted cells, a second PCR reaction was performed, where the forward primer was replaced with a primer corresponding to the final 22 nucleotides from the HiBiT sequence. This demonstrated a specific product with DNA from exon 8a targeted HUVECs, but no observable product with DNA from exon 8b targeted cells (5.5b). These data demonstrate that the CRISPR editing strategy led to the successful insertion of HiBiT at exon 8a, but not exon 8b.

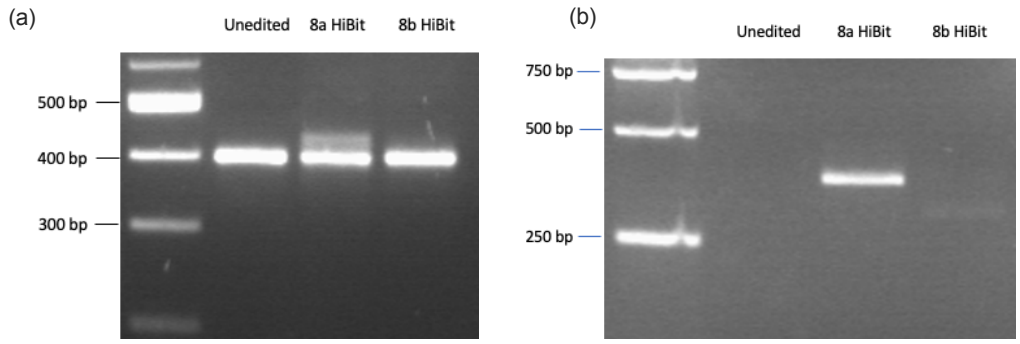


Fig. 5.5 Assessment of CRISPR mediated HiBiT tagging of VEGF-A exon 8a and 8b. Genomic DNA was edited from WT HUVECS, and HUVECS CRISPR edited to target the addition of the HiBiT sequence to the c terminal of either exon 8a or 8b of the VEGF-A gene. DNA was amplified via PCR with primers targeting a 399 bp region of the VEGF-A gene, flanking exons 8a and 8b and separated on a 3% agarose gel. DNA from exon 8a targeted cells demonstrates a double band, with the upper band representing a 33 bp increase in product size (i.e. the size of the HiBiT insert). DNA from 8b targeted cells did not display a double band (a). To give further confirmation of effective HiBiT addition to exon 8a but not 8b, an additional PCR reaction was performed, with the forward primer replaced with a primer corresponding to the final 22 nucleotides of the HiBiT sequence (b). This showed effective amplification of exon 8a targeted DNA, but no product in 8b targeted DNA.

In an attempt to optimise the CRISPR editing at exon 8b the quantity of both the RNP complex (guide RNA and Cas9 protein) and the ssODN were varied. Pools of HUVECs were electroporated with CRISPR reagents targeting exon 8b, with either double the concentration of RNP, or double the concentration of ssODN. Genomic DNA was extracted from these cells and PCR performed in the same way as described for figure 5.5. Neither the increase in amount of the RNP complex, nor the ssODN delivered to cells, led to any detection of a 33 bp shift in the 399 bp PCR reaction (figure 5.6a). Similarly, none of the trialled optimisations led to a detectable product in the PCR reaction with the forward primer based on the HiBiT sequence (figure 5.6b). Collectively these data suggest that CRISPR mediated HiBiT tagging of VEGF exon 8b at this PAM site is not possible, at least to any degree that has experimental utility. As such CRISPR targeting of exon 8b was not performed in any subsequent experiments.

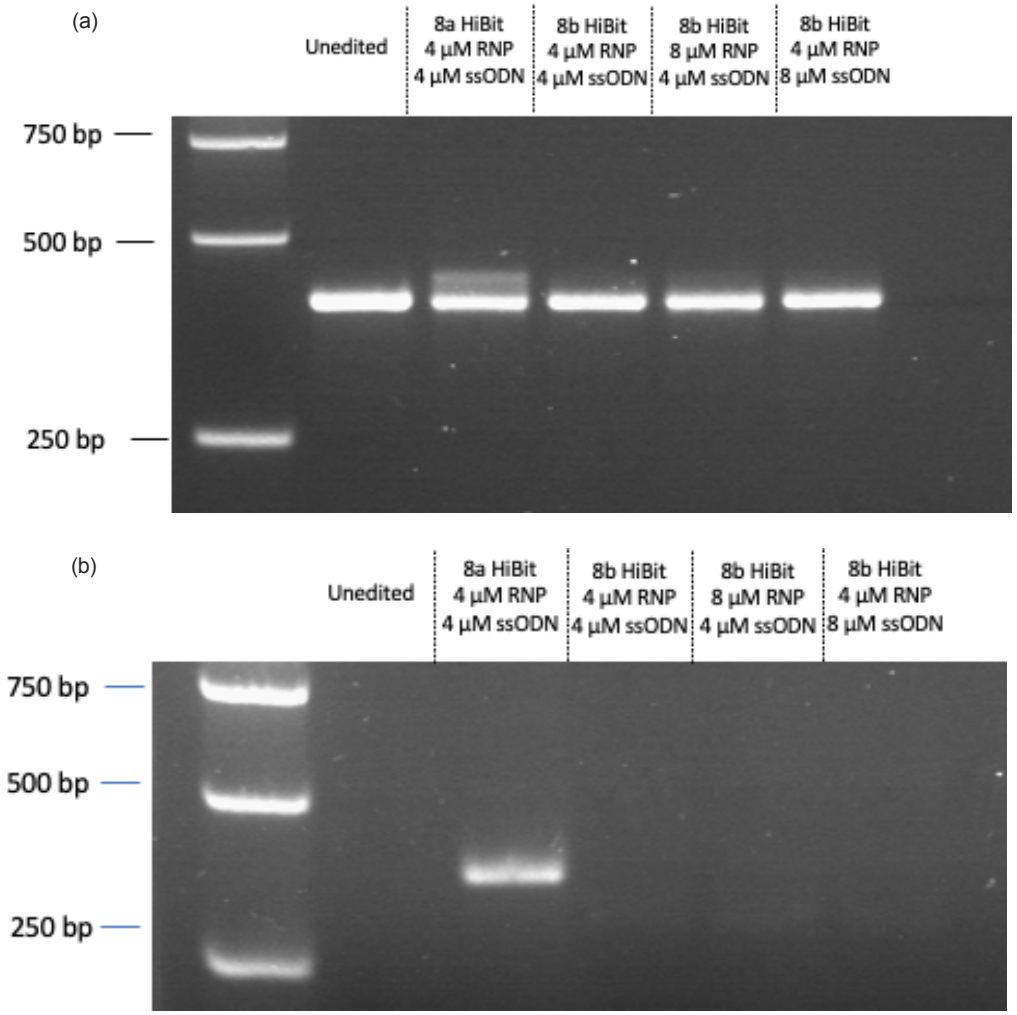


Fig. 5.6 Optimisation of CRISPR mediated HiBiT tagging of VEGF-A exon 8b. Amounts of either RNP complex or ssODN were increased in an attempt to improve the efficacy of exon 8b HiBiT tagging. Genomic DNA was extracted from cells, PCR performed with primers flanking exon 8a and 8B of the VEGF-A gene, and PCR products separated on a 3% agarose gel (a). There was no evidence of a 33 bp shift in PCR product that would indicate successful incorporation of the HiBiT sequence. A second PCR reaction was performed with the forward primer replaced with a primer corresponding to the final 22 nucleotides of the HiBiT sequence. This confirmed an absence of HiBiT sequence incorporation in any of the exon 8b targeted cells (b).

Assessment of the effect of DM-NOFD treatment upon VEGF production in HUVECs

To address the core question of whether the inhibition of FIH1, through DM-NOFD treatment, can enhance the production of VEGF under hypoxia, experiments were performed in HUVECs utilising the HiBiT tagged exon 8a strategy. Cells were electroporated with CRISPR RNP complex and ssODN to append the HiBiT tag onto exon 8a, as in figures 5.4 & 5.5. Following electroporation cells were plated into 96 well plates at a density of $6x10^3$ per well and cultured for two days. Subsequently, cells were treated with experimental media conditions (control (M200 +2% LVES), control + vehicle (0.5% dimethyl sulfoxide (DMSO)), or control + DM-NOFD (500 μM)). Cells were then cultured in either normoxia or hypoxia (1% O_2), and VEGF production assessed at 24, 48, and 72 hours.

At the desired time points, media was sampled from cells, and cells treated with glycosaminoglycan inhibitor surfen (Schuksz et al., 2008) (10 μM) for 30 minutes to release any remaining VEGF bound extracellularly, and then washed twice with HEPES buffered saline solution (HBSS). Cells where then subjected to a lytic assay, as performed for HIF-1α (figures 5.1 & 5.2d), affording the determination of intracellular VEGF via luminescent measurement. The sampled media was then assayed to quantify the degree of VEGF secretion.

A representative experiment is shown in figure 5.7, showing both secretion of VEGF into media (a) and the intracellular VEGF (b). These data demonstrate the utility of this experimental approach. There is a clear hypoxia induced up-regulation of VEGF production, detected both intracellularly and secreted into the media. There was however no significant effect of DM-NOFD treatment upon VEGF production.

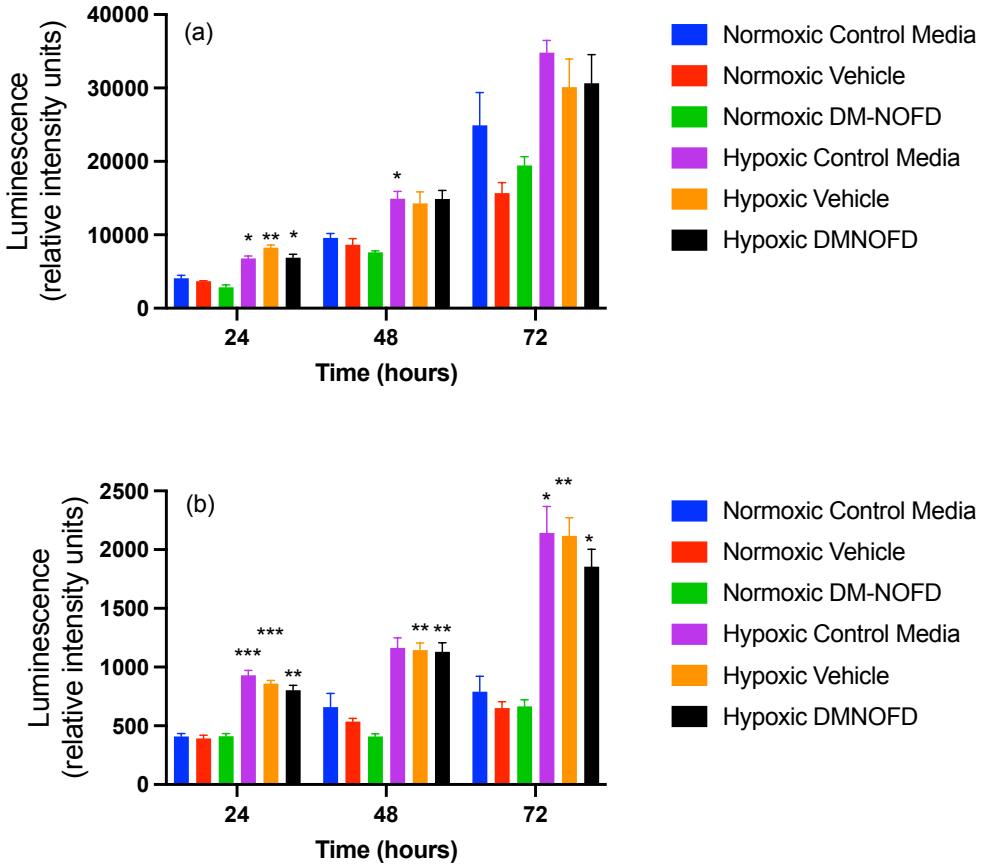


Fig. 5.7 The effect of DM-NOFD (500 µM) and hypoxia (1% O2) upon VEGF-A production in HUVECs with HiBiT tagged Exon 8A. CRISPR edited cells were plated in quadruplicate in 96 well plates, at 6,000 cells per well. Following 48 hours cells were treated with either control media (M200 +2% LVES), control media + vehicle (0.5% DMSO), or control media + 500 μM DM-NOFD, and cultured in normoxia or hypoxia for the indicated time periods. VEGF secreted into media is shown in (a) and intracellular VEGF represented in (b). Bars represent the mean of four replicate values $\pm$ standard error. Stars represent significant difference from corresponding normoxic value (Two-way ANOVA with Tukey post-hoc test; * p<0.05, ** p<0.005, ***p<0.001). No significant treatment effects within oxygen concentrations were present.

In order to confirm the absence of effect DM-NOFD treatment upon VEGF secretion further pools of HUVECs were CRISPR edited and the experiment shown in figure 5.7 repeated. Aggregate data from four independent pools of cells is shown in figure 5.8. The effect of DM-NOFD upon VEGF production in hypoxia was assessed via Wilcoxon matched-pairs signed rank test, demonstrating no significant effect in either secreted (figure 5.8a,c,e) or intracellular (figure 5.8b,d,f) VEGF-A production at either 24, 48, or 72 hours.

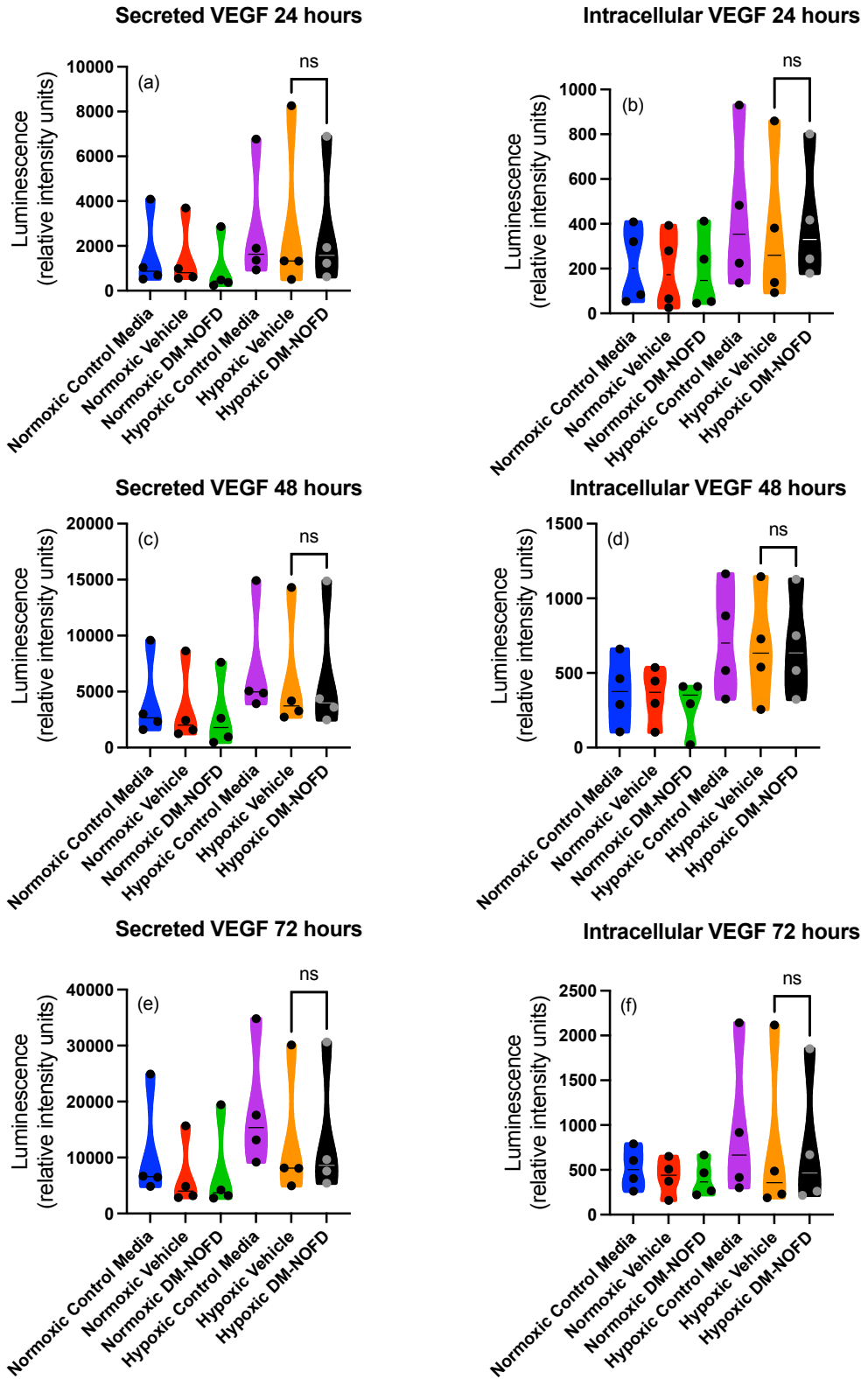


Fig. 5.8 Pooled data from n = 4 independent experiments each using unique pools of CRISPR edited HUVECs on the effect of DM-NOFD (500 μM) and hypoxia (1% O2) upon VEGF-A production. CRISPR edited cells were plated in quadruplicate in 96 well plates, at 6,000 cells per well. Following 48 hours cells were treated with either control media (M200 +2% LVES), control media + vehicle (0.5% DMSO), or control media + 500 μM DM-NOFD, and cultured in normoxia or hypoxia for the indicated time periods.

(continued overleaf)

Fig. 5.8 *(continued)* VEGF secreted into media is represented as Luminescence (relative intensity units) at indicated time points in (a,c,e) and intracellular VEGF represented in (b,d,e). Violin plots represent the median of four independent experiments with independent pools of edited cells, with individual values shown. The effect of DM-NOFD treatment upon VEGF production in hypoxia was assessed via a Wilcoxon matched-pairs signed rank test and found to be non-significant ($p > 0.05$; ns) in all cases.

CRISPR edited cells maintain HUVEC phenotype

In order to assess the effect of CRISPR editing upon HUVEC cell phenotype a pool of cells were either CRISPR edited (HiBiT addition to exon 8a), or left as un-edited WT controls, and seeded in 96 well plates. Media was refreshed following two days of culture, after which cells were cultured for a further 72 hours to give an equivalent time point to the longest time points used in VEGF production assays (figures 5.7 & 5.8). Cells were then fixed and co-stained for nuclei and endothelial marker CD31. Cells were subsequently imaged using an ImageXpress Micro widefield platereader (Molecular Devices, USA). Results from three independent pools of cells are shown in figure 5.9 a,b, and c. Both edited and WT cells show clear expression of CD31, and typical HUVEC cobblestone morphology (Jiménez et al., 2013; Müller et al., 2002). In a subset of cells primary antibody staining was omitted and cells stained with Hoerscht and secondary antibody alone. These cells show no green fluorescence (figure 5.9d), demonstrating that the CD31 signal from fully stained cells is not an artefact of aberrant secondary antibody staining. Collectively, these data show that the HUVECs used in VEGF production assays (figures 5.7 & 5.8) represent a valid endothelial cell model with no signs of loss of phenotype.

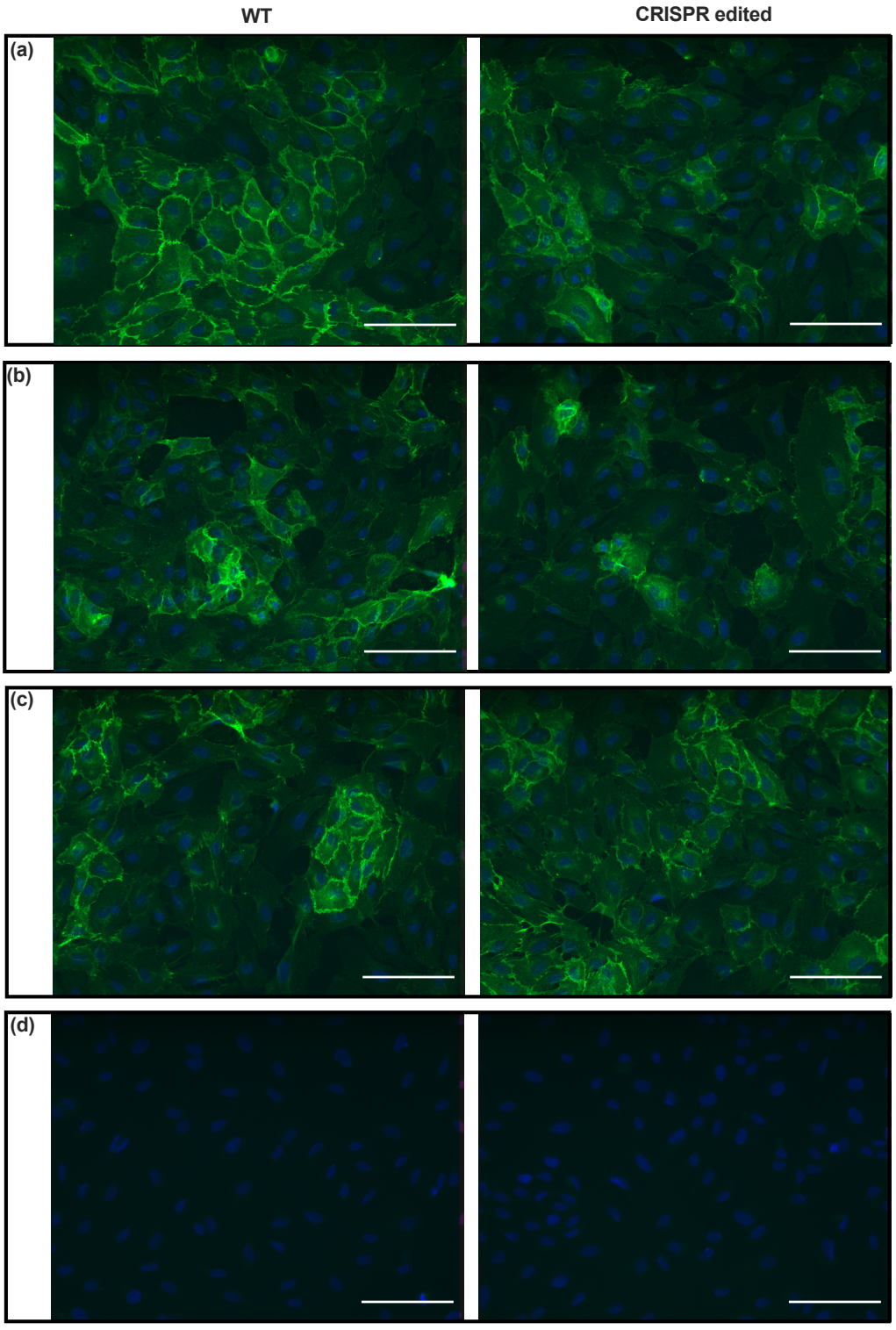


Fig. 5.9 CD31 expression in WT and CRISPR edited HUVECs. Unedited and CRISPR edited cells were seeded in black 96 well plates, and cultured for 5 days. Cells were fixed and stained for CD31 (green) and nuclei (blue) and imaged with a 20x objective. A, B, and C each represent independent experiments with unique pools of edited cells. D represents cells where primary CD31 antibody staining was omitted, demonstrating the absence of non specific secondary antibody binding. Scale bars represent 100 μm.

HiBiT tagged VEGF secreted from edited HUVECs binds to canonical receptors.

In order to determine the ability of HiBiT tagged VEGF to bind to its canonical receptors, conditioned media experiments were performed in HEK293T cells expressing either VEGFR2 or NRP1. To generate media containing HiBiT tagged VEGF, HUVECS were electroporated with CRISPR reagents to append the HiBiT sequence to VEGF 8a. Cells were subsequently cultured in a T25 flask in 4 ml of media, which was collected after 5 days.

HEK293T cells were transfected with plasmids encoding either VEGFR2 or NRP1, both with an LgBiT tag on the extracellular N terminus (Peach et al., 2021). Following transfection, cells were plated into 96 well plates at a density of $30x10^3$/well and allowed to attach for 24 hours. To perform the conditioned media assay, growth media from transfected HEK293T cells were washed with HBSS. Cells were then treated with conditioned media from CRISPR edited HUVECs for a period of 1 hour at 37 °C. Subsequently Furimazine was added, and bioluminescence read. To act as a positive control, a series of cells was treated with unconditioned media supplemented with 100 pM purified HiBiT. Cells treated with unconditioned media alone served as a negative control.

Conditioned media treatment of HEK293T cells expressing LgBiT tagged VEGFR2 displayed increased luminescence, indicating that the HiBiT tagged VEGF secreted by the edited HUVECs is biologically active and binds to this receptor (figure 5.10a). Similarly, treatment of HEK293T cells expressing LgBiT tagged NRP1, display a large luminescent signal when treated with CRISPR edited HUVEC conditioned media. Furthermore, the signal generated from conditioned media treatment of LgBiT tagged NRP1 transfected HEK293T cells could be greatly reduced (approximately 62%) by co treatment with 100 nM recombinant VEGF 165a (figure 5.10b).

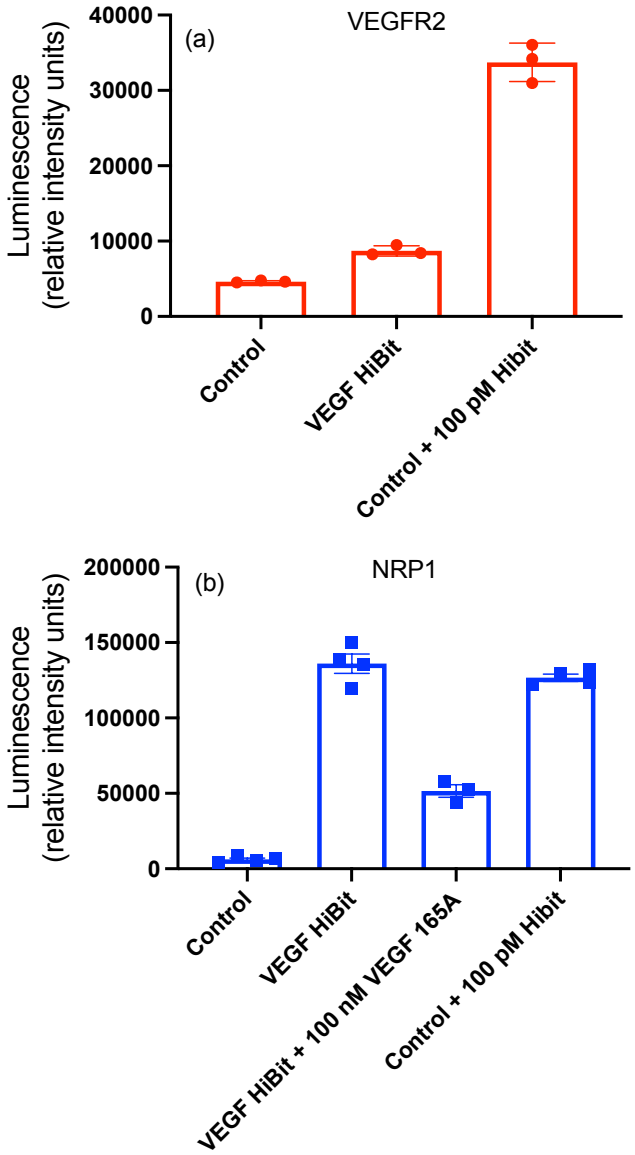


Fig. 5.10 HiBiT tagged VEGF from CRISPR edited HUVECs binding to LgBiT tagged receptors. LgBiT tagged VEGFR2 (a) and NRP1 (b) were transfected in to HEK293T cells. Cells were subsequently treated for one hour with either control media, conditioned media from CRISPR edited VEGF Exon 8a HiBiT tagged HUVECS, or control media supplemented with 100 pM purified HiBiT. Treatment with conditioned media led to bioluminescence. Co-treatment with recombinant VEGF165A alongside conditioned media from edited cells was able to substantially reduce luminescence produced from binding to LgBiT tagged NRP1 (b). Data are from a representative experiment, bars represent mean $\pm$ standard error, points represent individual data points.

5.4 Discussion

There is substantial evidence that promoting angiogenesis following myocardial infarction can enhance the recovery of cardiac function. Exploitation of the HIF-VEGF-A axis represents one possible avenue to achieve this. HIF signalling is constrained by both PHDs and FIH1, with the latter remaining active to lower oxygen tensions (Tian et al., 2011). The principal aims of the present study, therefore, were to assess the ability of FIH1 inhibitor DM-NOFD to enhance HIF-signalling in hypoxia and to develop bioluminescent methods to assess VEGF-A production as a means to do so.

CRISPR mediated HiBiT tagging of VEGF-A at exon 8a, but not exon 8b facilitated the development of an assay to monitor VEGF-A production in HUVEC cells. This technique was shown to be sensitive to hypoxia induced increases in VEGF-A production and demonstrated this effect not to be potentiated by treatment with the FIH1 inhibitor DM-NOFD. This is despite the finding that DM-NOFD treatment caused an approximate doubling of hypoxia response element signalling in hypoxic HeLa cells.

DM-NOFD can increase HRE signalling in hypoxia

The finding that DM-NOFD treatment can potentiate HRE signalling in hypoxia (figure 5.2) demonstrates the role of FIH1 in constraining the activity of HIF-1α signalling complexes at 1% O_2 culture conditions. These data suggest that HIF-1α is being Asn803 hydroxylated, impairing transcriptional activation, which can be overcome by treatment with the FIH1 inhibitor DM-NOFD. The assertion that this effect is mediated by FIH1 inhibition and therefore that DM-NOFD is specific to FIH1 as previously reported (McDonough et al., 2005), is supported by the finding that DM-NOFD treatment does not enhance HIF-1α protein expression, only its signalling. This finding could be further confirmed via the use of alternative

methods to disrupt FIH1, such as siRNA, which could also be used to ensure the specificity and mechanism of action of DM-NOFD (i.e. assessment of DM-NOFD treatment on FIH1 depleted cells).

A HiBiT tag could successfully be incorporated into the VEGF-A gene via CRISPR editing

A principal finding and success of the present chapter is that a HiBiT tag could successfully be incorporated into the VEGF-A gene and be used to assay VEGF-A production, and furthermore that this provided a sensitive assay of hypoxia induced VEGF-A production. This is the first report of utilisation of these techniques to monitor hypoxia induced protein expression in primary cells.

DM-NOFD treatment does not enhance hypoxic VEGF-A production

The third aim of the present investigation was to evaluate if DM-NOFD treatment could enhance the hypoxia induced expression of VEGF-A. Although hypoxia upregulated the expression of VEGF-A (figures 5.7, & 5.8), this effect was not potentiated by DM-NOFD treatment. This is in contrast to data from both genetic (Huang et al., 2011) and chemical (Chan et al., 2016) models of HIF manipulation, which have demonstrated that FIH1 inhibition can enhance the HIF signalling effects. One possible explanation for the discrepancy in these findings is that the degree of hypoxia utilised in the present experiment did not give a large enough window for the effect of FIH1 inhibition to be observed.

The degree of hypoxia experienced by a particular cell or tissue can be thought of relative to the normal oxygen supply. In cell culture models, therefore it is important to consider the 'dose'of hypoxia is relative to that which a cell type may normally experience. Human umbilical vein blood has PO_2 of 3.8 kPa (Keeley and Mann, 2019), making the normal physiological exposure to oxygen of endothelial

cells in this vessel relatively low. Previous reports have demonstrated HIF-1α accumulation to comparable levels in HUVECs cultured in both 1% and also at 3%- O_2 (Keeley et al., 2017). It is unlikely, therefore, that conditions used in the present investigation failed to initiate HIF signalling. Indeed, there was a clear enhancement of VEGF-A production in cells exposed to hypoxia, indicative of HIF signalling.

It is interesting to consider that if HIF-1α accumulates at 3% O_2 in HUVECs (Keeley et al., 2017), what would be the effect of FIH1 inhibition at this oxygen tension. As there is likely a greater degree of Asn803 hydroxylation at 3% O_2 (Tian et al., 2011), FIH1 inhibition may have more potential to increase the degree of HIF signalling. This is a clear area in which the present investigation could be extended, to investigate the effect of FIH1 inhibition at a wider range of oxygen tensions.

The binding of HiBiT tagged VEGF-A to LgBiT tagged receptors

The ability of HiBiT tagged VEGF-A to bind to LgBiT tagged receptors and produce bioluminescence (figure 5.10) provides evidence that it still acts as a biologically active ligand. This is imperative, as, if the addition of HiBiT blocked biological activity, the utility of the model to assay VEGF-A production would be compromised. A system in which the function of a ligand is impaired cannot be viewed as a valid model to assay the production of that ligand. It is interesting, however, to consider the difference in signal generated between the binding of HiBiT tagged VEGF-A conditioned media treatment of VEGFR2 expressing cells and NRP1 expressing cells.

An obvious difference between VEGFR2 and NRP1 is the different binding sites on the VEGF-A ligand, and its position relative to the HiBit tag. Consequently there may be some degree of inhibition of HiBiT-LgBiT complementation

due to the accessibility of the LgBiT tag. NRP1, on the other hand does not form dimers and as such the LgBiT tag may be more readily available to complement with the HiBiT tag on the VEGF-A. Previous investigations utilising HiBiT tagged receptors have demonstrated that the conformational constraints can influence the interaction with LgBiT (White et al., 2020). It may be therefore, that VEGF-A HiBiT interaction with LgBiT VEGFR2 is limited by the conformation of ligand-receptor complex. Additionally, VEGF-A interacts with glycosaminoglycans (GAG) in the extracellular matrix, which modulate VEGFR2 activation (Ashikari-Hada et al., 2005). In the present investigation it could be that the GAG interaction differentially affects NRP1 and VEGFR2 binding, possibly by differentially affecting VEGF-A concentration local to receptors, or the ability of the NanoBiT subunits to complement.

An alternative approach could be taken to monitor and confirm the interaction of HiBiT tagged VEGF-A with VEGFR2, which would overcome the possible inhibitory effects described above. Use of bioluminescent resonance energy transfer (BRET) can effectively monitor ligand-receptor interaction in living cells (Stoddart et al., 2015). This proximity based technique relies upon the excitation of a fluorophore by the bioluminescence generated by a luciferase. With reference to the present investigation, therefore, this technique could be used to monitor HiBiT tagged VEGF-A binding to a fluorescently labelled VEGFR2. This could be readily performed utilising the previously described HaloTag-VEGFR2 construct, which can be fluorescently labelled and utilised for bioluminescence based proximity assays (Kilpatrick et al., 2019). This would allow interaction between HiBiT tagged VEGF-A in conditioned media for CRISPR cells to be applied to cells expressing HaloTag VEGFR2. Supplementation with purified LgBiT protein would form a functional luciferase with the HiBiT tag (as in the media assays of the present investigation), and excitation of the receptor fluorophore upon receptor binding. This experimental aproach has previously been

demonstrated as an effective way to monitor HiBiT tagged CXCL 12 interacting with fluorescently labelled CXCR4 (White et al., 2021).

Although the LgBiT tagged receptor experiments provided good evidence of HiBiT tagged VEGF engaging with receptors, they do not confirm an equal ability to activate down stream signalling. This could be achieved by utilising reporter gene assays, such as the nuclear factor of activated T-cells (NFAT) reporter gene assay that has been extensively used to investigate VEGFR2 signalling (Carter et al., 2015; Kilpatrick et al., 2017). Comparison of the ability of WT HUVEC conditioned media and CRISPR edited VEGF-A HiBiT HUVEC conditioned media to activate NFAT regulated gene expression would allow any differences in down stream signalling due to HiBiT addition to be identified.

Methods to further develop CRISPR editing strategy

In the present investigation RNP complexes and ssODN repair templates were delivered to HUVECs via electroporation. There are several benefits to this approach. The transient expression of CRISPR components within the cells limits the potential for off target Cas9 effects, that may be associated with other delivery systems (e.g. viral delivery). Furthermore this approach allows the use of a physiologically relevant primary cell model. The downside to this approach is that editing efficiency is variable, and was low in some instances. Although this limitation is overcome to a degree by the excellent sensitivity of the HiBiT system, enhancing the editing efficiency would be beneficial.

A relatively minor modification that could be made to the protocols utilised in the present investigation would be to use Cas9 fusion proteins, such as a Cas9:GFP fusion. This would then afford the use of fluorescence-activated cell sorting (FACS) to select green fluorescent protein (GFP) positive cells, which would therefore represent those cells to which the RNP complex was successfully

delivered. This strategy would allow assays to be performed with cell populations with a greater proportion of edited cells.

Alternatively the use of immortalised HUVEC cell lines may afford different CRISPR editing approaches. HUVECs can be successfully immortalised through the expression of telomerase reverse transcriptase (TERT2). Expression of TERT2 by HUVECs gives substantial extension of lifespan and importantly does not lead to a change in core phenotypical characteristics (Chang et al., 2005). Furthermore, TERT2 expressing HUVECs can be used effectively to generate clonal CRISPR edited cell lines (Carretero-Ortega et al., 2019). Utilising a similar approach, the present investigation could be extended to generate a clonal line expressing HiBiT tagged VEGF-A, as has previously been performed for HEK293T cells expressing HiBiT tagged CXCL12 (White et al., 2021). This would give a cell population where all VEGF-A produced would be HiBiT tagged, therefore increasing bioluminescent signal. Furthermore, this approach may have the benefit of being able to overcome the limitations of targets with very low editing efficiency, such as the addition of HiBiT to VEGF-A exon 8b.

Possibility to further expand HiBiT tagged protein approach

As discussed in Chapter 1 (table 1.1), VEGF-A has several splice variants. There is potential to investigate additional splice variants, by altering the position of HiBiT tag insertion. The present investigation focussed on tagging exon 8a, to monitor VEGF-A_{xxx}a isoforms, as attempts to tag exon 8b were unsuccessful. Tagging of exon 8b my be improved by attempting to utilise an alternative PAM site. Additionally, alternative isoforms could be monitored by targeting the HiBiT tag to other loci. One particular interesting idea, would be place a tag in the 'intron' between the proximal and distal splice sites of exon 8, i.e. between exon 8a and 8b. This would allow for assessment of production of the programmed

read through variant VEGF-Ax (Eswarappa et al., 2014). This, combined with successful tagging at the 3' end of exon 8b, would allow a thorough investigation of the expression of VEGF-A_{165}b, which has attracted some degree of contention (Bridgett et al., 2017).

The demonstration of luminescence upon HiBiT tagged VEGF-A binding to LgBiT tagged receptors gives an insight into the avenues that these techniques could be expanded into. For example, co-culture experiments, with cells expressing tagged receptors would allow for endogenously expressed ligand-receptor interactions to be studied in live cells in real-time. Additionally, this could also be extended into BRET techniques as described above, with fluorescently labelled ligands expressed in either the HiBiT edited cells or another cell type within a co-culture system. Furthermore these methods of VEGF-A HiBiT tagging could be readily applied to alternative cell types to investigate VEGF-A biology. This may be of particular relevance may be to the cancer field, given the focus on anti-VEGF therapeutics (Ferrara and Adamis, 2016).

The techniques used in the present chapter could be readily applied to alternative protein targets. The CRISPR mediated HiBiT tagging system can be readily adapted, through identification of PAM sites in an alternative target protein, and appropriate design of gRNA and HDR constructs. This could allow for monitoring of hypoxic regulation alternative HIF regulated proteins, or to cell systems beyond the sphere of hypoxia research.

Conclusions

The present chapter has demonstrated that it is possible to CRISPR edit endothelial cells to incorporate a HiBiT signal in the VEGF-A gene, which can be utilised to assay VEGF-A production. This assay system is sensitive to hypoxia induced increases in VEGF-A signalling, but did not demonstrate an enhancement in

VEGF-A production due to FIH1 inhibition. The techniques developed and utilised in the present investigation have several avenues for further development and to broaden their application.

Chapter 6

General Discussion

The cardiovascular system experiences hypoxia in a variety of physiological and pathophysiological states. In heart failure, for example, the human heart experiences hypoperfusion and hypoxia (Karamitsos et al., 2013; Mahmod et al., 2014). Hypoxia is also a central component of ischaemia (Bishop and Ratcliffe, 2015). Much of the molecular signalling response to hypoxia is governed by the HIF signalling system. Oxygen sensitivity is conferred upon the HIF system by the PHD enzymes, which control HIF degradation, and FIH1 which regulates the ability of HIF to bind DNA and affect target gene expression (Semenza, 2011).

The overarching aim of this thesis was to explore the role of FIH1 in the cardiovascular response to hypoxia. To this end, both a genetic loss of function model and a specific chemical inhibitor were utilised to study the effect of a loss of FIH1 in the regulation of cardiac metabolism, the response to hypoxic and ischaemic stress, and the potential for FIH1 inhibition to augment hypoxia induced angiogenic signalling.

6.1 Discussion of principle findings

Cardiac metabolism in the FIH1$^{-/-}$ mouse

Modulation of metabolism is a core response to hypoxia. The HIF system has a multitude of metabolic gene targets, the induction of which act to maintain energy production whilst reducing oxygen cost.

In contrast to previous reports of loss of PHD function, the present investigation did not find any evidence of reduced mitochondrial function in the heart due to loss of FIH1. Loss of PHD2 in cardiomyocytes of mouse hearts is associated with increased BNIP3 expression, and reduction in mitochondrial content (Moslehi et al., 2010). BNIP3 is a well established HIF target gene, and has been demonstrated to induce mitophagy in MEFs in response to hypoxia (Zhang et al., 2008). In the present study, however, there was no evidence of a reduction of mitochondrial content in the FIH1$^{-/-}$ heart, therefore suggesting that loss of FIH1 does not activate the HIF-1 - BNIP3 axis in the heart. Furthermore, there was no evidence of reductions in mitochondrial content in the hearts or skeletal muscle of either WT or FIH1$^{-/-}$ exposed to moderate chronic hypoxia in the present investigation. These discrepancies raise interesting considerations around the regulation of mitochondria by hypoxia, and also the relevance of metabolic data from some cell culture models with respect to hypoxia.

As outlined at length in chapter one, the heart is metabolically omnivorous, with large ATP demands being met predominantly by oxidative phosphorylation. The constant hydraulic work done by the heart means that large energy demands must be constantly met for survival. It is perhaps not surprising therefore, to see that mitochondrial content is maintained in modest hypoxia and in spite of FIH1 deletion. Furthermore, the ability of MEFS to maintain sufficient energy production through fermentation of glucose, when cultured in a high glucose hypoxic environment, likely explains the severity of reduction in mitochondrial

activity. This underlines the importance of data from more physiological models, such as the isolated perfused heart in the present investigation.

The rates of fatty acid oxidation observed in the present investigation were equivalent in WT and FIH1$^{-/-}$ hearts. This finding is in agreement with the absence of any effect of FIH1 loss upon mitochondrial content and function in the heart. Equivalent rates of fatty acid oxidation also mirror that seen in the Chuvash polycythaemia mouse (a model of moderately upregulated HIF signalling (Slingo et al., 2016)). This differs, however, from the rates of fatty acid oxidation seen in hearts from chronically hypoxic animals, which display reductions of 20-25% (Cole et al., 2016; Mansor et al., 2016). These data highlight that the cardiac phenotype of the FIH1$^{-/-}$ mouse is not simply a phenocopy of that of a mouse exposed to chronic hypoxia.

The rates of fatty acid oxidation observed in the hearts should be considered in the context in which they were measured i.e. an isolated system. Cardiac lipid uptake and oxidation is directly proportional to the circulating lipid concentration (Wisneski et al., 1987). Previous studies of a FIH1$^{-/-}$ mice have described a reduction in the circulating lipid concentrations (Zhang et al., 2010). It may be, therefore, that in vivo, the FIH1$^{-/-}$ mouse heart is oxidising fatty acids at a lower rate than WT controls. However, in the present investigation, when fatty acids were provided to isolated hearts at the same concentrations in the perfusate (0.4 mM), the rate of oxidation was the same.

The increased glycolytic flux seen in FIH1$^{-/-}$ hearts in the present study parallels findings from previous genetic models of upregulated HIF signalling in the heart (Hyvärinen et al., 2010; Slingo et al., 2016). This is also seen in the hypoxic heart (Cole et al., 2016; Handzlik et al., 2018; Mansor et al., 2016). This is likely due to the presence of HRE in the promoter regions of many of the genes encoding for glycolytic enzymes (Semenza et al., 1994). Furthermore there was an increase in net lactate efflux from the FIH1$^{-/-}$ heart, this again mirroring

the effects of both chronic hypoxia (Cole et al., 2016) and upregulation of HIF signalling (Hyvärinen et al., 2010; Slingo et al., 2016). Again this may be due to upregulation of lactate dehydrogenase, which is a HIF target gene (Semenza et al., 1994). Furthermore, the upregulation of lactate production permits continued high rates of glycolytic activity by regenerating NAD^+, required for the conversion of glyceraldehyde 3-phosphate to 1,3-bisphosphoglycerate.

In summary, the present investigation found that the FIH1$^{-/-}$ heart displays some, but not all, of the metabolic characteristics of the chronically hypoxic heart. The metabolic and mitochondrial consequences of FIH1 loss appear similar to some of the characteristics of moderate upregulation of HIF signalling (Hyvärinen et al., 2010; Slingo et al., 2016), but not more severe phenotypes associated with PHD2 complete loss of function (Minamishima et al., 2008; Moslehi et al., 2010).

Improved recovery from ischaemic injury in the FIH1$^{-/-}$ mouse heart

One of the principal findings of the present investigation was that hearts from FIH1$^{-/-}$ mice had enhanced recovery relative to baseline function (figure 4.2). This effect was predominantly driven by improved recovery of left ventricular developed pressure. Improved cardiac functional recovery in the FIH1$^{-/-}$ heart is in agreement with previous investigations that have studied both PHD specific loss of function (Adluri et al., 2011; Hyvärinen et al., 2010; Kerkelä et al., 2013; Xie et al., 2015), PHD specific acute chemical inhibition (Ong et al., 2014b), and pan hydroxylase inhibition (Eckle et al., 2008; Ockaili et al., 2005; Poynter et al., 2011).

Several different mechanisms have been proposed to explain the cardioprotective effects of increased HIF activity, from differences in reactive oxygen species (ROS) production and mitochondrial behaviour, differences in energy metabolism, and effects of increased angiogenic signalling. The range of mechanisms de-

scribed likely reflects the array of methods used to study this process. These range from germline genetic deletions, inducible genetic deletions, to chronic pharmacological treatments, through to more acute or single dose pharmacological experiments (table 4.1).

In the present investigation, a key difference between the FIH1$^{-/-}$ and the WT, which may explain the improved functional recovery, is the enhanced rate of glycolysis. In the baseline and reperfusion period, glycolysis was significantly greater in the FIH1$^{-/-}$ heart, as well the accumulation of tissue lactate under low flow conditions. It is likely that the enhanced glycolysis seen in reperfusion is, at least in part, responsible for some fo the improvement in cardiac function.

Ischaemic pre conditioning (application of short periods of ischaemia preceding a long damaging period) is one of the strongest cardioprotective interventions against ischaemia reperfusion injury across all species (Murry et al., 1986; Zuurbier et al., 2020). Ischaemic preconditioning enhances glycolysis both pre and post ischaemia (Zuurbier et al., 2020). Ischaemic preconditioning is lost in the absence of glucose, demonstrating the importance of this substrate in mediating the protective effect (Nadtochiy et al., 2015). Enhanced glycolysis in early reperfusion has been suggested to be protective due to preferential utilisation of glycolytically derived ATP by ion pumps to maintain cardiac function (Jeremy et al., 1993). Furthermore, increased glycolysis contributes to a lower pH, which may in turn delay the opening of the mitochondrial permeability transition pore, therefore conferring cardioprotection (Halestrap, 1991). These mechanisms may link the enhanced glycolytic flux with the enhanced functional recovery in FIH1$^{-/-}$ hearts.

The present study investigated hearts from mice with a chronic loss of FIH1 function. This does not necessarily provide support for intervention with FIH1 inhibition during ischaemia prior to reperfusion, as would be required in a patient presenting with acute coronary syndrome. Nevertheless, there may be scenarios

where FIH1 inhibition could be effective as a prophylactic measure, for example to mitigate against ischaemia reperfusion injury during surgery or transplant. Furthermore, there is scope to expand on the present investigation to evaluate FIH1 inhibition at different time points, as outlined below.

FIH1 inhibition did not enhance hypoxic VEGF production

The principal finding of chapter 5 was that inhibition of FIH1 did not enhance hypoxia induced increase in VEGF-A production. The ability of DM-NOFD to inhibit FIH1 and promote HIF signalling was confirmed and shown to approximately double HRE signalling in 1% hypoxia in HeLa cells. This was not associated with enhanced HIF-1α protein stabilisation, therefore confirming that the increase HRE signal was due to reduced FIH1 mediated hydroxylation.

In HUVECs, hypoxia (1% O_2) resulted in an increase in VEGF-A production, as would be anticipated. This was not enhanced with FIH1 inhibition, suggesting that asparagine hydroxylation of HIF is not limiting VEGF-A production in this setting. It may be that in conditions of more mild hypoxia, where FIH1 remains more active relative to PHD enzymes, that DM-NOFD treatment my enhance the production of VEGF-A. The accumulation of HIF-1α in HUVECs is broadly equivalent at 3% O_2 and 1% O_2 (Keeley et al., 2017). As the degree of FIH1 activity is greater at 3% O_2, adding FIH1 inhibition may have a greater impact upon the HIF-VEGF-A signalling axis.

6.2 Experimental models employed: limitations and potential for further development

6.2.1 Langendorff heart perfusion

Assessment of cardiac function and metabolism in the present study was all performed utilising Langendorff isolated perfused heart models. This approach has distinct benefits, but also distinct limitations. The use of this model afforded the assessment of metabolic fluxes utilising both ^{3}H glucose and palmitate. These therefore give direct measurements of metabolic pathway flux, that could not be achieved using in vivo models. Additionally, the Langendorff system allows for hearts to be immediately snap frozen in Wollenberger tongs cooled to the temperature of liquid nitrogen, therefore allowing measurements of metabolites to be made in pristine samples that have not degraded, particularly important for the measurement of high energy phosphate metabolites (Lu et al., 2017). However, the metabolic measurements made do not give a full understanding of cardiac metabolism and there is substantial scope to investigate further. A limitation was the absence of any measurement of glucose oxidation, which was not possible due to safety restrictions in the laboratory. This would give a more comprehensive analysis of the effect of FIH1 loss on mitochondrial metabolism performed in chapter 3, and expand upon the finding of accelerated glycolysis in chapter 4. Use of a ^{14}C glucose tracer would allow measurement of glucose oxidation in the isolated heart and could be coupled with ^{3}H glucose measurements, to investigate the coupling of cardiac glycolysis and glucose oxidation, which has been shown to be important in understanding ischaemic reperfusion (Ussher et al., 2012). Furthermore, the exact mechanism by which glycolysis is upregulated in the FIH1 heart was not determined in the present study. This could be expanded upon by utilising ^{13}C glucose tracers in the isolated heart perfusion system, coupled with

mass spectrometry based metabolomic measurements, to understand differences in regulation within the metabolic pathway.

The use of an ex vivo heart preparation has the benefit of providing insight into the isolated organ without neural, endocrine, or other external influence. However although this gives more direct understanding the behaviour of the myocardium, it is an oversimplification and negates the influence of important factors that occur in vivo (Bell et al., 2011). The present study could be extended, therefore, by investigation of cardiac ischaemia reperfusion in vivo. Such models, including, for example, temporary ligation of the LAD, have the benefit of being closer to the clinical relevance and allow follow up assessment of cardiac recovery over a longer time period (Lindsey et al., 2018). Furthermore, investigations could be developed further by study of permanent LAD ligation models, discussed in more detail below.

6.2.2 FIH1$^{-/-}$ mouse

The mouse model employed was a global disruption of the FIH1 gene. As such, there was no expression of FIH1 in any tissue at any point through development. It is difficult to delineate, therefore, the exact mechanism and at what time point the phenotypic traits of the FIH1$^{-/-}$ mouse manifest. It may be that the loss of FIH1 through development shapes the phenotype seen in the adult mouse, and that the absence of FIH1 in adulthood is of lesser importance than this model may imply. Conversely, it may be that the phenotype seen in the FIH1$^{-/-}$ mouse represents a large degree of compensation for FIH1 loss that has occurred through development. This could be explored by the deletion of FIH1 in adulthood, such as by inducible cre-lox system or inducible shRNA, and the resultant phenotype compared with the present model with germline deletion.

The use of conditional genetic knock out models could also significantly broaden the scope of the experimental designs that have been employed. In the present investigation, the finding of enhanced recovery from acute ischaemic injury in hearts from FIH1$^{-/-}$ may support the use of a prophylactic treatment with FIH1 inhibition, as described above. If the timing of FIH1 deletion could be manipulated, this finding could be expanded upon. Firstly, the use of an inducible knockout model, with FIH1 deletion in close proximity prior to an ischaemia reperfusion experiment would, aid understanding of whether the beneficial effects seen in the present investigation are reliant on long-term FIH1 loss or developmental effects. Furthermore, the experimental approach could be broadened into an infarction model, such as by LAD ligation. This could allow longer-term follow up of mice to study the degree of cardiac recovery, therefore broadening the clinical relevance of the findings. Perhaps most importantly, a LAD ligation model could be combined with a post ligation deletion of FIH1. This would give insight into the effect of FIH1 loss in the most clinically relevant time period (i.e. post infarction) and give insight into the potential for clinical translation FIH1 inhibition post infarction, as has been elegantly performed for each of the PHD isoforms (Jatho et al., 2021).

A limitation of the present investigation, with respect to the use of the FIH1$^{-/-}$ mouse, is the fact that the effects of FIH1 loss on the behaviour of the HIF signalling system were not fully explored. Previous reports from FIH1$^{-/-}$ mice, have reported transcriptional changes in vivo due to FIH1 loss. Additionally, profiling of FIH1$^{-/-}$ MEFs shows enhanced HRE signalling and differences in expression of a large number of genes (Sim et al., 2018; Zhang et al., 2010). The degree, if any, of compensation in the HIF system due to FIH1 loss has not been defined, either in the present investigation, or by previous investigators. Clearly the phenotypic differences between WT and FIH1$^{-/-}$ mice show that the loss of the FIH1 gene is not completely compensated for. It is still possible, however,

that there are changes in expression of other proteins that lessen the impact of FIH1 deletion. Changes in the expression of PHD enzymes, the HIF-β subunit, or the transcription of the HIF-α subunit may plausibly occur in compensation. It has been demonstrated, for example, that PHD2 has a hypoxia response element and is, therefore, induced by the HIF signalling (Metzen et al., 2005). As such, future work should look to understand the consequences of FIH1 loss of function on the whole of the HIF signalling system, both with respect to genetic loss in the mouse, and also chemical inhibition.

6.2.3 Cell models

HeLa cells were utilised in initial studies of FIH1 inhibition upon hypoxic signalling and HIF-1α protein stabilisation. Although these cells could be readily transfected to perform signalling assays, their physiological relevance as a model system is less than other cell types. HeLa cells have a relatively low oxygen consumption in relation to other cell models, making them less sensitive to hypoxia (Keeley and Mann, 2019). The present investigation could be improved, therefore, by performing these assays in a more physiological and oxygen sensitive cell type for greater translational relevance.

In all cell culture experiments, routine culture, and "normoxic" control conditions were performed in room air supplemented with 5% CO_2, resulting in an oxygen concentration of approximately 18% (Newby et al., 2005). As such these cells can be considered to be in a hyperoxic environment, as oxygen exposure is much greater than would be experienced in vivo (Keeley and Mann, 2019). Although this is common within the scientific literature, it must be acknowledged that this practice reduces the translational validity of resultant findings. With particular respects to HUVECs, it has been previously demonstrated that cellular behaviour changes when cultured at physiological normoxia of 5% O_2 (Keeley

and Mann, 2019; Keeley et al., 2017). To remedy this, and provide more physiologically relevant data, future investigations should aim to perform routine and control culture in conditions of physiological normoxia.

6.3 Future Directions

The present investigation has shown that the loss of FIH1 is cardioprotective in ischaemia reperfusion injury, and modulates cardiac metabolism. The recent licencing of PHD inhibitors for treatment of anaemia associated with chronic kidney disease (Dhillon, 2019, 2020; Markham, 2020), demonstrates that the HIF signalling pathway can successfully be promoted for clinical benefit. The present investigation suggests that there may be merit in targeting HIF signalling via FIH1 inhibition in the heart. As described above, there is certainly more that could be done with different genetic models and pre clinical investigations to understand and evaluate the effect of FIH1 loss of function. Furthermore, there is scope to develop more small molecule inhibitors for FIH1, the number of which substantially lags behind that available for PHDs. Evidence suggests that this should be possible (Wu et al., 2021b). Development and application of further FIH1 inhibitors will allow greater insight into therapeutic potential to be explored. Furthermore, the possibility to combine FIH1 inhibition with PHD inhibition may be a therapeutic strategy to induce a greater degree of HIF signalling for a given level of HIF protein stabilisation.

The techniques developed in chapter 5, utilising split luciferase tags to monitor protein production, show great promise for further development. In this chapter a HiBiT tag was successfully appended to VEGF-A to allow production to be monitored. This could be readily applied to other proteins, to monitor production, either under hypoxia, or other experimental conditions. Furthermore, this technology is powerful in the study of protein-protein interactions, as demonstrated by

the receptor binding experiments shown in the present investigation. This could allow a variety of experimental approaches, such as co culture studies, where the binding of secreted tagged proteins from one cell type to tagged receptors in a different cell type could be studied.

6.4 Concluding remarks

In summary, loss of FIH1 was shown to modulate carbohydrate, but not lipid metabolism in the heart. FIH1 loss is associated with a degree of protection from ischaemic injury in the isolated heart, associated with upregulation of glycolysis. Although the inhibition of FIH1 in HeLa cells demonstrated a doubling of hypoxia induced HIF signalling, it did not translate to an increase in VEGF-A production by vascular endothelial cells. The techniques developed for monitoring VEGF-A production (split luciferase tag by CRISPR editing) show promise for broader application.

References

Abdul Kadir, A., Clarke, K., and Evans, R. D. (2020). Cardiac ketone body metabolism. *Biochimica et Biophysica Acta - Molecular Basis of Disease*, 1866(6):165739.

Adluri, R. S., Thirunavukkarasu, M., Dunna, N. R., Zhan, L., Oriowo, B., Takeda, K., Sanchez, J. A., Otani, H., Maulik, G., Fong, G. H., and Maulik, N. (2011). Disruption of hypoxia-inducible transcription factor-prolyl hydroxylase domain-1 (PHD-1 -/-) Attenuates ex vivo myocardial ischemia/reperfusion injury through hypoxia-inducible factor-1α transcription factor and its target genes in mice. *Antioxidants and Redox Signaling*, 15(7):1789–1797.

Ahmed, S., Ayscough, A., Barker, G. R., Canning, H. E., Davenport, R., Downham, R., Harrison, D., Jenkins, K., Kinsella, N., Livermore, D. G., Wright, S., Ivetac, A. D., Skene, R., Wilkens, S. J., Webster, N. A., and Hendrick, A. G. (2017). 1,2,4-Triazolo-[1,5-a]pyridine HIF Prolylhydroxylase Domain-1 (PHD-1) Inhibitors with a Novel Monodentate Binding Interaction. *Journal of Medicinal Chemistry*, 60(13):5663–5672.

Amin, E. M., Oltean, S., Hua, J., Gammons, M. V., Hamdollah-Zadeh, M., Welsh, G. I., Cheung, M. K., Ni, L., Kase, S., Rennel, E. S., Symonds, K. E., Nowak, D. G., Royer-Pokora, B., Saleem, M. A., Hagiwara, M., Schumacher, V. A., Harper, S. J., Hinton, D. R., Bates, D. O., and Ladomery, M. R. (2011). WT1 Mutants Reveal SRPK1 to Be a Downstream Angiogenesis Target by Altering VEGF Splicing. *Cancer Cell*, 20(6):768–780.

Aragonés, J., Schneider, M., Van Geyte, K., Fraisl, P., Dresselaers, T., Mazzone, M., Dirkx, R., Zacchigna, S., Lemieux, H., Jeoung, N. H., Lambrechts, D., Bishop, T., Lafuste, P., Diez-Juan, A., Harten, S. K., Van Noten, P., De Bock, K., Willam, C., Tjwa, M., Grosfeld, A., Navet, R., Moons, L., Vandendriessche, T., Deroose, C., Wijeyekoon, B., Nuyts, J., Jordan, B., Silasi-Mansat, R., Lupu, F., Dewerchin, M., Pugh, C., Salmon, P., Mortelmans, L., Gallez, B., Gorus, F., Buyse, J., Sluse, F., Harris, R. a., Gnaiger, E., Hespel, P., Van Hecke, P., Schuit, F., Van Veldhoven, P., Ratcliffe, P., Baes, M., Maxwell, P., and Carmeliet, P. (2008). Deficiency or inhibition of oxygen sensor Phd1 induces hypoxia tolerance by reprogramming basal metabolism. *Nature genetics*, 40(2):170–80.

Ariazi, J. L., Duffy, K. J., Adams, D. F., Fitch, D. M., Luo, L., Pappalardi, M., Biju, M., DiFilippo, E. H., Shaw, T., Wiggall, K., and Erickson-Miller, C. (2017). Discovery and preclinical characterization of gsk1278863 (daprodustat), a small molecule hypoxia inducible factor-prolyl hydroxylase inhibitor for anemias. *Journal of Pharmacology and Experimental Therapeutics*, 363(3):336–347.

Ashikari-Hada, S., Habuchi, H., Kariya, Y., and Kimata, K. (2005). Heparin regulates vascular endothelial growth factor165- dependent mitogenic activity, tube formation, and its receptor phosphorylation of human endothelial cells: Comparison of the effects of heparin and modified heparins. *Journal of Biological Chemistry*, 280(36):31508–31515.

Atkinson, D. E. and Walton, G. M. (1967). Adenosine triphosphate conservation in metabolic regulation. Rat liver citrate cleavage enzyme. *The Journal of biological chemistry*, 242(13):3239–41.

Bao, W., Qin, P., Needle, S., Erickson-Miller, C. L., Duffy, K. J., Ariazi, J. L., Zhao, S., Olzinski, A. R., Behm, D. J., Teg Pipes, G. C., Jucker, B. M., Hu, E., Lepore, J. J., and Willette, R. N. (2010). Chronic inhibition of hypoxia-inducible factor prolyl 4-hydroxylase improves ventricular performance, remodeling, and vascularity after myocardial infarction in the rat. *Journal of Cardiovascular Pharmacology*, 56(2):147–155.

Bates, D. O., Cui, T. G., Doughty, J. M., Winkler, M., Sugiono, M., Shields, J. D., Peat, D., Gillatt, D., and Harper, S. J. (2002). VEGF165b, an inhibitory splice variant of vascular endothelial growth factor, is down-regulated in renal cell carcinoma. *Cancer Research*, 62(14):4123–4131.

Bell, R. M., Mocanu, M. M., and Yellon, D. M. (2011). Retrograde heart perfusion: the Langendorff technique of isolated heart perfusion. *Journal of molecular and cellular cardiology*, 50(6):940–50.

Berra, E., Benizri, E., Ginouvès, A., Volmat, V., Roux, D., and Pouysségur, J. (2003). HIF prolyl-hydroxylase 2 is the key oxygen sensor setting low steady-state levels of HIF-1α in normoxia. *EMBO Journal*, 22(16):4082–4090.

Bishop, T. and Ratcliffe, P. J. (2015). HIF Hydroxylase Pathways in Cardiovascular Physiology and Medicine. *Circulation Research*, 117(1):65–79.

Boardman, N., Hafstad, A. D., Larsen, T. S., Severson, D. L., and Aasum, E. (2009). Increased O 2 cost of basal metabolism and excitation-contraction coupling in hearts from type 2 diabetic mice. *American Journal of Physiology - Heart and Circulatory Physiology*, 296(5):1373–1379.

Boateng, S. and Sanborn, T. (2013). Acute myocardial infarction. *Disease-a-Month*, 59(3):83–96.

Bonen, A. (2001). The expression of lactate transporters (MCT1 and MCT4) in heart and muscle. / L ' Expression des transporteurs de lactate (mct1 et mct4) dans le coeur et le muscle. *European Journal of Applied Physiology*, 86(1):6–11.

Bowler, E. and Oltean, S. (2019). Alternative splicing in angiogenesis. *International Journal of Molecular Sciences*, 20(9).

Bowler, E., Porazinski, S., Uzor, S., Thibault, P., Durand, M., Lapointe, E., Rouschop, K. M., Hancock, J., Wilson, I., and Ladomery, M. (2018). Hypoxia leads to significant changes in alternative splicing and elevated expression of CLK splice factor kinases in PC3 prostate cancer cells. *BMC Cancer*, 18(1):1–11.

Bracken, C. P., Fedele, A. O., Linke, S., Balrak, W., Lisy, K., Whitelaw, M. L., and Peet, D. J. (2006). Cell-specific regulation of hypoxia-inducible factor (HIF)-1α and HIF-2α stabilization and transactivation in a graded oxygen environment. *Journal of Biological Chemistry*, 281(32):22575–22585.

Bridgett, S., Dellett, M., and Simpson, D. A. (2017). RNA-Sequencing data supports the existence of novel VEGFA splicing events but not of VEGFAxxxb isoforms. *Scientific reports*, 7(1):58.

Cahill, G. F. (2006). Fuel Metabolism in Starvation. *Annual Review of Nutrition*, 26(1):1–22.

Cai, X., Zhang, D., Wang, J., Liu, X., Ouyang, G., and Xiao, W. (2018). Deletion of the fih gene encoding an inhibitor of hypoxiainducible factors increases hypoxia tolerance in zebrafish. *Journal of Biological Chemistry*, 293(40):15370–15380.

Cai, Z., Zhong, H., Bosch-Marce, M., Fox-Talbot, K., Wang, L., Wei, C., Trush, M. A., and Semenza, G. L. (2008). Complete loss of ischaemic preconditioning-induced cardioprotection in mice with partial deficiency of HIF-1α. *Cardiovascular Research*, 77(3):463–470.

Campbell, F. M., Kozak, R., Wagner, A., Altarejos, J. Y., Dyck, J. R., Belke, D. D., Severson, D. L., Kelly, D. P., and Lopaschuk, G. D. (2002). A role for peroxisome proliferator-activated receptor α (PPARα) in the control of cardiac malonyl-CoA levels: Reduced fatty acid oxidation rates and increased glucose oxidation rates in the hearts of mice lacking PPARα are associated with higher concentra. *Journal of Biological Chemistry*, 277(6):4098–4103.

Carmeliet, P. (2005). VEGF as a key mediator of angiogenesis in cancer. *Oncology*, 69(SUPPL. 3):4–10.

Carretero-Ortega, J., Chhangawala, Z., Hunt, S., Narvaez, C., Menéndez-González, J., Gay, C. M., Zygmunt, T., Li, X., and Torres-Vázquez, J. (2019). GIPC proteins negatively modulate Plexind1 signaling during vascular development. *eLife*, 8:1–38.

Carter, J. J., Wheal, A. J., Hill, S. J., and Woolard, J. (2015). Effects of receptor tyrosine kinase inhibitors on VEGF165a- and VEGF165b-stimulated gene transcription in HEK-293 cells expressing human VEGFR2. *British Journal of Pharmacology*, 172(12):3141–3150.

Cave, A. C., Ingwall, J. S., Friedrich, J., Liao, R., Saupe, K. W., Apstein, C. S., and Eberli, F. R. (2000). ATP synthesis during low-flow ischemia: Influence of increased glycolytic substrate. *Circulation*, 101(17):2090–2096.

Chan, M. C., Ilott, N. E., Schödel, J., Sims, D., Tumber, A., Lippl, K., Mole, D. R., Pugh, C. W., Ratcliffe, P. J., Ponting, C. P., and Schofield, C. J. (2016). Tuning the transcriptional response to hypoxia by inhibiting Hypoxia-inducible Factor (HIF) prolyl and asparaginyl hydroxylases. *Journal of Biological Chemistry*, 291(39):20661–20673.

Chang, M. W.-F., Grillari, J., Mayrhofer, C., Fortschegger, K., Allmaier, G., Marzban, G., Katinger, H., and Voglauer, R. (2005). Comparison of early passage, senescent and hTERT immortalized endothelial cells. *Experimental cell research*, 309(1):121–36.

Chatham, J. C., Zhang, J., and Wende, A. R. (2021). Role of o-linked n-acetylglucosamine proteinmodification in cellular (Patho) physiology. *Physiological Reviews*, 101(2):427–493.

Chen, T. T., Luque, A., Lee, S., Anderson, S. M., Segura, T., and Iruela-Arispe, M. L. (2010). Anchorage of VEGF to the extracellular matrix conveys differential signaling responses to endothelial cells. *Journal of Cell Biology*, 188(4):595–609.

Cheng, L., Ding, G., Qin, Q., Huang, Y., Lewis, W., He, N., Evans, R. M., Schneider, M. D., Brako, F. A., Xiao, Y., Chen, Y. E., and Yang, Q. (2004). Cardiomyocyte-restricted peroxisome proliferator-activated receptor-δ deletion perturbs myocardial fatty acid oxidation and leads to cardiomyopathy. *Nature Medicine*, 10(11):1245–1250.

Cockman, M. E., Lippl, K., Tian, Y.-M., Pegg, H. B., Figg, W. D., Abboud, M. I., Heilig, R., Fischer, R., Myllyharju, J., Schofield, C. J., and Ratcliffe, P. J. (2019). Lack of activity of recombinant HIF prolyl hydroxylases (PHDs) on reported non-HIF substrates. *eLife*, 8:1–27.

Cockman, M. E., Webb, J. D., Kramer, H. B., Kessler, B. M., and Ratcliffe, P. J. (2009). Proteomics-based identification of novel factor inhibiting hypoxia-inducible factor (FIH) substrates indicates widespread asparaginyl hydroxylation of ankyrin repeat domain-containing proteins. *Molecular and Cellular Proteomics*, 8(3):535–546.

Cole, M. A., Abd Jamil, A. H., Heather, L. C., Murray, A. J., Sutton, E. R., Slingo, M., Sebag-Montefiore, L., Tan, S. C., Aksentijević, D., Gildea, O. S., Stuckey, D. J., Yeoh, K. K., Carr, C. A., Evans, R. D., Aasum, E., Schofield, C. J., Ratcliffe, P. J., Neubauer, S., Robbins, P. A., and Clarke, K. (2016). On the pivotal role of PPARα in adaptation of the heart to hypoxia and why fat in the diet increases hypoxic injury. *The FASEB Journal*, pages 1–14.

Concordet, J. P. and Haeussler, M. (2018). CRISPOR: Intuitive guide selection for CRISPR/Cas9 genome editing experiments and screens. *Nucleic Acids Research*, 46(W1):W242–W245.

Cung, T.-T., Morel, O., Cayla, G., Rioufol, G., Garcia-Dorado, D., Angoulvant, D., Bonnefoy-Cudraz, E., Guerin, P., Elbaz, M., Delarche, N., Coste, P., Vanzetto, G., Metge, M., Aupetit, J.-F., Jouve, B., Motreff, P., Tron, C., Labeque, J.-N., Steg, P. G., Cottin, Y., Range, G., Clerc, J., Claeys, M. J., Coussement, P., Prunier, F., Moulin, F., Roth, O., Belle, L., Dubois, P., Barragan, P., Gilard, M., Piot, C., Colin, P., De Poli, F., Morice, M.-C., Ider, O., Dubois-Rande, J.-L., Unterseeh, T., Le Breton, H., Beard, T., Blanchard, D., Grollier, G., Malquarti, V., Staat, P., Sudre, A., Elmer, E., Hansson, M. J., Bergerot, C., Boussaha, I., Jossan, C., Derumeaux, G., Mewton, N., and Ovize, M. (2015). Cyclosporine before PCI in Patients with Acute Myocardial Infarction. *The New England journal of medicine*, 373(11):1021–1031.

Dann, C. E., Bruick, R. K., and Deisenhofer, J. (2002). Structure of factor-inhibiting hypoxia-inducible factor 1: An asparaginyl hydroxylase involved in the hypoxic response pathway. *Proceedings of the National Academy of Sciences of the United States of America*, 99(24):15351–15356.

Debevec, T. (2017). Hypoxia-related hormonal appetite modulation in humans during rest and exercise: Mini review. *Frontiers in Physiology*, 8(MAY):1–8.

Depré, C., Rider, M. H., and Hue, L. (1998). Mechanisms of control of heart glycolysis. *European Journal of Biochemistry*, 258(2):277–290.

Depre, C., Vanoverschelde, J. L., and Taegtmeyer, H. (1999). Glucose for the heart. *Circulation*, 99(4):578–88.

Dhillon, S. (2019). Roxadustat: First Global Approval. *Drugs*, 79(5):563–572.

Dhillon, S. (2020). Daprodustat: First Approval. *Drugs*, 80(14):1491–1497.

Dixon, A. S., Schwinn, M. K., Hall, M. P., Zimmerman, K., Otto, P., Lubben, T. H., Butler, B. L., Binkowski, B. F., MacHleidt, T., Kirkland, T. A., Wood, M. G., Eggers, C. T., Encell, L. P., and Wood, K. V. (2016). NanoLuc Complementation Reporter Optimized for Accurate Measurement of Protein Interactions in Cells. *ACS Chemical Biology*, 11(2):400–408.

Dyck, J. R., Cheng, J. F., Stanley, W. C., Barr, R., Chandler, M. P., Brown, S., Wallace, D., Arrhenius, T., Harmon, C., Yang, G., Nadzan, A. M., and Lopaschuk, G. D. (2004). Malonyl coenzyme a decarboxylase inhibition protects the ischemic heart by inhibiting fatty acid oxidation and stimulating glucose oxidation. *Circulation research*, 94(9).

Eckle, T., Kohler, D., Lehmann, R., Kasmi, K. C., and Eltzschig, H. K. (2008). Hypoxia-inducible factor-1 is central to cardioprotection a new paradigm for ischemic preconditioning. *Circulation*, 118(2):166–175.

Ehrismann, D., Flashman, E., Genn, D. N., Mathioudakis, N., Hewitson, K. S., Ratcliffe, P. J., and Schofield, C. J. (2007). Studies on the activity of the hypoxia-inducible-factor hydroxylases using an oxygen consumption assay. *Biochemical Journal*, 401(1):227–234.

Elkins, J. M., Hewitson, K. S., McNeill, L. A., Seibel, J. F., Schlemminger, I., Pugh, C. W., Ratcliffe, P. J., and Schofield, C. J. (2003). Structure of factor-inhibiting hypoxia-inducible factor (HIF) reveals mechanism of oxidative modification of HIF-1α. *Journal of Biological Chemistry*, 278(3):1802–1806.

Emerling, B. M., Weinberg, F., Liu, J. L., Mak, T. W., and Chandel, N. S. (2008). PTEN regulates p300-dependent hypoxia-inducible factor 1 transcriptional activity through Forkhead transcription factor 3a (FOXO3a). *Proceedings of the National Academy of Sciences of the United States of America*, 105(7):2622–2627.

Essop, M. F. (2007). Cardiac metabolic adaptations in response to chronic hypoxia. *The Journal of physiology*, 584(Pt 3):715–26.

Eswarappa, S. M., Potdar, A. A., Koch, W. J., Fan, Y., Vasu, K., Lindner, D., Willard, B., Graham, L. M., Dicorleto, P. E., and Fox, P. L. (2014). Programmed translational readthrough generates antiangiogenic VEGF-Ax. *Cell*, 157(7):1605–1618.

Ferrara, N. and Adamis, A. P. (2016). Ten years of anti-vascular endothelial growth factor therapy. *Nature Reviews Drug Discovery*, 15(6):385–403.

Fillmore, N., Wagg, C. S., Zhang, L., Fukushima, A., and Lopaschuk, G. D. (2018). Cardiac branched-chain amino acid oxidation is reduced during insulin resistance in the heart. *American Journal of Physiology - Endocrinology and Metabolism*, 315(5):E1046–E1052.

Finck, B. N., Lehman, J. J., Leone, T. C., Welch, M. J., Bennett, M. J., Kovacs, A., Han, X., Gross, R. W., Kozak, R., Lopaschuk, G. D., and Kelly, D. P. (2002). The cardiac phenotype induced by PPARα overexpression mimics that caused by diabetes mellitus. *Journal of Clinical Investigation*, 109(1):121–130.

Forsythe, J. A., Jiang, B. H., Iyer, N. V., Agani, F., Leung, S. W., Koos, R. D., and Semenza, G. L. (1996). Activation of vascular endothelial growth factor gene transcription by hypoxia-inducible factor 1. *Molecular and Cellular Biology*, 16(9):4604–4613.

Frayn, K. N. and Evans, R. D. (2019). *Human Metabolism: A Regulatory Perspective*. Wiley Blackwell, fourth edition.

Gimeno, R. E., Ortegon, A. M., Patel, S., Punreddy, S., Ge, P., Sun, Y., Lodish, H. F., and Stahl, A. (2003). Characterization of a heart-specific fatty acid transport protein. *Journal of Biological Chemistry*, 278(18):16039–16044.

Giordano, F. J. (2005). Oxygen, oxidative stress, hypoxia, and heart failure. *Journal of Clinical Investigation*, 115(3):500–508.

Giordano, F. J., Gerber, H. P., Williams, S. P., Vanbruggen, N., Bunting, S., Ruiz-Lozano, P., Gu, Y., Nath, A. K., Huang, Y., Hickey, R., Dalton, N., Peterson, K. L., Ross, J., Chien, K. R., and Ferrara, N. (2001). A cardiac myocyte vascular endothelial growth factor paracrine pathway is required to maintain cardiac function. *Proceedings of the National Academy of Sciences of the United States of America*, 98(10):5780–5785.

Guo, H. F. and Vander Kooi, C. W. (2015). Neuropilin functions as an essential cell surface receptor. *Journal of Biological Chemistry*, 290(49):29120–29126.

Guyot, M. and Pagès, G. (2015). VEGF Splicing and the Role of VEGF Splice Variants: From Physiological-Pathological Conditions to Specific Pre-mRNA Splicing. *Methods in molecular biology (Clifton, N.J.)*, 1332:3–23.

Halestrap, A. P. (1991). Calcium-dependent opening of a non-specific pore in the mitochondrial inner membrane is inhibited at pH values below 7. Implications for the protective effect of low pH against chemical and hypoxic cell damage. *The Biochemical journal*, 278 (Pt 3(3):715–9.

Hall, M. P., Unch, J., Binkowski, B. F., Valley, M. P., Butler, B. L., Wood, M. G., Otto, P., Zimmerman, K., Vidugiris, G., MacHleidt, T., Robers, M. B., Benink, H. A., Eggers, C. T., Slater, M. R., Meisenheimer, P. L., Klaubert, D. H., Fan, F., Encell, L. P., and Wood, K. V. (2012). Engineered luciferase reporter from a deep sea shrimp utilizing a novel imidazopyrazinone substrate. *ACS Chemical Biology*, 7(11):1848–1857.

Hamada, M., Takayama, T., Shibata, T., Hiratate, A., Takahashi, M., Yashiro, M., Takayama, N., Okumura-Kitajima, L., Koretsune, H., Kajiyama, H., Naruse, T., Kato, S., Takano, H., and Kakinuma, H. (2018). Discovery of novel 2-[(4-hydroxy-6-oxo-2,3-dihydro-1H-pyridine-5-carbonyl)amino]acetic acid derivatives as HIF prolyl hydroxylase inhibitors for treatment of renal anemia. *Bioorganic and Medicinal Chemistry Letters*, 28(10):1725–1730.

Handzlik, M. K., Constantin-Teodosiu, D., Greenhaff, P. L., and Cole, M. A. (2018). Increasing cardiac pyruvate dehydrogenase flux during chronic hypoxia improves acute hypoxic tolerance. *The Journal of physiology*, 0:1–13.

Harris, R. C., Hultman, E., and Nordesjö, L. O. (1974). Glycogen, glycolytic intermediates and high-energy phosphates determined in biopsy samples of musculus quadriceps femoris of man at rest. Methods and variance of values. *Scandinavian Journal of Clinical and Laboratory Investigation*, 33(2):109–120.

Hausenloy, D. and Yellon, D. (2013). Myocardial ischemia-reperfusion injury: a neglected therapeutic target. *J Clin Invest*, 123(1):92–100.

Heather, L. C., Cole, M. A., Tan, J. J., Ambrose, L. J. A., Pope, S., Abd-Jamil, A. H., Carter, E. E., Dodd, M. S., Yeoh, K. K., Schofield, C. J., and Clarke, K. (2012). Metabolic adaptation to chronic hypoxia in cardiac mitochondria. *Basic Research in Cardiology*, 107(3).

Heather, L. C., Pates, K. M., Atherton, H. J., Cole, M. A., Ball, D. R., Evans, R. D., Glatz, J. F., Luiken, J. J., Griffin, J. L., and Clarke, K. (2013). Differential translocation of the fatty acid transporter, FAT/CD36, and the glucose transporter, GLUT4, coordinates changes in cardiac substrate metabolism during ischemia and reperfusion. *Circulation: Heart Failure*, 6(5):1058–1066.

Hirsch, D., Stahl, A., and Lodish, H. F. (1998). A family of fatty acid transporters conserved from mycobacterium to man. *Proceedings of the National Academy of Sciences of the United States of America*, 95(15):8625–8629.

Ho, K. L., Zhang, L., Wagg, C., Al Batran, R., Gopal, K., Levasseur, J., Leone, T., Dyck, J. R., Ussher, J. R., Muoio, D. M., Kelly, D. P., and Lopaschuk, G. D. (2019). Increased ketone body oxidation provides additional energy for the failing heart without improving cardiac efficiency. *Cardiovascular Research*, 115(11):1606–1616.

Holloway, C., Cochlin, L., Codreanu, I., Bloch, E., Fatemian, M., Szmigielski, C., Atherton, H., Heather, L., Francis, J., Neubauer, S., Robbins, P., Montgomery, H., and Clarke, K. (2011a). Normobaric hypoxia impairs human cardiac energetics. *FASEB journal : official publication of the Federation of American Societies for Experimental Biology*, 25(9):3130–5.

Holloway, C. J., Montgomery, H. E., Murray, A. J., Cochlin, L. E., Codreanu, I., Hopwood, N., Johnson, A. W., Rider, O. J., Levett, D. Z. H., Tyler, D. J., Francis, J. M., Neubauer, S., Grocott, M. P. W., and Clarke, K. (2011b). Cardiac response to hypobaric hypoxia: persistent changes in cardiac mass, function, and energy metabolism after a trek to Mt. Everest Base Camp. *FASEB journal : official publication of the Federation of American Societies for Experimental Biology*, 25(2):792–6.

Holmes, D. I. and Zachary, I. (2005). The vascular endothelial growth factor (VEGF) family: Angiogenic factors in health and disease. *Genome Biology*, 6(2).

Holness, M. J. and Sugden, M. C. (2003). Regulation of pyruvate dehydrogenase complex activity by reversible phosphorylation. *Biochemical Society transactions*, 31(Pt 6):1143–51.

Hölscher, M., Silter, M., Krull, S., Von Ahlen, M., Hesse, A., Schwartz, P., Wielockx, B., Breier, G., Katschinski, D. M., and Zieseniss, A. (2011). Cardiomyocyte-specific prolyl-4-hydroxylase domain 2 knock out protects from acute myocardial ischemic injury. *Journal of Biological Chemistry*, 286(13):11185–11194.

Huang, M., Nguyen, P., Jia, F., Hu, S., Gong, Y., De Almeida, P. E., Wang, L., Nag, D., Kay, M. A., Giaccia, A. J., Robbins, R. C., and Wu, J. C. (2011). Double knockdown of prolyl hydroxylase and factor-inhibiting hypoxia-inducible factor with nonviral minicircle gene therapy enhances stem cell mobilization and angiogenesis after myocardial infarction. *Circulation*, 124(11 SUPPL. 1):46–54.

Huang, Y., Hickey, R. P., Yeh, J. L., Liu, D., Dadak, A., Young, L. H., Johnson, R. S., and Giordano, F. J. (2004). Cardiac myocyte-specific HIF-1alpha deletion alters vascularization, energy availability, calcium flux, and contractility in the normoxic heart. *Faseb J*, 18(10):1138–1140.

Hyde, R., Taylor, P. M., and Hundal, H. S. (2003). Amino acid transporters: Roles in amino acid sensing and signalling in animal cells. *Biochemical Journal*, 373(1):1–18.

Hyvärinen, J., Hassinen, I. E., Sormunen, R., Mäki, J. M., Kivirikko, K. I., Koivunen, P., and Myllyharju, J. (2010). Hearts of hypoxia-inducible factor prolyl 4-hydroxylase-2 hypomorphic mice show protection against acute ischemia-reperfusion injury. *Journal of Biological Chemistry*, 285(18):13646–13657.

Ishida, A., Murray, J., Saito, Y., Kanthou, C., Benzakour, O., Shibuya, M., and Wijelath, E. S. (2001). Expression of vascular endothelial growth factor receptors in smooth muscle cells. *Journal of Cellular Physiology*, 188(3):359–368.

Ivan, M., Kondo, K., Yang, H., Kim, W., Valiando, J., Ohh, M., Salic, A., Asara, J. M., Lane, W. S., and Kaelin, W. G. (2001). HIFalpha targeted for VHL-mediated destruction by proline hydroxylation: implications for O2 sensing. *Science (New York, N.Y.)*, 292(5516):464–468.

Iyer, N. V., Kotch, L. E., Agani, F., Leung, S. W., Laughner, E., Wenger, R. H., Gassmann, M., Gearhart, J. D., Lawler, a. M., Yu, a. Y., and Semenza, G. L. (1998). Cellular and developmental control of O2 homeostasis by hypoxia-inducible factor 1 alpha. *Genes & development*, 12(2):149–162.

Jaakkola, P., Mole, D. R., Tian, Y. M., Wilson, M. I., Gielbert, J., Gaskell, S. J., von Kriegsheim, A., Hebestreit, H. F., Mukherji, M., Schofield, C. J., Maxwell, P. H., Pugh, C. W., and Ratcliffe, P. J. (2001). Targeting of HIF-alpha to the von Hippel-Lindau ubiquitylation complex by O2-regulated prolyl hydroxylation. *Science*, 292(5516):468–472.

James, D. E., Brown, R., Navarro, J., and Pilch, P. F. (1988). Insulin-regulatable tissues express a unique insulin-sensitive glucose transport protein. *Nature*, 333(6169):183–185.

Jatho, A., Zieseniss, A., Brechtel-Curth, K., Yamamoto, A., Coleman, M. L., Vergel Leon, A. M., Biggs, D., Davies, B., Pugh, C. W., Ratcliffe, P. J., and Katschinski, D. M. (2021). Precisely Tuned Inhibition of HIF Prolyl Hydroxylases Is Key for Cardioprotection After Ischemia. *Circulation research*, 128(8):1208–1210.

Jeremy, R. W., Ambrosio, G., Pike, M. M., Jacobus, W. E., and Becker, L. C. (1993). The functional recovery of post-ischemic myocardium requires glycolysis during early reperfusion. *Journal of molecular and cellular cardiology*, 25(3):261–76.

Jiménez, N., Krouwer, V. J., and Post, J. A. (2013). A new, rapid and reproducible method to obtain high quality endothelium in vitro. *Cytotechnology*, 65(1):1–14.

Kaelin, W. G. and Ratcliffe, P. J. (2008). Oxygen Sensing by Metazoans: The Central Role of the HIF Hydroxylase Pathway. *Molecular Cell*, 30(4):393–402.

Karamitsos, T. D., Dass, S., Suttie, J., Sever, E., Birks, J., Holloway, C. J., Robson, M. D., Jerosch-Herold, M., Watkins, H., and Neubauer, S. (2013). Blunted myocardial oxygenation response during vasodilator stress in patients with hypertrophic cardiomyopathy. *Journal of the American College of Cardiology*, 61(11):1169–1176.

Kato, S., Ochiai, N., Takano, H., Io, F., Takayama, N., Koretsune, H., ichi Kunioka, E., Uchida, S., and Yamamoto, K. (2019). TP0463518, a novel prolyl hydroxylase inhibitor, specifically induces erythropoietin production in the liver. *Journal of Pharmacology and Experimental Therapeutics*, 371(3):675–683.

Kato, S., Takayama, N., Takano, H., Koretsune, H., Koizumi, C., ichi Kunioka, E., Uchida, S., Takahashi, T., and Yamamoto, K. (2018). TP0463518, a novel inhibitor for hypoxia-inducible factor prolyl hydroxylases, increases erythropoietin in rodents and monkeys with a good pharmacokinetics-pharmacodynamics correlation. *European Journal of Pharmacology*, 838(May):138–144.

Keeley, T. P. and Mann, G. E. (2019). Defining Physiological Normoxia for Improved Translation of Cell Physiology to Animal Models and Humans. *Physiological reviews*, 99(1):161–234.

Keeley, T. P., Siow, R. C., Jacob, R., and Mann, G. E. (2017). A PP2A-mediated feedback mechanism controls Ca2+-dependent no synthesis under physiological oxygen. *FASEB Journal*, 31(12):5172–5183.

Kerendi, F., Kirshbom, P. M., Halkos, M. E., Wang, N. P., Kin, H., Jiang, R., Zhao, Z. Q., Kanter, K. R., Guyton, R. A., and Vinten-Johansen, J. (2006). Cobalt Chloride Pretreatment Attenuates Myocardial Apoptosis After Hypothermic Circulatory Arrest. *Annals of Thoracic Surgery*, 81(6):2055–2062.

Kerkelä, R., Karsikas, S., Szabo, Z., Serpi, R., Magga, J., Gao, E., Alitalo, K., Anisimov, A., Sormunen, R., Pietilä, I., Vainio, L., Koch, W. J., Kivirikko, K. I., Myllyharju, J., and Koivunen, P. (2013). Activation of Hypoxia Response in Endothelial Cells Contributes to Ischemic Cardioprotection. *Molecular and Cellular Biology*, 33(16):3321–3329.

Kido, M., Du, L., Sullivan, C. C., Li, X., Deutsch, R., Jamieson, S. W., and Thistlethwaite, P. A. (2005). Hypoxia-inducible factor 1-alpha reduces infarction and attenuates progression of cardiac dysfunction after myocardial infarction in the mouse. *Journal of the American College of Cardiology*, 46(11):2116–2124.

Kilpatrick, L. E., Alcobia, D. C., White, C. W., Peach, C. J., Glenn, J. R., Zimmerman, K., Kondrashov, A., Pfleger, K. D., Ohana, R. F., Robers, M. B., Wood, K. V., Sloan, E. K., Woolard, J., and Hill, S. J. (2019). Complex Formation between VEGFR2 and the β2-Adrenoceptor. *Cell Chemical Biology*, 26(6):830–841.e9.

Kilpatrick, L. E., Friedman-Ohana, R., Alcobia, D. C., Riching, K., Peach, C. J., Wheal, A. J., Briddon, S. J., Robers, M. B., Zimmerman, K., Machleidt, T., Wood, K. V., Woolard, J., and Hill, S. J. (2017). Real-time analysis of the binding of fluorescent VEGF165a to VEGFR2 in living cells: Effect of receptor tyrosine kinase inhibitors and fate of internalized agonist-receptor complexes. *Biochemical Pharmacology*, 136:62–75.

King, L. M., Boucher, F., and Opie, L. H. (1995). Coronary flow and glucose delivery as determinants of contracture in the ischemic myocardium. *Journal of Molecular and Cellular Cardiology*, 27(1):701–720.

Knowles, H. J., Tian, Y. M., Mole, D. R., and Harris, A. L. (2004). Novel mechanism of action for hydralazine: Induction of hypoxia-inducible factor-1 α, vascular endothelial growth factor, and angiogenesis by inhibition of prolyl hydroxylases. *Circulation Research*, 95(2):162–169.

Koivunen, P., Hirsilä, M., Günzler, V., Kivirikko, K. I., and Myllyharju, J. (2004). Catalytic Properties of the Asparaginyl Hydroxylase (FIH) in the Oxygen Sensing Pathway Are Distinct from Those of Its Prolyl 4-Hydroxylases. *Journal of Biological Chemistry*, 279(11):9899–9904.

Kolwicz, S. C., Olson, D. P., Marney, L. C., Garcia-Menendez, L., Synovec, R. E., and Tian, R. (2012). Cardiac-specific deletion of acetyl CoA carboxylase 2 prevents metabolic remodeling during pressure-overload hypertrophy. *Circulation Research*, 111(6):728–738.

Kolwicz, S. C., Purohit, S., and Tian, R. (2013). Cardiac metabolism and its interactions with contraction, growth, and survival of cardiomyocytes. *Circulation Research*, 113(5):603–616.

Kraegen, E. W., Sowden, J. A., Halstead, M. B., Clark, P. W., Rodnick, K. J., Chisholm, D. J., and James, D. E. (1993). Glucose transporters and in vivo glucose uptake in skeletal and cardiac muscle: Fasting, insulin stimulation and immunoisolation studies of GLUT1 and GLUT4. *Biochemical Journal*, 295(1):287–293.

Krishnan, J., Suter, M., Windak, R., Krebs, T., Felley, A., Montessuit, C., Tokarska-Schlattner, M., Aasum, E., Bogdanova, A., Perriard, E., Perriard, J. C., Larsen, T., Pedrazzini, T., and Krek, W. (2009). Activation of a HIF1α-PPARγ Axis Underlies the Integration of Glycolytic and Lipid Anabolic Pathways in Pathologic Cardiac Hypertrophy. *Cell Metabolism*, 9(6):512–524.

Kudo, N., Barr, A. J., Barr, R. L., Desai, S., and Lopaschuk, G. D. (1995). High Rates of Fatty Acid Oxidation during Reperfusion of Ischemic Hearts Are Associated with a Decrease in Malonyl-CoA Levels Due to an Increase in 5'-AMP-activated Protein Kinase Inhibition of Acetyl-CoA Carboxylase. *Journal of Biological Chemistry*, 270(29):17513–17520.

Lando, D., Peet, D. J., Gorman, J. J., Whelan, D. A., Whitelaw, M. L., and Bruick, R. K. (2002a). FIH-1 is an asparaginyl hydroxylase enzyme that regulates the transcriptional activity of hypoxia-inducible factor. *Genes & development*, 16(12):1466–71.

Lando, D., Peet, D. J., Whelan, D. A., Gorman, J. J., and Whitelaw, M. L. (2002b). Asparagine Hydroxylation of the HIF Transactivation Domain: A Hypoxic Switch. *Science*, 295(5556):858–861.

Lee, S. H., Wolf, P. L., Escudero, R., Deutsch, R., Jamieson, S. W., and Thistlethwaite, P. A. (2000). Early expression of angiogenesis factors in acute myocardial ischemia and infarction. *The New England journal of medicine*, 342(9):626–33.

Lehman, J. J., Boudina, S., Banke, N. H., Sambandam, N., Han, X., Young, D. M., Leone, T. C., Gross, R. W., Lewandowski, E. D., Abel, E. D., and Kelly, D. P. (2008). The transcriptional coactivator PGC-1α is essential for maximal and efficient cardiac mitochondrial fatty acid oxidation and lipid homeostasis. *American Journal of Physiology - Heart and Circulatory Physiology*, 295(1):185–196.

Leung, D. W., Cachianes, G., Kuang, W. J., Goeddel, D. V., and Ferrara, N. (1989). Vascular endothelial growth factor is a secreted angiogenic mitogen. *Science*, 246(4935):1306–1309.

Levett, D. Z., Radford, E. J., Menassa, D. A., Graber, E. F., Morash, A. J., Hoppeler, H., Clarke, K., Martin, D. S., Ferguson-Smith, A. C., Montgomery, H. E., Grocott, M. P. W., Murray, A. J., and Caudwell Xtreme Everest Research Group (2012). Acclimatization of skeletal muscle mitochondria to high-altitude hypoxia during an ascent of Everest. *FASEB journal : official publication of the Federation of American Societies for Experimental Biology*, 26(4):1431–41.

Lieb, M. E., Menzies, K., Moschella, M. C., Ni, R., and Taubman, M. B. (2002). Mammalian EGLN genes have distinct patterns of mRNA expression and regulation. *Biochemistry and cell biology = Biochimie et biologie cellulaire*, 80(4):421–426.

Lindsey, M. L., Bolli, R., Canty, J. M., Du, X.-J., Frangogiannis, N. G., Frantz, S., Gourdie, R. G., Holmes, J. W., Jones, S. P., Kloner, R. A., Lefer, D. J., Liao, R., Murphy, E., Ping, P., Przyklenk, K., Recchia, F. A., Schwartz Longacre, L., Ripplinger, C. M., Van Eyk, J. E., and Heusch, G. (2018). Guidelines for experimental models of myocardial ischemia and infarction. *American Journal of Physiology-Heart and Circulatory Physiology*, 314(4):H812–H838.

Lippl, F. J., Neubauer, S., Schipfer, S., Lichter, N., Tufman, A., Otto, B., and Fischer, R. (2010). Hypobaric hypoxia causes body weight reduction in obese subjects. *Obesity*, 18(4):675–681.

Livak, K. J. and Schmittgen, T. D. (2001). Analysis of relative gene expression data using real-time quantitative PCR and the 2-ΔΔCT method. *Methods*, 25(4):402–408.

Lopaschuk, G. D. and Barr, R. L. (1997). Measurements of fatty acid and carbohydrate metabolism in the isolated working rat heart. *Molecular and cellular biochemistry*, 172(1-2):137–47.

Lopaschuk, G. D., Karwi, Q. G., Tian, R., Wende, A. R., and Abel, E. D. (2021). Cardiac Energy Metabolism in Heart Failure. *Circulation research*, 128(10):1487–1513.

Lopaschuk, G. D., Ussher, J. R., Folmes, C. D. L., Jaswal, J. S., and STANLEY, W. C. (2010). Myocardial Fatty Acid Metabolism in Health and Disease. *Physiological Reviews*, 90(1):207–258.

Lozano, R., Naghavi, M., Foreman, K., Lim, S., Shibuya, K., Aboyans, V., Abraham, J., Adair, T., Aggarwal, R., Ahn, S. Y., Alvarado, M., Anderson, H. R., Anderson, L. M., Andrews, K. G., Atkinson, C., Baddour, L. M., Barker-Collo, S., Bartels, D. H., Bell, M. L., Benjamin, E. J., Bennett, D., Bhalla, K., Bikbov, B., Abdulhak, A. B., Birbeck, G., Blyth, F., Bolliger, I., Boufous, S., Bucello, C., Burch, M., Burney, P., Carapetis, J., Chen, H., Chou, D., Chugh, S. S., Coffeng, L. E., Colan, S. D., Colquhoun, S., Colson, K. E., Condon, J., Connor, M. D., Cooper, L. T., Corriere, M., Cortinovis, M., De Vaccaro, K. C., Couser, W., Cowie, B. C., Criqui, M. H., Cross, M., Dabhadkar, K. C., Dahodwala, N., De Leo, D., Degenhardt, L., Delossantos, A., Denenberg, J., Des Jarlais, D. C., Dharmaratne, S. D., Dorsey, E. R., Driscoll, T., Duber, H., Ebel, B., Erwin, P. J., Espindola, P., Ezzati, M., Feigin, V., Flaxman, A. D., Forouzanfar, M. H., Fowkes, F. G. R., Franklin, R., Fransen, M., Freeman, M. K., Gabriel, S. E., Gakidou, E., Gaspari, F., Gillum, R. F., Gonzalez-Medina, D., Halasa, Y. A., Haring, D., Harrison, J. E., Havmoeller, R., Hay, R. J., Hoen, B., Hotez, P. J., Hoy, D., Jacobsen, K. H., James, S. L., Jasrasaria, R., Jayaraman, S., Johns, N., Karthikeyan, G., Kassebaum, N., Keren, A., Khoo, J. P., Knowlton, L. M., Kobusingye, O., Koranteng, A., Krishnamurthi, R., Lipnick, M., Lipshultz, S. E., Ohno, S. L., Mabweijano, J., MacIntyre, M. F., Mallinger, L., March, L., Marks, G. B., Marks, R., Matsumori, A., Matzopoulos,

R., Mayosi, B. M., McAnulty, J. H., McDermott, M. M., McGrath, J., Mensah, G. A., Merriman, T. R., Michaud, C., Miller, M., Miller, T. R., Mock, C., Mocumbi, A. O., Mokdad, A. A., Moran, A., Mulholland, K., Nair, M. N., Naldi, L., Narayan, K. M. V., Nasseri, K., Norman, P., O'Donnell, M., Omer, S. B., Ortblad, K., Osborne, R., Ozgediz, D., Pahari, B., Pandian, J. D., Rivero, A. P., Padilla, R. P., Perez-Ruiz, F., Perico, N., Phillips, D., Pierce, K., Pope, C. A., Porrini, E., Pourmalek, F., Raju, M., Ranganathan, D., Rehm, J. T., Rein, D. B., Remuzzi, G., Rivara, F. P., Roberts, T., De Le??n, F. R., Rosenfeld, L. C., Rushton, L., Sacco, R. L., Salomon, J. A., Sampson, U., Sanman, E., Schwebel, D. C., Segui-Gomez, M., Shepard, D. S., Singh, D., Singleton, J., Sliwa, K., Smith, E., Steer, A., Taylor, J. A., Thomas, B., Tleyjeh, I. M., Towbin, J. A., Truelsen, T., Undurraga, E. A., Venketasubramanian, N., Vijayakumar, L., Vos, T., Wagner, G. R., Wang, M., Wang, W., Watt, K., Weinstock, M. A., Weintraub, R., Wilkinson, J. D., Woolf, A. D., Wulf, S., Yeh, P. H., Yip, P., Zabetian, A., Zheng, Z. J., Lopez, A. D., and Murray, C. J. L. (2012). Global and regional mortality from 235 causes of death for 20 age groups in 1990 and 2010: A systematic analysis for the Global Burden of Disease Study 2010. *The Lancet*, 380(9859):2095–2128.

Lu, W., Su, X., Klein, M. S., Lewis, I. A., Fiehn, O., and Rabinowitz, J. D. (2017). Metabolite Measurement: Pitfalls to Avoid and Practices to Follow. *Annual review of biochemistry*, 86(1):277–304.

Lundholm, L., Mohme-Lundholm, E., and Vamos, N. (1963). Lactic Acid Assay with L(+)lactic Acid Dehydrogenase from Rabbit Muscle. *Acta Physiologica Scandinavica*, 58(2-3):243–249.

Luptak, I., Yan, J., Cui, L., Jain, M., Liao, R., and Tian, R. (2007). Long-term effects of increased glucose entry on mouse hearts during normal aging and ischemic stress. *Circulation*, 116(8):901–909.

Mahmod, M., Francis, J. M., Pal, N., Lewis, A., Dass, S., De Silva, R., Petrou, M., Sayeed, R., Westaby, S., Robson, M. D., Ashrafian, H., Neubauer, S., and Karamitsos, T. D. (2014). Myocardial perfusion and oxygenation are impaired during stress in severe aortic stenosis and correlate with impaired energetics and subclinical left ventricular dysfunction. *Journal of cardiovascular magnetic resonance : official journal of the Society for Cardiovascular Magnetic Resonance*, 16(1):29.

Mahon, P. C., Hirota, K., and Semenza, G. L. (2001). FIH-1: A novel protein that interacts with HIF-1a and VHL to mediate repression of HIF-1 transcriptional activity. *Genes and Development*, 15(20):2675–2686.

Mann, D. L. and Bristow, M. R. (2005). Mechanisms and models in heart failure: The biomechanical model and beyond. *Circulation*, 111(21):2837–2849.

Mansor, L. S., Mehta, K., Aksentijevic, D., Carr, C. A., Lund, T., Cole, M. A., Page, L. L., Fialho, M. d. L. S., Shattock, M. J., Aasum, E., Clarke, K., Tyler, D. J., and Heather, L. C. (2016). Increased oxidative metabolism following hypoxia in the type 2 diabetic heart, despite normal hypoxia signalling and metabolic adaptation. *The Journal of Physiology*, 594(2):307–320.

Markham, A. (2020). Vadadustat: First Approval. *Drugs*, 80(13):1365–1371.

Masson, N., Singleton, R. S., Sekirnik, R., Trudgian, D. C., Ambrose, L. J., Miranda, M. X., Tian, Y.-M., Kessler, B. M., Schofield, C. J., and Ratcliffe, P. J. (2012). The FIH hydroxylase is a cellular peroxide sensor that modulates HIF transcriptional activity. *EMBO reports*, 13(3):251–7.

Masson, N., Willam, C., Maxwell, P. H., Pugh, C. W., and Ratcliffe, P. J. (2001). Independent function of two destruction domains in hypoxia-inducible factor-alpha chains activated by prolyl hydroxylation. *The EMBO journal*, 20(18):5197–206.

McDonough, M. A., McNeill, L. A., Tilliet, M., Papamicaël, C. A., Chen, Q. Y., Banerji, B., Hewitson, K. S., and Schofield, C. J. (2005). Selective inhibition of factor inhibiting hypoxia-inducible factor. *Journal of the American Chemical Society*, 127(21):7680–7681.

McGarry, J. D. and Brown, N. F. (1997). The mitochondrial carnitine palmitoyltransferase system. From concept to molecular analysis. *European Journal of Biochemistry*, 244(1):1–14.

Metallo, C. M. and Vander Heiden, M. G. (2013). Understanding metabolic regulation and its influence on cell physiology. *Molecular cell*, 49(3):388–98.

Metzen, E., Stiehl, D. P., Doege, K., Marxsen, J. H., Hellwig-Bürgel, T., and Jelkmann, W. (2005). Regulation of the prolyl hydroxylase domain protein 2 (phd2/egln-1) gene: Identification of a functional hypoxia-responsive element. *Biochemical Journal*, 387(3):711–717.

Milavetz, J. J., Giebel, D. W., Christian, T. F., Schwartz, R. S., Holmes, D. R., and Gibbons, R. J. (1998). Time to therapy and salvage in myocardial infarction. *Journal of the American College of Cardiology*, 31(6):1246–1251.

Milewski, S. (2002). Glucosamine-6-phosphate synthase–the multi-facets enzyme. *Biochimica et biophysica acta*, 1597(2):173–92.

Minamishima, Y. A., Moslehi, J., Bardeesy, N., Cullen, D., Bronson, R. T., and Kaelin, W. G. (2008). Somatic inactivation of the PHD2 prolyl hydroxylase causes polycythemia and congestive heart failure. *Blood*, 111(6):3236–3244.

Mineur, P., Colige, A. C., Deroanne, C. F., Dubail, J., Kesteloot, F., Habraken, Y., Noël, A., Vöö, S., Waltenberger, J., Lapière, C. M., Nusgens, B. V., and Lambert, C. A. (2007). Newly identified biologically active and proteolysis-resistant VEGF-A isoform VEGF111 is induced by genotoxic agents. *Journal of Cell Biology*, 179(6):1261–1273.

Moran, A. E., Forouzanfar, M. H., Roth, G. A., Mensah, G. A., Ezzati, M., Flaxman, A., Murray, C. J. L., and Naghavi, M. (2014). The global burden of ischemic heart disease in 1990 and 2010: The global burden of disease 2010 study. *Circulation*, 129(14):1493–1501.

Moslehi, J., Minamishima, Y. A., Shi, J., Neuberg, D., Charytan, D. M., Padera, R. F., Signoretti, S., Liao, R., and Kaelin, W. G. (2010). Loss of hypoxia-inducible factor prolyl hydroxylase activity in cardiomyocytes phenocopies ischemic cardiomyopathy. *Circulation*, 122(10):1004–16.

Mozaffarian, D., Benjamin, E. J., Go, A. S., Arnett, D. K., Blaha, M. J., Cushman, M., Das, S. R., de Ferranti, S., Després, J.-P., Fullerton, H. J., Howard, V. J., Huffman, M. D., Isasi, C. R., Jiménez, M. C., Judd, S. E., Kissela, B. M., Lichtman, J. H., Lisabeth, L. D., Liu, S., Mackey, R. H., Magid, D. J., McGuire, D. K., Mohler, E. R., Moy, C. S., Muntner, P., Mussolino, M. E., Nasir, K., Neumar, R. W., Nichol, G., Palaniappan, L., Pandey, D. K., Reeves, M. J., Rodriguez, C. J., Rosamond, W., Sorlie, P. D., Stein, J., Towfighi, A., Turan, T. N., Virani, S. S., Woo, D., Yeh, R. W., Turner, M. B., Committee, A. H. A. S., and Stroke Statistics Subcommittee (2016). Heart Disease and Stroke Statistics-2016 Update: A Report From the American Heart Association. *Circulation*, 133(4):e38–360.

Müller, A. M., Hermanns, M. I., Skrzynski, C., Nesslinger, M., Müller, K. M., and Kirkpatrick, C. J. (2002). Expression of the endothelial markers PECAM-1, vWF, and CD34 in Vivo and in Vitro. *Experimental and Molecular Pathology*, 72(3):221–229.

Murry, C. E., Jennings, R. B., and Reimer, K. A. (1986). Preconditioning with ischemia: a delay of lethal cell injury in ischemic myocardium. *Circulation*, 74(5):1124–36.

Nadtochiy, S. M., Urciuoli, W., Zhang, J., Schafer, X., Munger, J., and Brookes, P. S. (2015). Metabolomic profiling of the heart during acute ischemic preconditioning reveals a role for SIRT1 in rapid cardioprotective metabolic adaptation. *Journal of Molecular and Cellular Cardiology*, 88:64–72.

Nakada, Y., Canseco, D. C., Thet, S., Abdisalaam, S., Asaithamby, A., Santos, C. X., Shah, A. M., Zhang, H., Faber, J. E., Kinter, M. T., Szweda, L. I., Xing, C., Hu, Z., Deberardinis, R. J., Schiattarella, G., Hill, J. A., Oz, O., Lu, Z., Zhang, C. C., Kimura, W., and Sadek, H. A. (2017). Hypoxia induces heart regeneration in adult mice. *Nature*, 541(7636):222–227.

Nanayakkara, G., Alasmari, A., Mouli, S., Eldoumani, H., Quindry, J., McGinnis, G., Fu, X., Berlin, A., Peters, B., Zhong, J., and Amin, R. (2015). Cardioprotective hif-1α-frataxin signaling against ischemia-reperfusion injury. *American Journal of Physiology - Heart and Circulatory Physiology*, 309(5):H867–H879.

Natarajan, R., Salloum, F. N., Fisher, B. J., Kukreja, R. C., and Fowler, A. A. (2006). Hypoxia inducible factor-1 activation by prolyl 4-hydroxylase-2 gene silencing attenuates myocardial ischemia reperfusion injury. *Circulation Research*, 98(1):133–140.

Neubauer, S. (2007). The Failing Heart - An Engine Out of Fuel. *The New England Journal of Medicine*, 356(11):1140–1151.

Newby, D., Marks, L., and Lyall, F. (2005). Dissolved oxygen concentration in culture medium: Assumptions and pitfalls. *Placenta*, 26(4):353–357.

Nissen, N. N., Polverini, P. J., Koch, A. E., Volin, M. V., Gamelli, R. L., and DiPietro, L. A. (1998). Vascular endothelial growth factor mediates angiogenic activity during the proliferative phase of wound healing. *American Journal of Pathology*, 152(6):1445–1452.

Ockaili, R., Natarajan, R., Salloum, F., Fisher, B. J., Jones, D., Fowler, A. A., and Kukreja, R. C. (2005). HIF-1 activation attenuates postischemic myocardial injury: Role for heme oxygenase-1 in modulating microvascular chemokine generation. *American Journal of Physiology - Heart and Circulatory Physiology*, 289(2 58-2):542–548.

Ogoshi, Y., Matsui, T., Mitani, I., Yokota, M., Terashita, M., Motoda, D., Ueyama, K., Hotta, T., Ito, T., Hase, Y., Fukui, K., Deai, K., Yoshiuchi, H., Ito, S., and Abe, H. (2017). Discovery of JTZ-951: A HIF Prolyl Hydroxylase Inhibitor for the Treatment of Renal Anemia. *ACS Medicinal Chemistry Letters*, 8(12):1320–1325.

Okumura, C. Y., Hollands, A., Tran, D. N., Olson, J., Dahesh, S., Von Köckritz-Blickwede, M., Thienphrapa, W., Corle, C., Jeung, S. N., Kotsakis, A., Shalwitz, R. A., Johnson, R. S., and Nizet, V. (2012). A new pharmacological agent (AKB-4924) stabilizes hypoxia inducible factor-1 (HIF-1) and increases skin innate defenses against bacterial infection. *Journal of Molecular Medicine*, 90(9):1079–1089.

Olson, A. K., Bouchard, B., Zhu, W. Z., Chatham, J. C., and Rosiers, C. D. (2020). First characterization of glucose flux through the hexosamine biosynthesis pathway (HBP) in ex vivo mouse heart. *Journal of Biological Chemistry*, 295(7):2018–2033.

Oltean, S., Gammons, M., Hulse, R., Hamdollah-Zadeh, M., Mavrou, A., Donaldson, L., Salmon, A. H., Harper, S. J., Ladomery, M. R., and Bates, D. O. (2012). SRPK1 inhibition in vivo: Modulation of VEGF splicing and potential treatment for multiple diseases. *Biochemical Society Transactions*, 40(4):831–835.

Ong, S.-g., Lee, W. H., Theodorou, L., Kodo, K., Lim, S. Y., Shukla, D. H., Briston, T., Kiriakidis, S., Ashcroft, M., Davidson, S. M., Maxwell, P. H., Yellon, D. M., and Hausenloy, D. J. (2014a). HIF-1 reduces ischaemia-reperfusion injury in the heart by targeting the mitochondrial permeability transition pore. *Cardiovascular research*, 104(1):24–36.

Ong, S.-G., Lee, W. H., Theodorou, L., Kodo, K., Lim, S. Y., Shukla, D. H., Briston, T., Kiriakidis, S., Ashcroft, M., Davidson, S. M., Maxwell, P. H., Yellon, D. M., and Hausenloy, D. J. (2014b). HIF-1 reduces ischaemia–reperfusion injury in the heart by targeting the mitochondrial permeability transition pore. *Cardiovascular Research*, 104(1):24–36.

Opie, L. H. (2004). *Heart Physiology From Cell to Circulation*. Lippincott Williams & Wilkins, Philadelphia, 4th edition.

Ortiz-Prado, E., Dunn, J. F., Vasconez, J., Castillo, D., and Viscor, G. (2019). Partial pressure of oxygen in the human body: a general review. *American journal of blood research*, 9(1):1–14.

Palmer, J. W., Tandler, B., and Hoppel, C. L. (1977). Biochemical properties of subsarcolemmal and interfibrillar mitochondria isolated from rat cardiac muscle. *The Journal of biological chemistry*, 252(23):8731–9.

Pande, S. V. (1975). A mitochondrial carnitine acylcarnitine translocase system. *Proceedings of the National Academy of Sciences of the United States of America*, 72(3):883–887.

Peach, C. J., Kilpatrick, L. E., Woolard, J., and Hill, S. J. (2021). Use of NanoBiT and NanoBRET to monitor fluorescent VEGF-A binding kinetics to VEGFR2/NRP1 heteromeric complexes in living cells. *British journal of pharmacology*, 178(12):2393–2411.

Peach, C. J., Mignone, V. W., Arruda, M. A., Alcobia, D. C., Hill, S. J., Kilpatrick, L. E., and Woolard, J. (2018). Molecular pharmacology of VEGF-A isoforms: Binding and signalling at VEGFR2. *International Journal of Molecular Sciences*, 19(4).

Ponikowski, P., Anker, S. D., AlHabib, K. F., Cowie, M. R., Force, T. L., Hu, S., Jaarsma, T., Krum, H., Rastogi, V., Rohde, L. E., Samal, U. C., Shimokawa, H., Budi Siswanto, B., Sliwa, K., and Filippatos, G. (2014). Heart failure: preventing disease and death worldwide. *ESC Heart Failure*, 1(1):4–25.

Poynter, J. A., Manukyan, M. C., Wang, Y., Brewster, B. D., Herrmann, J. L., Weil, B. R., Abarbanell, A. M., and Meldrum, D. R. (2011). Systemic pretreatment with dimethyloxalylglycine increases myocardial HIF-1α and VEGF production and improves functional recovery after acute ischemia/reperfusion. *Surgery*, 150(2):278–283.

Puchalska, P. and Crawford, P. A. (2017). Multi-dimensional Roles of Ketone Bodies in Fuel Metabolism, Signaling, and Therapeutics. *Cell Metabolism*, 25(2):262–284.

Quiros, P. M., Goyal, A., Jha, P., and Auwerx, J. (2017). Analysis of mtDNA/nDNA Ratio in Mice. *Current protocols in mouse biology*, 7(1):47–54.

Ran, F. A., Hsu, P. D., Wright, J., Agarwala, V., Scott, D. A., and Zhang, F. (2013). Genome engineering using the CRISPR-Cas9 system. *Nature Protocols*, 8(11):2281–2308.

Ratcliffe, P. J. (2013). Oxygen sensing and hypoxia signalling pathways in animals: the implications of physiology for cancer. *The Journal of physiology*, 591(July 2012):2027–42.

Robinson, A. M. and Williamson, D. H. (1980). Physiological roles of ketone bodies as substrates and signals in mammalian tissues. *Physiological Reviews*, 60(1):143–187.

Rovetto, M. J., Lamberton, W. F., and Neely, J. R. (1975). Mechanisms of glycolytic inhibition in ischemic rat hearts. *Circulation Research*, 37(6):742–751.

Sabia, P. J., Powers, E. R., Ragosta, M., Sarembock, I. J., Burwell, L. R., and Kaul, S. (1992). An association between collateral blood flow and myocardial viability in patients with recent myocardial infarction. *The New England journal of medicine*, 327(26):1825–31.

Sano, M., Minamino, T., Toko, H., Miyauchi, H., Orimo, M., Qin, Y., Akazawa, H., Tateno, K., Kayama, Y., Harada, M., Shimizu, I., Asahara, T., Hamada, H., Tomita, S., Molkentin, J. D., Zou, Y., and Komuro, I. (2007). p53-induced inhibition of Hif-1 causes cardiac dysfunction during pressure overload. *Nature*, 446(7134):444–448.

Schaper, J., Meiser, E., and Stammler (1985). Ultrastructural morphometric analysis of myocardium from dogs, rats, hamsters, mice, and from human hearts. *Circulation Research*, 56(3):377–391.

Schofield, C. J. and Ratcliffe, P. J. (2004). Oxygen sensing by HIF hydroxylases. *Nature Reviews Molecular Cell Biology*, 5(5):343–354.

Schuksz, M., Fuster, M. M., Brown, J. R., Crawford, B. E., Ditto, D. P., Lawrence, R., Glass, C. A., Wang, L., Tor, Y., and Esko, J. D. (2008). Surfen, a small molecule antagonist of heparan sulfate. *Proceedings of the National Academy of Sciences of the United States of America*, 105(35):13075–13080.

Schwinn, M. K., Machleidt, T., Zimmerman, K., Eggers, C. T., Dixon, A. S., Hurst, R., Hall, M. P., Encell, L. P., Binkowski, B. F., and Wood, K. V. (2018). CRISPR-Mediated Tagging of Endogenous Proteins with a Luminescent Peptide. *ACS Chemical Biology*, 13(2):467–474.

Scrutton, M. C. and Utter, M. F. (1968). The Regulation of Glycolysis and Gluconeogenesis in Animal Tissues. *Annual Review of Biochemistry*, 37(1):249–302.

Selim, M., Foster, L. D., Moy, C. S., Xi, G., Hill, M. D., Morgenstern, L. B., Greenberg, S. M., James, M. L., Singh, V., Clark, W. M., Norton, C., Palesch, Y. Y., Yeatts, S. D., Dolan, M., Yeh, E., Sheth, K., Kunze, K., Muehlschlegel, S., Nieto, I., Claassen, J., Falo, C., Huang, D., Beckwith, A., Messe, S., Yates, M., O'Phelan, K., Escobar, A., Becker, K., Tanzi, P., Gonzales, N., Tremont, C., Venkatasubramanian, C., Thiessen, R., Save, S., Verrault, S., Collard, K., DeGeorgia, M., Cwiklinski, V., Thompson, B., Wasilewski, L., Andrews, C., Burfeind, R., Torbey, M., Hamed, M., Butcher, K., Sivakumar, L., Varelas, N., Mays-Wilson, K., Leira, E., Olalde, H., Silliman, S., Calhoun, R., Dangayach, N., Renvill, R., Malhotra, R., Kordesch, K., Lord, A., Calahan, T., Geocadin, R., Parish, M., Frey, J., Harrigan, M., Leifer, D., Mathias, R., Schneck, M., Bernier, T., Gonzales-Arias, S., Elysee, J., Lopez, G., Volgi, J., Brown, R., Jasak, S., Phillips, S., Jarrett, J., Gomes, J., McBride, M., Aldrich, F., Aldrich, C., Kornbluth, J., Bettle, M., Goldstein, J., Tirrell, G., Shaw, Q., and Jonczak, K. (2019). Deferoxamine mesylate in patients with intracerebral haemorrhage (i-DEF): a multicentre, randomised, placebo-controlled, double-blind phase 2 trial. *The Lancet Neurology*, 18(5):428–438.

Semenza, G. L. (2010). Vascular responses to hypoxia and ischemia. *Arteriosclerosis, Thrombosis, and Vascular Biology*, 30(4):648–652.

Semenza, G. L. (2011). Oxygen sensing, homeostasis, and disease. *The New England journal of medicine*, 365(6):537–47.

Semenza, G. L. (2012). Hypoxia-inducible factors in physiology and medicine. *Cell*, 148(3):399–408.

Semenza, G. L., Roth, P. H., Fang, H. M., and Wang, G. L. (1994). Transcriptional regulation of genes encoding glycolytic enzymes by hypoxia-inducible factor 1. *The Journal of biological chemistry*, 269(38):23757–63.

Shao, D. and Tian, R. (2016). Glucose transporters in cardiac metabolism and hypertrophy. *Comprehensive Physiology*, 6(1):331–351.

Shinfuku, A., Shimazaki, T., Fujiwara, M., Sato, F., Watase, H., Numazaki, T., Kawakita, Y., Mutoh, M., Yamasaki, H., Takayama, N., Kato, S., Sugimoto, T., and Maruyama, J. (2018). Novel compound induces erythropoietin secretion through liver effects in chronic kidney disease patients and healthy volunteers. *American Journal of Nephrology*, 48(3):157–164.

Sim, J., Cowburn, A. S., Palazon, A., Madhu, B., Tyrakis, P. A., Macías, D., Bargiela, D. M., Pietsch, S., Gralla, M., Evans, C. E., Kittipassorn, T., Chey, Y. C., Branco, C. M., Rundqvist, H., Peet, D. J., and Johnson, R. S. (2018). The Factor Inhibiting HIF Asparaginyl Hydroxylase Regulates Oxidative Metabolism and Accelerates Metabolic Adaptation to Hypoxia. *Cell Metabolism*, 27(4):898–913.e7.

Simons, M., Gordon, E., and Claesson-Welsh, L. (2016). Mechanisms and regulation of endothelial VEGF receptor signalling. *Nature Reviews Molecular Cell Biology*, 17(10):611–625.

Slingo, M., Cole, M. A., Carr, C. A., Curtis, M. K., Dodd, M. S., Giles, L., Heather, L. C., Tyler, D. J., Clarke, K., and Robbins, P. A. (2016). The von Hippel-Lindau Chuvash mutation in mice alters cardiac substrate and high energy phosphate metabolism. *American journal of physiology. Heart and circulatory physiology*, 44(0):ajpheart.00912.2015.

Slot, J. A. N. W., Geuze, H. J., Gigengack, S., Jamest, D. E., and Lienhardt, G. E. (1991). Translocation of the glucose. *Proceedings of the National Academy of Sciences of the United States of America*, 88(September):7815–7819.

Srere, P. (1969). Citrate synthase. *Methods in Enzymology*, 13:3–11.

Stanley, W. W. C., Recchia, F. a., and Lopaschuk, G. D. (2005). Myocardial Substrate Metabolism in the Normal and Failing Heart. *Physiological ...*, 85(3):1093–1129.

Stoddart, L. A., Johnstone, E. K., Wheal, A. J., Goulding, J., Robers, M. B., MacHleidt, T., Wood, K. V., Hill, S. J., and Pfleger, K. D. (2015). Application of BRET to monitor ligand binding to GPCRs. *Nature Methods*, 12(7):661–663.

Sulser, P., Pickel, C., Günter, J., Leissing, T. M., Crean, D., Schofield, C. J., Wenger, R. H., and Scholz, C. C. (2020). HIF hydroxylase inhibitors decrease cellular oxygen consumption depending on their selectivity. *FASEB journal : official publication of the Federation of American Societies for Experimental Biology*, 34(2):2344–2358.

Takeda, K., Aguila, H. L., Parikh, N. S., Li, X., Lamothe, K., Duan, L.-J., Lee, F. S., Fong, G.-H., and Takeda, H. (2008). Regulation of adult erythropoiesis by prolyl hydroxylase domain proteins Regulation of adult erythropoiesis by prolyl hydroxylase domain proteins. *Blood*, 111(6):3229–3235.

Tanhauser, S. M. and Laipis, P. J. (1995). Multiple deletions are detectable in mitochondrial DNA of aging mice. *Journal of Biological Chemistry*, 270(42):24769–24775.

Tarhonskaya, H., Hardy, A. P., Howe, E. A., Loik, N. D., Kramer, H. B., McCullagh, J. S., Schofield, C. J., and Flashman, E. (2015). Kinetic investigations of the role of factor inhibiting hypoxia-inducible factor (FIH) as an oxygen sensor. *Journal of Biological Chemistry*, 290(32):19726–19742.

Tian, Y. M., Yeoh, K. K., Lee, M. K., Eriksson, T., Kessler, B. M., Kramer, H. B., Edelmann, M. J., Willam, C., Pugh, C. W., Schofield, C. J., and Ratcliffe, P. J. (2011). Differential sensitivity of hypoxia inducible factor hydroxylation sites to hypoxia and hydroxylase inhibitors. *Journal of Biological Chemistry*, 286(15):13041–13051.

Townsend, N., Wickramasinghe, K Bhatnagar, P., Smolina, K., Nichols, M., Leal, J., Luengo-Fernandez, R., and Rayner, M. (2012). *Coronary heart disease statistics*.

Uchida, K., Uchida, S., Nitta, K., Yumura, W., Marumo, F., and Nihei, H. (1994). Glomerular endothelial cells in culture express and secrete vascular endothelial growth factor. *American Journal of Physiology - Renal Fluid and Electrolyte Physiology*, 266(1 35-1):81–88.

Uddin, G. M., Zhang, L., Shah, S., Fukushima, A., Wagg, C. S., Gopal, K., Al Batran, R., Pherwani, S., Ho, K. L., Boisvenue, J., Karwi, Q. G., Altamimi, T., Wishart, D. S., Dyck, J. R., Ussher, J. R., Oudit, G. Y., and Lopaschuk, G. D. (2019). Impaired branched chain amino acid oxidation contributes to cardiac insulin resistance in heart failure. *Cardiovascular Diabetology*, 18(1):1–12.

Ussher, J. R., Wang, W., Gandhi, M., Keung, W., Samokhvalov, V., Oka, T., Wagg, C. S., Jaswal, J. S., Harris, R. A., Clanachan, A. S., Dyck, J. R., and Lopaschuk, G. D. (2012). Stimulation of glucose oxidation protects against acute myocardial infarction and reperfusion injury. *Cardiovascular Research*, 94(2):359–369.

van der Vusse, G. J., van Bilsen, M., and Glatz, J. F. (2000). Cardiac fatty acid uptake and transport in health and disease. *Cardiovascular research*, 45(2):279–293.

Van Weeghel, M., Abdurrachim, D., Nederlof, R., Argmann, C. A., Houtkooper, R. H., Hagen, J., Nabben, M., Denis, S., Ciapaite, J., Kolwicz, S. C., Lopaschuk, G. D., Auwerx, J., Nicolay, K., Des Rosiers, C., Wanders, R. J., Zuurbier, C. J., Prompers, J. J., and Houten, S. M. (2018). Increased cardiac fatty acid oxidation in a mousemodel with decreasedmalonyl-CoA sensitivity of CPT1B. *Cardiovascular Research*, 114(10):1324–1334.

Wang, D., Eraslan, B., Wieland, T., Hallström, B., Hopf, T., Zolg, D. P., Zecha, J., Asplund, A., Li, L., Meng, C., Frejno, M., Schmidt, T., Schnatbaum, K., Wilhelm, M., Ponten, F., Uhlen, M., Gagneur, J., Hahne, H., and Kuster, B. (2019). A deep proteome and transcriptome abundance atlas of 29 healthy human tissues. *Molecular Systems Biology*, 15(2):1–16.

Wang, G. L., Jiang, B. H., Rue, E. A., and Semenza, G. L. (1995). Hypoxia-inducible factor 1 is a basic-helix-loop-helix-PAS heterodimer regulated by cellular O2 tension. *Proceedings of the National Academy of Sciences of the United States of America*, 92(12):5510–5514.

Wang, Y., Zhong, S., Schofield, C. J., Ratcliffe, P. J., and Lu, X. (2018). Nuclear entry and export of FIH are mediated by HIF1α and exportin1, respectively. *Journal of Cell Science*, 131(22):1–8.

Wells, L., Vosseller, K., and Hart, G. W. (2001). Glycosylation of nucleocytoplasmic proteins: Signal transduction and O-GlcNAc. *Science*, 291(5512):2376–2378.

White, C. W., Caspar, B., Vanyai, H. K., Pfleger, K. D., and Hill, S. J. (2020). CRISPR-Mediated Protein Tagging with Nanoluciferase to Investigate Native Chemokine Receptor Function and Conformational Changes. *Cell Chemical Biology*, 27(5):499–510.e7.

White, C. W., Kilpatrick, L. E., Pfleger, K. D., and Hill, S. J. (2021). A nanoluciferase biosensor to investigate endogenous chemokine secretion and receptor binding. *iScience*, 24(1):102011.

Willam, C., Maxwell, P. H., Nichols, L., Lygate, C., Tian, Y. M., Bernhardt, W., Wiesener, M., Ratcliffe, P. J., Eckardt, K. U., and Pugh, C. W. (2006). HIF prolyl hydroxylases in the rat; organ distribution and changes in expression following hypoxia and coronary artery ligation. *Journal of Molecular and Cellular Cardiology*, 41(1):68–77.

Wisneski, J. A., Gertz, E. W., Neese, R. A., and Mayr, M. (1987). Myocardial metabolism of free fatty acids. Studies with 14C-labelled substrates in humans. *Journal of Clinical Investigation*, 79(June 1986):359–366.

Witmer, A. N., Dai, J., Weich, H. A., Vrensen, G. F., and Schlingemann, R. O. (2002). Expression of vascular endothelial growth factor receptors 1, 2, and 3 in quiescent endothelia. *Journal of Histochemistry and Cytochemistry*, 50(6):767–777.

Woolard, J., Wang, W. Y., Bevan, H. S., Qiu, Y., Morbidelli, L., Pritchard-Jones, R. O., Cui, T. G., Sugiono, M., Waine, E., Perrin, R., Foster, R., Digby-Bell, J., Shields, J. D., Whittles, C. E., Mushens, R. E., Gillatt, D. A., Ziche, M., Harper, S. J., and Bates, D. O. (2004). VEGF165b, an inhibitory vascular endothelial growth factor splice variant: Mechanism of action, in vivo effect on angiogenesis and endogenous protein expression. *Cancer Research*, 64(21):7822–7835.

Wright, J. N., Collins, H. E., Wende, A. R., and Chatham, J. C. (2017). O-GlcNAcylation and cardiovascular disease. *Biochemical Society transactions*, 45(2):545–553.

Wu, N., Zhang, X., Du, S., Chen, D., and Che, R. (2018). Upregulation of miR-335 ameliorates myocardial ischemia reperfusion injury via targeting hypoxia inducible factor 1-alpha subunit inhibitor. *American Journal of Translational Research*, 10(12):4082–4094.

Wu, X., Reboll, M. R., Korf-Klingebiel, M., and Wollert, K. C. (2021a). Angiogenesis after acute myocardial infarction. *Cardiovascular research*, 117(5):1257–1273.

Wu, Y., Li, Z., McDonough, M. A., Schofield, C. J., and Zhang, X. (2021b). Inhibition of the Oxygen-Sensing Asparaginyl Hydroxylase Factor Inhibiting Hypoxia-Inducible Factor: A Potential Hypoxia Response Modulating Strategy. *Journal of Medicinal Chemistry*.

Xi, L., Taher, M., Yin, C., Salloum, F., and Kukreja, R. C. (2004). Cobalt chloride induces delayed cardiac preconditioning in mice through selective activation of HIF-1α and AP-1 and iNOS signaling. *American Journal of Physiology - Heart and Circulatory Physiology*, 287(6 56-6):2369–2375.

Xie, L., Pi, X., Wang, Z., He, J., Willis, M. S., and Patterson, C. (2015). Depletion of PHD3 protects heart from ischemia/reperfusion injury by inhibiting cardiomyocyte apoptosis. *Journal of molecular and cellular cardiology*, 80:156–65.

Xin, H., Zhong, C., Nudleman, E., and Ferrara, N. (2016). Evidence for Pro-angiogenic Functions of VEGF-Ax. *Cell*, 167(1):275–284.e6.

Yancy, C. W., Jessup, M., Bozkurt, B., Butler, J., Casey, D. E., Drazner, M. H., Fonarow, G. C., Geraci, S. A., Horwich, T., Januzzi, J. L., Johnson, M. R., Kasper, E. K., Levy, W. C., Masoudi, F. A., McBride, P. E., McMurray, J. J. V., Mitchell, J. E., Peterson, P. N., Riegel, B., Sam, F., Stevenson, L. W., Tang, W. H. W., Tsai, E. J., and Wilkoff, B. L. (2013). 2013 ACCF/AHA guideline for the management of heart failure: A report of the American college of cardiology foundation/american heart association task force on practice guidelines. *Journal of the American College of Cardiology*, 62(16):e147–e239.

Yu, A. Y., Shimoda, L. A., Iyer, N. V., Huso, D. L., Sun, X., McWilliams, R., Beaty, T., Sham, J. S., Wiener, C. M., Sylvester, J., and Semenza, G. L. (1999). Impaired physiological responses to chronic hypoxia in mice partially deficient for hypoxia-inducible factor 1α. *Journal of Clinical Investigation*, 103(5):691–696.

Yuan, Y., Hilliard, G., Ferguson, T., and Millhorn, D. E. (2003). Cobalt inhibits the interaction between hypoxia-inducible factor-α and von Hippel-Lindau protein by direct binding to hypoxia-inducible factor-α. *Journal of Biological Chemistry*, 278(18):15911–15916.

Zhang, H., Bosch-Marce, M., Shimoda, L. A., Yee, S. T., Jin, H. B., Wesley, J. B., Gonzalez, F. J., and Semenza, G. L. (2008). Mitochondrial autophagy is an HIF-1-dependent adaptive metabolic response to hypoxia. *Journal of Biological Chemistry*, 283(16):10892–10903.

Zhang, N., Fu, Z., Linke, S., Chicher, J., Gorman, J. J., Visk, D., Haddad, G. G., Poellinger, L., Peet, D. J., Powell, F., and Johnson, R. S. (2010). The asparaginyl hydroxylase factor inhibiting HIF-1alpha is an essential regulator of metabolism. *Cell metabolism*, 11(5):364–78.

Zimmer, H. G. (1996). Regulation of and intervention into the oxidative pentose phosphate pathway and adenine nucleotide metabolism in the heart. *Molecular and Cellular Biochemistry*, 160-161:101–109.

Zuurbier, C. J., Bertrand, L., Beauloye, C. R., Andreadou, I., Ruiz-Meana, M., Jespersen, N. R., Kula-Alwar, D., Prag, H. A., Eric Botker, H., Dambrova, M., Montessuit, C., Kaambre, T., Liepinsh, E., Brookes, P. S., and Krieg, T. (2020). Cardiac metabolism as a driver and therapeutic target of myocardial infarction. *Journal of cellular and molecular medicine*, 24(11):5937–5954.

Appendix A

Reagent details

A.1 Sequence of CRISPR components for addition of HiBit sequence to VEGF-A exon 8a and 8b

Sequences of CRISPR components utilised for the addition of HiBit sequences to the 3' end of VEGF-A exons 8a and 8b (chapter 5) are shown below in table A.1.

Table A.1 CRISPR Components for targeting HiBiT addition to VEGF-A exons 8a and 8b

Target	**Component**	**Sequence**
VEGF-A Exon 8a	gRNA	5'- UCAGAUGUGACAAGCCGAGGGUUUUAGAGCUAUGCU -3'
	ssODN	5'- CATCGCCAGGCCTCCTCACTTGGCCCTAACCCCAGCCTTTG TTTTCCATTTCCCTCAGATGTGACAAGCCGAGGCGAGTGAGCGG CTGGCGGCTGTTCAAGAAGATTAGCTGAgccgggcaggaggaaggag cctccctcagggtttcgggaaccagatctctcaccaggaaagactgatacagaacgatcga -3'
VEGF-A Exon 8b	gRNA	5'- CGGGAACCAGAUCUCUCACCGUUUUAGAGCUAUGCU -3'
	ssODN	5'- GCCGAGGCGGTGAGCCGGGCAGGAGGAAGGAGCCTCCC TCAGGGTTTCGGGAACCAGATCTCTCACCAGAAAAAGACGTGA GCGGCTGGCGGCTGTTCAAGAAGATTAGCTGAtacagaacgatcgatac agaaaccacgctgccgccaccacaccatcaccatcgacagaacagtccttaatccag -3'

Appendix B

Professional internship for PhD students

Note to examiners

This statement is included as an appendix to the thesis in order that the thesis accurately captures the PhD training experienced by the candidate as a BBSRC Doctoral Training Partnership student. The Professional Internship for PhD Students is a compulsory 3-month placement which must be undertaken by DTP students. It is usually centred on a specific project and must not be related to the PhD project. This reflective statement is designed to capture the skills development which has taken place during the student's placement and the impact on their career plans it has had.

Reflective statement

As a student of the Nottingham - BBSRC Doctoral training partnership I undertook a 3 month professional internship during the course of my PhD. The Professional internship for PhD students (PIP) is designed give PhD students a broader experience than their doctoral research project alone. For my PIP, I elected to travel to Stockholm and work in Professor Juleen Zierath's laboratory at Karolinska Institutet. The work in Professor Zierath's lab revolves around the study of diabetes, with particular focus on the study of skeletal muscle in type two diabetes. As such my work there represented a significant change from my PhD research and offered a unique opportunity to explore a new field, a new culture, country, and working environment.

The work I undertook on my PIP revolved around investigating novel type two diabetes targets in primary human skeletal muscle cultures. These targets had been identified by large scale profiling of muscle biopsies from type two diabetic

patients and non diabetic control volunteers. The functions of target genes were investigated by small interfering RNA manipulation, treatment with insulin, and in vitro exercise simulation via electrical pulse stimulation. Down stream assays including gene and protein expression analysis and metabolic measurements. Practically, therefore, my work gave me an opportunity to learn and develop a number of new technical skills.

In addition to the hands on practical skills that I developed, I benefited from exposure to a new scientific environment, institute, city and country. Being part of an international, dynamic group of motivated and welcoming scientists was a fantastic opportunity to learn. I received great scientific and technical support, but also I am grateful for the time that my colleagues took to discuss their experiences of navigating a scientific career following a PhD.

Working in Stockholm gave me a fantastic opportunity to explore a vibrant city and become more familiar with the Swedish way of life; two opportunities I am extremely grateful for. The working environment in Sweden is clearly quite different from the U.K., and it was brilliant to be able to experience this first hand. I am pleased that I have been able to maintain some of the positive working practices since returning to the U.K. If nothing else, my rate of coffee consumption remains distinctly Swedish.

In summary, my PIP was a very positive experience. I gained practical skills that will be useful throughout my career, and also experience of a different working culture and environment. I made a number of friendships and professional connections that I hope will continue throughout my career. I am very grateful to Professor Zierath for hosting me in her laboratory, to Brendan Gabriel for helping to arrange my time there, and to all of my other great colleagues, particularly Jonathon Smith, who helped make my time in Stockholm so much fun. Tack så mycket!